ENERGY LABORATORY

MASSACHUSETTS INSTITUTE
OF TECHNOLOGY

EVALUATION OF MODELS FOR PREDICTING EVAPORATIVE WATER LOSS IN COOLING IMPOUNDMENTS

by

Karl R. Helfrich, E. Eric Adams,
Alice L. Godbey and Donald R.F. Harleman

Energy Laboratory Report No. MIT-EL 82-017
March 1982

EVALUATION OF MODELS FOR PREDICTING EVAPORATIVE WATER LOSS IN COOLING IMPOUNDMENTS

Karl R. Helfrich
E. Eric Adams
Alice L. Godbey
Donald R.F. Harleman

Energy Laboratory

and

Ralph M. Parsons Laboratory
for
Water Resources and Hydrodynamics
Department of Civil Engineering

Massachusetts Institute of Technology
Cambridge, Massachusetts 02139

Prepared under the Support of

Electric Power Research Institute
Palo Alto, California

Energy Laboratory Report No. MIT-EL 82-017

March 1982

ACKNOWLEDGMENTS

This study was supported by the Electric Power Research Institute under Contract No. RP 1260-17 (MIT OSP No. 88945). Mr. John Bartz was project manager at EPRI and his administrative help was greatly appreciated.

With minor modification, this report represents the thesis of Mr. Karl R. Helfrich, submitted to the Department of Civil Engineering in partial fulfillment of the degree of Master of Science in Civil Engineering. Thesis supervision was provided by Dr. E. Eric Adams of the MIT Energy Laboratory and the Department of Civil Engineering. Mrs. Alice L. Godbey, graduate research assistant worked on several parts of the report including the analysis of data averaging described in Section 4.7, and Professor Donald R. F. Harleman of the Department of Civil Engineering provided overall project supervision. The report was typed by Mrs. Carole J. Solomon.

TABLE OF CONTENTS

LIST OF FIGURES

LIST OF TABLES

LIST OF SYMBOLS

Symbol	Definition
A	water surface area
A	constant
A'	constant
$A*$	atmospheric stability parameter
a	empirical constant
B	buoyancy flux
$B*$	atmospheric stability parameter
b	empirical constant
Δb	buoyancy difference = $g(\rho_a-\rho_s)/\rho_a$
c_{p_a}	specific heat of air at constant pressure
C	cloud cover factor
D_s	lateral entrance dilution factor
D_v	vertical volumetric dilution factor
D_w	molecular diffusivity of water vapor
d	empirical constance
e_2	vapor pressure at 2 meters height
e_a	vapor pressure of air (at some height)
e_{a_o}	vapor pressure of air upstream of lake
e_s	vapor pressure at water surface temperature
e_z	vapor pressure of air at height z above water surface
Δe	$= e_s - e_z$

Symbol	Definition
E	evaporative mass loss rate
E_h	evaporative mass loss rate under heated conditions
E_L	longitudinal dispersion coefficient
E_{L_F}	longitudinal dispersion coefficient, Fisher (1967)
E_n	evaporative mass loss rate under natural conditions
f_i	interfacial friction factor
f_o	bottom friction factor
$f(W_z)$	empirical wind speed function
G	groundwater inflows, outflows
g	acceleration due to gravity
$g(T_n)$	empirical function for linearizing back radiation
H	plant heat rejection rate
H	pond depth
h_c	heat transfer coefficient for sensible heat flux
h_e	heat transfer coefficient for evaporative heat flux
h_s	depth of heated surface layer
K	surface heat transfer coefficient
K_e	evaporative heat transfer coefficient
$K_{W,H,M}$	turbulent eddy diffusivities for mass, heat and momentum respectively
L	pond length along flow path
L	latent heat of vaporization

Symbol	Definition
L	Monin-Obukov length
ℓ	length scale or fetch length
N_u	Nusselt number
n	empirical constant
P	precipitation
P_a	atmospheric pressure
Q_o	condenser flow rate
q	jet surface area factor
$\bar{q}$	mean specific humidity
q'	turbulent specific humidity fluctuation
$\bar{q}_{1,2}$	mean specific humidity at vertical level 1, 2 etc.
$\bar{q}_s$	specific humidity at water surface temperature
R	Bowen Ratio
R	overland runoff
R_a	Rayleigh number
R_e	Reynolds number
R_i	bulk Richardson number
R_f	flux Richardson number
$S_{i,o}$	stream inflows or outflows respecitvely
ΔS	change in energy content of water body
s	$= \partial q_s / \partial T$
$\bar{T}_a$	mean air temperature
T_e	equilibrium temperature
T_h	water surface temperature under heated conditions
T_n	water surface temperature under natural conditions

Symbol	Definition
T_s	water surface temperature
$\bar{T}_z$	mean air temperature at height z
T^*	$= (T_s + T_e)/2$
ΔT	temperature difference between water surface and air $= T_s - T_a$
ΔT	temperature difference between heated and natural conditions $= T_h - T_n$
ΔT_o	temperature rise across condenser
ΔT_v	vertical temperature difference in cooling pond
U	cross-sectionally averaged water velocity
$\bar{u}$	mean horizontal velocity
u_*	friction velocity
$\bar{u}_{1,2}$	mean horizontal velocity at vertical level 1,2 etc.
u_∞	free stream velocity
W	flow path width
W_z	wind speed at height z
W_2	wind speed at 2 meters height
w'	turbulent vertical velocity fluctuation
z	vertical coordinate
$z_{1,2}$	measurement heights
z_o	roughness height
z_w	"roughness" height for water vapor
α	empirical constant
α	molecular diffusivity of heat

Symbol	Definition
ϕ	thermal loading factor
ϕ_{ad}	advected heat flux
ϕ_{an}	net incoming longwave atmospheric radiation
ϕ_{br}	longwave back radiation from water surface
ϕ_c	sensible (conductive) heat flux
ϕ_e	evaporative heat flux
ϕ_ℓ	net surface heat loss = $\phi_e + \phi_c + \phi_{br}$
ϕ_{LW}	long-wave radiation flux
ϕ_n	net surface heat transfer = $\phi_r - \phi_e$
ϕ_r	net incident shortwave solar and longwave atmospheric radiation
ϕ_{sn}	net incoming solar radiation heat flux
Ψ_m	$= \int_0^{z/L} \frac{1 - \phi_m(z/L)}{(z/L)} \, d(z/L)$
Ψ_w	$= \int_0^{z/L} \frac{1 - \phi_w(z/L)}{(z/L)} \, d(z/L)$

Symbol	Definition
β	coefficient of thermal expansion of air $= -\frac{1}{\rho}\frac{\partial \rho}{\partial T}$
γ	$= (0.61 \times 10^{-3}\ ^{o}c^{-1})P_a$
γ	$= c_{p_a}/L$
$\gamma_{1,2,3,4}$	empirical constants
ε	emissivity
ε_a	emissivity of atmosphere
ε_{a_c}	emissivity of atmosphere under clear skies
ζ	measurement height/Monin-Obukov length
θ_2	air temperature at 2 meters
θ_s	water surface temperature
θ_{v_a}	virtual air temperature at some height
θ_{v_s}	virtual water surface temperature
$\Delta\theta$	$= \theta_s - \theta_a$
$\Delta\theta_v$	$= \theta_{v_s} - \theta_{v_a}$
κ	von Karmon's constant (=.4)
ν	viscosity of air
ρ	density
ρ_a	density of air
ρ'	turbulent density fluctuation
σ	Stephan - Boltzman constant
τ	shear stress (momentum flux)
$\Phi_{W,H,M}$	empirical functions which account for buoyancy effects on mean vertical profiles of water vapor, heat and momentum respectively

SUMMARY

Cooling impoundments can offer a number of advantages over cooling towers for condenser water cooling at steam electric power plants. However, a major disadvantage of cooling ponds is a lack of confidence in the ability to predict various aspects of their hydrothermal performance and consumptive water use. This report focuses on evaporation, which is related to both pond performance (temperatures) and consumptive water use.

A discussion of evaporation equations from both a theoretical and an empirical basis is presented. Several empirical evaporation equations falling into three basic categories - Dalton Law, Modified Dalton Law and Stability Dependent - have been compared to determine accuracy and confidence limits for evaporation from heated water bodies. Comparisons have been carried out using MIT's dynamic cooling pond model MITEMP to evaluate the energy budget for six weeks of comprehensive meteorological and water temperature data taken at Dresden Cooling Pond in Illinois. Results show a large decrease in the variability among the different formulations (measured by mean error and variance of predicted and measured plant intake temperatures) when a dynamic model is used compared with the large variability among the equations for constant meteorological conditions and water surface temperature. Feedback between evaporation and temperature in the dynamic model is suggested as a reason for this decrease. Linear calibrations have been fitted to

each equation using these data. The consistency of calibration was then checked using similar data from Powerton Cooling Pond in Illinois. Due to the high non-linearity of some of the equations, the effects of meteorological data averaging period are examined by long term simulations.

Linearized surface heat loss formulations are discussed with emphasis on their use in long term forced evaporation water consumption estimates. An extension of the Harbeck Diagram concept (Harbeck, 1964; Ward, 1980) is presented to better account for non-linearities due to high temperature differences between heated and natural conditions. Surprisingly good agreement has been found between annual water consumption computed from diagram estimates and from dynamic hydrothermal model simulations involving full non-linear heat loss expressions.

CHAPTER 1

INTRODUCTION

1.1 Background and Objective

This effort is part of the research project entitled, "Evaluation of Models for Predicting Evaporative Water Loss and Hydrothermal Performance in Cooling Impoundments," sponsored by the Electric Power Research Institute. A cooling impoundment is a large body of water used to dissipate waste heat discharged by the condenser cooling water of a steam electric power plant. The dissipation occurs at the water surface through a combination of radiative, evaporative and conductive heat transfer.

Alternatives to cooling impoundments include once through (or open systems) and cooling towers. Once through cooling, however, is seldom planned for new generating stations because of the dwindling number of available sites and because of strict downstream or coastal zone water quality standards which must be met. The alternatives are then cooling impoundments or cooling towers.

Cooling impoundments have a number of advantages in comparison with cooling towers. Because of lower condenser intake temperatures, lower pumping head and absence of fans, the net efficiency of power production is increased; their thermal inertia reduces the short term fluctuations associated with towers, and their ability to store water on a seasonal basis reduces make-up water demand during low flow periods and increases siting flexibility in water short areas. Disadvantages include land availability for off-stream impoundments,

environmental constraints in the case of on-stream impoundments and most significantly, a lack of confidence in the ability to predict various aspects of their hydrothermal performance and consumptive water use.

Three areas of performance can be identified and, as suggested in Figure 1.1, each is centrally related to impoundment water temperature. Plant efficiency is a function of intake temperature which reflects the hydrothermal circulation within the impoundment and the selective withdrawal characteristics of the intake; impoundment (or downstream) water quality is dependent on water temperature in general and on thermal stratification in particular; and a major component of water consumption is evaporation which is closely keyed to impoundment surface temperature. Thus an improved understanding of hydrothermal performance - i.e., prediction of impoundment water temperatures - will lead to improved understanding of these three areas and thus to reduced uncertainty in the use of cooling lakes and ponds as alternatives to towers in closed-cycle cooling systems. Such improvement in the basic capabilities of hydrothermal modeling has been an objective of recent research at M.I.T. (e.g., Ryan et al (1973), Watanabe et al (1975), Brocard et al (1977), Jirka et al (1978, 1980), Octavio et al (1980) and Adams et al (1980) and has provided background motivation for the present project.

The specific objective of the project - and the focus of this report - is improved understanding and quantification of cooling pond evaporation. There are several fundamental reasons for interest in evaporation. The first is that evaporative mass loss is usually the major component in a water balance for a cooling impoundment and is

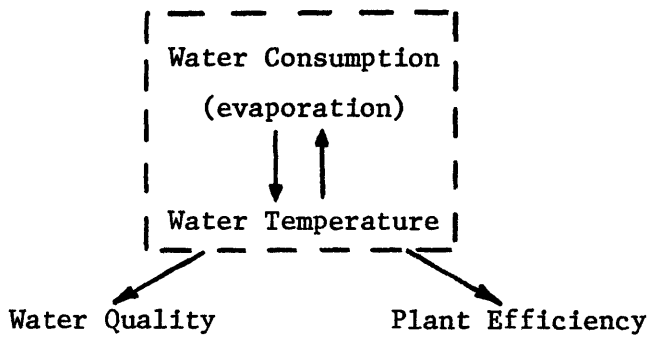

Figure 1.1: Relationships of Cooling Impoundment Performance and Impoundment Water Temperatures

almost always the major component in cooling pond water consumption. In view of the increasing demand on the nation's fresh water supplies it is important that we be able to quantify the amount of consumption involved in alternative processes and, to the extent possible, design these alternatives to minimize water consumption.

The primary reason for interest in evaporation is that evaporative

heat flux is also one of the dominant terms in the energy budget governing the transport of heat across the water surface. Therefore not only does water temperature affect evaporation, but evaporation affects water temperature and thus also exerts an influence on the water quality and station efficiency aspects of cooling impoundment performance. The link between evaporation and station efficiency is particularly important because both evaporation and land requirements - two negative attributes of cooling impoundments - decrease with decreasing pond area while water temperature, which is inversely related to plant performance, increases. In order to be able to design water and land efficient ponds, while maintaining an acceptable margin of station performance, it is necessary to have an accurate evaluation of evaporative heat transfer.

It should be noted that, even if one were exclusively interested in evaporation for the sake of evaluating water consumption, one must still employ hydrothermal models. This is because evaporation is a function of water surface temperature and, in order to predict evaporation at future sites, one must simultaneously predict water temperature. Also, hydrothermal models are useful in the interpretation of field data concerning evaporation. In this respect they may either be used directly, in an energy budget approach by adjusting evaporation rates such that measured and predicted temperatures agree, or indirectly to predict surface temperatures and thus supplement the measurement of surface temperature measurements needed as input to evaporation formulae.

1.2 Outline of Report

This report presents findings which attempt to answer the question: how good are existing approaches to predicting evaporation from cooling impoundments? Chapter II discusses the theoretical basis behind various evaporation formulations including the importance of boundary layer stability in evaporative heat and mass transfer. Empirical formulations are discussed and in particular ten equations which were selected for empirical testing in Chapter IV are introduced. Chapter III discusses the role of hydrothermal models which must be used along with an evaporation formula to capture the relevant spatial and temporal scales of water temperature, and therefore evaporation, that are characteristic of cooling impoundments. In particular the model MITEMP [Octavio et al. (1980)] is described in some detail as it was used extensively in the empirical testing of Chapter IV.

Chapter IV identifies a number of existing data bases which either have been or could be used to calibrate and/or verify evaporation models. Hydrothermal model predictions (pond temperature and evaporation) are made using data from the Dresden Cooling Pond with an appropriate hydrothermal model and the ten evaporation equations. Results are compared and the formulas are calibrated to this data set in the sense of zeroing the mean error between measured and predicted plant intake temperatures. Consistency of the calibrations is tested by a similar analysis using data from the Powerton Cooling Pond. Additionally, a hierarchy of evaporation prediction variability, associated with method of prediction, is identified. Finally, the sources of possible uncer-

tainty in the calibrations previously performed are identified and sensitivity studies are performed in order to quantify the confidence in the equation calibrations.

Chapter V presents an improvement upon the Harbeck Diagram [Harbeck (1964)] for estimating the forced evaporation due to the input of waste heat into a waterbody. Chapter VI summarizes the results and conclusions of the thesis.

CHAPTER 2

EVAPORATION MODEL FORMULATION

2.1 Theoretical Formulation

Evaporation is the vertical flux of water vapor from the surface of an open body of water. In the absence of any turbulence production (wind, etc.) the water vapor movement is dominated by molecular diffusion. Given enough kinetic energy water molecules can escape from the water surface and are transported upward into the air which has a lower water vapor content. Ideally a thin layer (saturated with water vapor) exists just above the water surface. In the absence of any limiting conditions this layer will increase in height so that eventually the evaporation rate will decrease. The air above the water surface will contain more and more water vapor.

However, under realistic atmospheric conditions this transport process is dominated by turbulence. The thin saturated molecular layer is limited in height. The turbulence, which is generated by wind, buoyancy or both, acts to supply "fresh" air above the saturated layer and thus the evaporation rate is enhanced. This turbulent transport of water vapor at a point is given by (following the Reynolds averaging approach)

$$E = \rho_a \overline{w'q'} \tag{2.1}$$

where E = evaporative mass loss rate, ρ_a = density of moist air, w' = turbulent vertical velocity fluctuation, q' = turbulent specific humidity fluctuation, and the overbar denotes a temporal average.

Equation (2.1) as an analytical tool is not readily useful. Generally little or no a priori information on w' and q' is available. Measurements of these quantities are possible [Hicks et al. (1977)] and are referred to as eddy flux measurements. To develop a more useful analytical tool use may be made of dynamic similarity arguments. For turbulent conditions the transfer laws for mass, heat and momentum (heat and momentum transfer are analogous to (2.1)) can be written as

$$E = -\rho_a K_W \frac{\partial \bar{q}}{\partial z} \tag{2.2a}$$

$$\phi_c = -\rho_a c_{p_a} K_H \frac{\partial \bar{T}}{\partial z} \tag{2.2b}$$

$$\tau = \rho_a K_M \frac{\partial \bar{u}}{\partial z} = \rho_a u_*^2 \tag{2.2c}$$

where ϕ_c = sensible heat flux, τ = shear stress (momentum flux), $\bar{q}$ = mean specific humidity, $\bar{T}$ = mean air temperature, c_{p_a} = specific heat of air at constant pressure, u_* = friction velocity, z = vertical coordinate and $K_{W,H,M}$ = turbulent eddy diffusivities for mass, heat and momentum, respectively.

Rearranging (2.2c) gives

$$K_M = \frac{u_*^2}{\partial \bar{u}/\partial z} \tag{2.3}$$

Multiplying and dividing equation (2.2a) by (2.3) one gets

$$E = -\frac{K_W}{K_M} \rho_a u_*^2 \frac{\partial \bar{q}/\partial z}{\partial \bar{u}/\partial z} \tag{2.4}$$

Because continuous measurements of the velocity and specific humidity

with height are generally not available, and thus $\partial\bar{u}/\partial z$ and $\partial\bar{q}/\partial z$ cannot be evaluated, Eqn. (2.4) is usually written in difference form

$$E = \frac{K_W}{K_M} \rho_a u_*^2 \frac{(\bar{q}_1 - \bar{q}_2)}{(\bar{u}_2 - \bar{u}_1)} \tag{2.5}$$

The subscripts on $\bar{q}$ and $\bar{u}$ refer to the heights, z, at which measurements are taken ($z_2 > z_1$).

Further refinement of equation (2.5) is necessary because knowledge of the shear stress $\rho_a u_*^2$ is generally not available. Flow over a water surface will usually be fully rough turbulent. For a neutrally stable boundary layer a log-law velocity profile can be used to relate $\bar{u}(z)$ and u_*:

$$u(z) = \frac{u_*}{\kappa} \ln(z/z_o) \tag{2.6}$$

where κ = van Karman's constant (= .4) and z_o = roughness height. This comes from dimensional reasoning which implies $\frac{\partial \bar{u}}{\partial z} = \frac{u_*}{\kappa z}$ and therefore $K_M = u_* \kappa z$ from Equation (2.2c).

Eliminating u_* in (2.5) using (2.6) gives

$$E = \frac{K_W}{K_M} \rho_a \kappa^2 \frac{(\bar{u}_2 - \bar{u}_1)(\bar{q}_1 - \bar{q}_2)}{[\ln(z_2/z_1)]^2} \tag{2.7}$$

It should be noted that equation (2.7) which is known as the Thornwaite-Holtzman equation gives a relationship for evaporation in terms of the specific humidity gradient and the horizontal wind speed directly. Equation (2.1) and (2.2a) do not directly reflect the influence of the horizontal windspeed. This influence is encountered indirectly because $w' \sim u_*$ and $K_W \sim u_* \ell$ where ℓ is an appropriate length scale.

Field studies at Lake Hefner [Harbeck (1952)] (a non-heated lake) indicated that equation (2.7) and some other similarly derived relationships did not predict evaporation adequately. Problems included specification of the measurement heights z_1 and z_2 and the assumption that the ratio K_W/K_M is a constant, usually taken to be 1 (the Reynolds analogy). This assumption in general is only good for conditions of no vertical density gradient [Turner (1973), p. 133]. The non-neutral situation will be discussed in Section 2.1.2.

To help correct the problem with the measurement heights, z_1 is usually taken to lie within the saturated vapor layer just above the water surface. In this molecularly dominated layer $\bar{q}_1$ is assumed to be equal to the saturation specific humidity, $\bar{q}_s$, a function of the local air temperature which is approximately equal to the water surface temperature. From (2.6) $\bar{u}_1 = 0$ when $z_1 = z_o$. If it is assumed that z_o lies within this saturated layer then equation (2.7) becomes

$$E = \left(0.622 \frac{K_W}{K_M} \frac{\rho_a}{P_a} \bar{u}_z\right) \frac{(e_s - e_z)}{[\ell n(z_2/z_o)]^2} \tag{2.8}$$

where $\bar{q} = 0.622\ e/P_a$, P_a is the atmospheric pressure and e is the vapor pressure. The subscript 2 referring to height z_2 on $\bar{u}$ and e has been replaced by z which indicates measurement at some height z.

In practice, equation (2.8) is often replaced by an empirical equation of the form

$$E = f(W_z)(e_s - e_z) \tag{2.9}$$

where $f(W_z)$ = empirical wind speed function, e_s = saturation vapor pressure at water surface temperature, e_z = vapor pressure of the air at some specified height z and W_z = wind speed at some specified height z. The value of the windspeed function varies widely among evaporation equations but it is commonly of the form $f(W_z) = a + bW_z$ where a and b are empirically determined constants. This type of equation is termed a Dalton Law equation. With $a = 0$ this wind speed function is analogous to equation (2.8), though empirical determination of b is often different from that implied by (2.8).

Equation (2.9) with non-zero value for "a", differs from equations (2.7) and (2.8) mainly in that it allows evaporation to continue in the absence of wind. Measurement of evaporation over both heated [Ryan and Harleman (1973), Brady et al. (1969)] and natural [Kohler (1954)] water bodies have shown this to occur. Evaporation at zero windspeed can be attributed to such factors as finite anemometer threshold, unsteady effects, and free convective heat transfer (which will be disucssed in Section 2.1.2 in more detail). For heated water bodies this last factor is extremely important because of the high temperature differences which can occur between the water surface and the overlying air.

A fundamental difference between equation (2.1) and the empirical evaporation equation (2.9) should be mentioned. The eddy flux of vapor given by equation (2.1) refers to evaporation from a point on the water surface. Equation (2.9), though "developed" (in form at least) from equation (2.1), is generally used to determine evaporation integrated

over some area. The coefficients a and b of the windspeed often have this areal dependence incorporated in them through their original calibration.

2.1.1 Bowen Ratio

At this time it is useful to introduce the Bowen ratio concept [Bowen (1926)] which is used to relate evaporative heat transfer and sensible heat transfer and to discuss some of the assumptions in this concept.

From equation (2.2a), and proceeding along the same lines as was done with evaporative mass loss, one can arrive at

$$\phi_c = \rho_a c_{p_a} \frac{K_H}{K_M} \bar{u}_z [\ell n(z/z_o)]^{-2} (\bar{T}_s - \bar{T}_z) \tag{2.10}$$

The Bowen ratio, R, is simply the ratio of the conductive heat flux to the evaporative heat flux ϕ_e (ϕ_e = LE where L = latent heat of vaporization)

$$R = \frac{\phi_c}{\phi_e} = \frac{c_{p_a} P_a}{0.622\ L} \quad \frac{K_H}{K_W} \quad \frac{(\bar{T}_s - \bar{T}_z)}{(e_s - e_z)} \tag{2.11}$$

Bowen gives

$$R = (0.61 \times 10^{-3}\ {}^{o}C^{-1}) \frac{(T_s - T_z)}{(e_s - e_z)} \quad P_a \tag{2.12}$$

which he arrived at by assuming the transfer of heat and water vapor were similar and that the transfer process was partially limited by molecular diffusion through a saturated layer. Using Bowen's suggested values for c_{p_a} and L we get $K_H/K_W = 0.92$.

Usually the Bowen ratio is used to compute conductive heat flux using an empirical evaporation equation:

$$\phi_c = R\ L\ f(W_z)(e_s - e_z)$$

$$\phi_c = (.61 \times 10^{-3}\ {}^{o}C^{-1}) P_a\ L\ f(W_z)(T_s - T_z) \qquad (2.13)$$

There is some question about the validity of the Bowen ratio concept in unstable situations, which are typical of cooling ponds. (See Section 2.1.2 for more discussion on stability.) Two assumptions are inherent in using the Bowen ratio in this fashion. First it assumes that the wind speed function $f(W_z)$ applicable for evaporation is also applicable for conduction. Secondly it assumes that the ratio K_H/K_W is constant. These two assumptions are related because the wind speed function implicitly contains information on turbulent transfer processes and as such K_H and K_W.

Monin and Yaglom (1971) state that all empirical evidence indicates $K_H = K_W$ in neutral and unstable conditions. Dyer (1974), after examining many sets of available field data, also states that the eddy diffusivities of heat and mass are equal in neutral and unstable situations. These results point to the applicability of equation (2.11) in neutral and unstable conditions.

Problems with application of equation (2.11) or (2.12) may arise because over a cooling pond the water vapor and thermal boundary layers may never reach an equilibrium situation. The measurements which indicate $K_H = K_W$ were made over land or water within a developed boundary layer. Very often in hydrothermal modeling measurements of the primary

meteorological variables used to determine evaporation and conduction (by way of Bowen ratio) are from off-pond met stations. Use of this data could lead to error in computing the Bowen ratio and therefore conductive heat flux. Furthermore, McNaughton (1976) points out the importance of a changing Bowen ratio with downwind distance from an abrupt change in surface wetness (e.g., land to water). Further work in this area as it pertains to cooling impoundments is necessary to gauge the probable magnitude of error when using equation (2.11) or (2.12) to compute conduction.

Other methods of computing the Bowen ratio have been suggested. Priestly and Taylor (1972) use a "meteorological" approach--which attempts to account for second order errors associated with a Taylor expansion of the specific humidity gradient near the water surface--to get

$$\frac{\phi_e}{\phi_c+\phi_e} = \alpha \frac{s}{s+\gamma} \tag{2.14}$$

where $s = \left.\frac{\partial q_s}{\partial T}\right|_{T_s}$, T_s = water surface temperature, $\gamma = c_{p_a}/L$, and α = empirical constant. Priestly and Taylor determine $\alpha = 1.26$ from experimental data whereby rearrangement gives

$$R = 0.79(\gamma/s)-0.21 \tag{2.15}$$

Hicks and Hess (1976) get the similar relation

$$R = 0.63(\gamma/s)-0.15 \tag{2.16}$$

from fitting experimental data. They caution, however, that this result be used only on long time and length scales (e.g., seasonal and zonal). It should also be noted that these two relations also assume $K_H = K_W$.

Although equation (2.15) and (2.16) do not depend on meteorological conditions in the air and are not subject to any possible errors associated with measurement location as mentioned earlier in this study we will use equation (2.12) to compute conduction given some empirical evaporation equation.

2.1.2 Stability

In the preceeding development it was assumed that the boundary layer above the water surface was neutrally stable. For cooling impoundments this is rarely the case. Water temperatures are often in the range 30^{o} - 40^{o} C and air temperatures are, on average, much less than this. The combination of higher temperature and greater water vapor content in the air nearest the water surface leads to lower density than the air above and a resulting vertical flux of buoyancy. Evaporative heat and mass transfer are therefore enhanced. Eqn. (2.8) with K_W/K_M assumed constant and Dalton Law type equation, with its constant coefficients, do not take this instability into account. The general inadequacy of equations developed for natural conditions when applied to heated situations is probably due to this effect.

Recently more investigators [Shulyakovsky (1969), Ryan and Harleman (1973), Hicks et al. (1975), Weisman and Brutsart (1973),

Quinn (1979) and others] have attempted to include the effect of atmospheric stability on the evaporation rate. The methods for doing this follow two different though related paths--forced convection augmentation and free convection.

2.1.2.1 Forced Convection Correction

Forced convection refers to the transfer of heat or mass (buoyancy) when the production of turbulence by velocity shear dominates over production or damping of turbulence by buoyancy [Turner (1973), p. 134]. The velocity scale for the problem is imposed by the presence of mean velocity shear. The balance between mean velocity shear turbulence production and buoyancy induced turbulence production (or damping in stable situations) is reflected in the flux Richardson number

$$R_f = \frac{\frac{g}{\rho}\overline{\rho' w'}}{-\overline{u'w'}\frac{\partial \bar{u}}{\partial z}} \qquad (2.17)$$

where ρ = mean density; ρ' = turbulent density fluctuation; u' = horizontal velocity fluctuation and g = acceleration due to gravity. When $R_f < 0$ the situation is unstable and buoyancy is generating turbulence. Neutral stability occurs when $R_f = 0$ and when $R_f > 0$ the flow is stable and buoyancy tends to damp out turbulence generated by shear. When $|R_f|$ is large buoyancy influences are dominant and when $|R_f|$ is small turbulence production by mean shear is most important. The flux Richardson number is a local measure of the importance of buoyancy and mean shear in a turbulent flow.

A commonly used parameterization of the same influences is z/L where z is the vertical coordinate and L is the Monin-Obukov length scale. For a neutral atmosphere the production of turbulence by mean shear is given by

$$-\overline{u'w'}\,\frac{\partial \bar{u}}{\partial z} = u_*^2\,\frac{u_*}{\kappa z} \tag{2.18}$$

The production (or damping) of turbulence by buoyancy is denoted by

$$\frac{g}{\rho_a}\,\overline{\rho'w'} = -B \tag{2.19}$$

B is the buoyancy flux:

$$B = \frac{\beta g(\phi_c + \phi_e)}{\rho_a\, c_{p_a}}$$

where β = coefficient of thermal expansion of air = $-\frac{1}{\rho}\frac{\partial \rho}{\partial T}$; and ϕ_c and ϕ_e are the heat fluxes for conduction and evaporation, respectively. $B > 0$ for a net outward evaporation and conduction heat flux. Now dividing equation (2.19) by (2.18) we have

$$\frac{\frac{g}{\rho}\,\overline{\rho'w'}}{-\overline{u'w'}\,\frac{\partial \bar{u}}{\partial z}} = -\frac{B\kappa z}{u_*^3} = \frac{z}{L} \tag{2.21}$$

where

$$L = -\frac{u_*^3}{\kappa B} \tag{2.22}$$

Notice that z/L is related to the flux Richardson number, but is not equal unless the velocity profile is actually logarithmic. In defining

the production term we assumed a logarithmic velocity profile (equation 2.14). Since z is a positive quantity, stability is related to the sign of L:

$L < 0 \rightarrow$ unstable

$L = 0 \rightarrow$ neutral

$L > 0 \rightarrow$ stable

At a level $z << |L|$ buoyancy influences may be neglected and for $z >> |L|$ buoyancy is dominant.

For non-neutral conditions the velocity profile is usually not logarithmic but rather given by

$$\frac{\partial \bar{u}}{\partial z} = \frac{u_*}{\kappa z} \Phi_M \tag{2.23}$$

$\Phi_M = \Phi_M(z/L)$ is a universal function which accounts for the effects of buoyancy on mean shear [Monin and Yaglon (1971), p. 428]. From equations (2.2c) and (2.23) one can infer $K_M = \frac{u_* \kappa z}{\Phi_M(z/L)}$. Similarly

$$K_W = \frac{\kappa u_* z}{\Phi_W(z/L)}$$

and

$$K_H = \frac{\kappa u_* z}{\Phi_H(z/L)}$$

From equations (2.2a and b):

$$E = -\rho_a \frac{u_* \kappa z}{\Phi_W(z/L)} \frac{\partial \bar{q}}{\partial z} \tag{2.24}$$

and

$$\phi_c = -\rho_a c_{p_a} \frac{u_* \kappa z}{\Phi_H(z/L)} \frac{\partial \bar{T}}{\partial z} \tag{2.25}$$

where $\Phi_H(z/L)$ and $\Phi_W(z/L)$ are universal functions for heat and water vapor (mass) transport and are usually assumed to be equal [Hicks et al. (1977) and Quinn (1979)].

Integration of equation (2.23) following Panofsky (1963) gives

$$\bar{u}_z = \frac{u_*}{\kappa} [\ell n(z/z_o) - \Psi_M(z/L)] \tag{2.26}$$

and from equation (2.24)

$$(\bar{q}_s - \bar{q}_z) = \frac{E}{\rho_a \kappa u_*} [\ell n(z/z_w) - \Psi_W(z/L)] \tag{2.27}$$

The subscripts z and s refer to values at some height z and in the saturated vapor layer respectively. z_W is the "roughness height" for water vapor. Hicks et al. (1977) suggest $z_W = D_W/\kappa u_*$ and $z_o = \alpha u_*^2/g$ where D_W is the molecular diffusion coefficient for water vapor and α is an empirical constant. Ψ_M and Ψ_W are given by

$$\Psi_M = \int_o^{z/L} \frac{1-\Phi_M(z/L)}{(z/L)} d(z/L) \tag{2.28}$$

and

$$\Psi_W = \int_o^{z/L} \frac{1-\Phi_W(z/L)}{(z/L)} d(z/L) \tag{2.29}$$

Solution of equation (2.27) for E along with use of (2.26) to eliminate u_* results in

$$E = \frac{\rho_a \kappa^2 \bar{u}_z (\bar{q}_s - \bar{q}_z)}{[\ell n(z/z_o) - \Psi_M][\ell n(z/z_w) - \Psi_W]} \tag{2.30}$$

This is similar to equation (2.8) except for the modification for buoyancy effects as represented by Ψ_M and Ψ_W.

Until now nothing has been said about the universal functions Φ_M and Φ_W except that they are functions of z/L. Many empirical forms exist in the literature [Dyer and Hicks (1970), Businger et al. (1971) and others] and experimental evidence is available to support many of them. Differences between evaporation equations which correct for buoyancy influences on forced convection are usually in the form of Φ_M and Φ_W rather than the form of the equation (2.30). Figures 2.1 and 2.2 show experimental results by Businger et al. (1971) performed over a Kansas wheat field. Dyer (1974) criticised these results, which indicated $\kappa = 0.35$ instead of the commonly accepted 0.4, but the behavior of Φ_M and Φ_W is typical of all such data over land or water. It is sufficient for our purposes to say that the most successful representations for Φ_M and Φ_W are:

for stable conditions ($z/L > 0$)

$$\Phi_M = (1 + \gamma_1 \, z/L)$$
$$\Phi_W = (1 + \gamma_2 \, z/L)$$

for unstable conditions ($z/L < 0$)

$$\Phi_M = (1 - \gamma_3 \, z/L)^{-1/4}$$
$$\Phi_W = (1 - \gamma_4 \, z/L)^{-1/2}$$

where $\gamma_{1,2,3,4}$ are empirically determined constants [Dyer (1974)].

Other attempts have been made [Wunderlich (1972) and Resch and Silva (1979)] to parameterize buoyancy influences on forced convection using the bulk Richardson number:

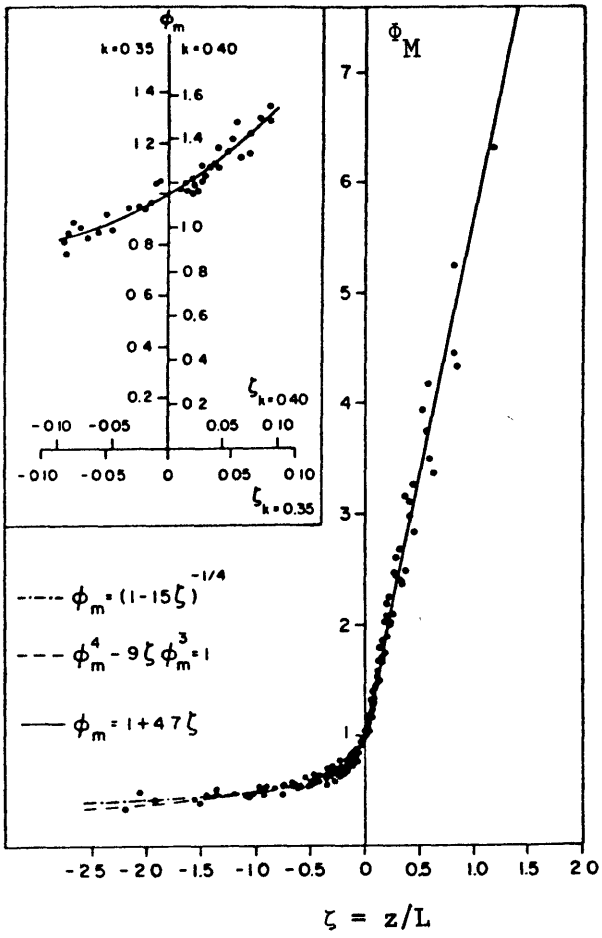

Figure 2.1: Φ_M vs. z/L. From Businger, et al., (1971) calculated with κ=0.35.

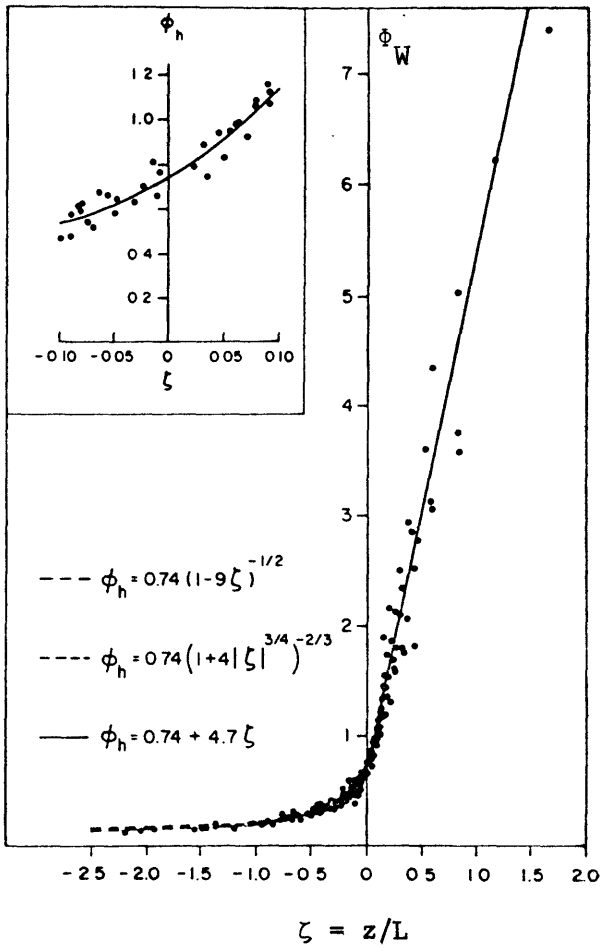

Figure 2.2: Φ_W vs. z/L. From Businger, et al., (1971) calculated with κ=0.35.

$$R_i = - \frac{\frac{g}{\rho}\frac{\partial \rho}{\partial z}}{\left(\frac{\partial \bar{u}}{\partial z}\right)^2} \qquad (2.31)$$

The bulk Richardson number indicates when hydrodynamic instability and breakdown to turbulence occurs in a stratified fluid rather than a relation between turbulent production (and thus transfer of heat and mass) and buoyancy influences in an already turbulent fluid. As such R_i is not as applicable as R_f or z/L for describing a process such as evaporation which is usually turbulent to begin with.

In summary,the approach described in this section in effect sets $a = 0$ and $b = b(z/L$, or possibly $R_i)$ rather than a constant in the empirical windspeed function, $f(W_z) = a + bW_z$. It is most applicable when measurements of the meteorological variables $\bar{u}_z$ and q_z are taken such that $|z/L| < 1$, in a region when forced convection is important.

2.1.2.2 Free Convection

Free convection is defined as the transfer of heat or mass (buoyancy) in the absence of any imposed velocity scale. The transfer is due primarily to buoyancy effects. For z/L negative and $|z/L) \gtrsim 1$ turbulence generated by buoyancy is equal in magnitude or larger than that generated by mean flow shear. In the limits of no mean flow $u_* \to 0$ and $L \to 0$ thus all transfer is by buoyant effects.

Since no velocity scale is imposed the relevant non-dimensional number for this situation is the Rayleigh number

$$R_a = \frac{\Delta b \ell^3}{\nu \alpha} \qquad (2.32)$$

where $\Delta b = g(\rho_a - \rho_s)/\rho_a$ is the buoyancy difference, ρ_s = air density near water surface, ρ_a = ambient air density, ℓ = length scale, ν = viscosity of air and α = molecular diffusivity of heat. The Rayleigh number is a ratio of buoyant forces to the molecular forces (diffusivities) which tend to stabilize the motion.

Shulyakovsky (1969) and later Ryan and Harleman (1973) made the analogy between a warm water surface and a heated flat plate to derive a free convection contribution to evaporation. If a flat plate is heated uniformly at the bottom of a semi-infinite fluid it can be shown from dimensional reasoning that the heat transfer rate as represented by the Nusselt number, Nu, is proportional to the Rayleigh number to some power

$$Nu \propto R_a^c$$

where $Nu = \phi_c \ell/(\rho_a c_{p_a} \alpha)\Delta T$, $\Delta T = T_s - T_a$, and c = constant. In the field when the free convection is turbulent c = 1/3 in order to eliminate any dependence on the length scale ℓ [Turner (1973), p. 213]

$$\frac{\phi_c \ell}{(\rho_a c_{p_a} \alpha)\Delta T} \propto \left(\frac{g\beta\Delta T \ell^3}{\nu\alpha}\right)^{1/3}$$

or

$$\phi_c = 0.14\ (\rho_a c_{p_a} \alpha)\left(\frac{g\beta\Delta T}{\nu\alpha}\right)^{1/3} \Delta T \qquad (2.33)$$

using an empirical proportionality constant of 0.14 suggested by Ryan and Harleman (1973).

To use this result for evaporation from a water surface we first rewrite equation (2.33) in a standard heat transfer coefficient form

$$\phi_c = h_c \Delta T$$

where

$$h_c = 0.14\ (\rho_a c_{p_a} \alpha)\left(\frac{g\beta\Delta T}{\nu\alpha}\right)^{1/3} \qquad (2.34)$$

Note that the heat transfer coefficient depends on the temperature difference from the plate to the ambient fluid. Similarly a transfer coefficient for evaporation h_e can be defined

$$\phi_e = \frac{Lh_e}{c_{p_a}} (q_s - q_a)$$

Assuming $h_c = h_e$ and using $q = 0.622\ e/p_a$ one gets

$$\phi_e = \frac{0.622\ L}{p_a\ c_{p_a}} h_c (e_s - e_a) \qquad (2.35)$$

The assumption of $h_c = h_e$ is equivalent to assuming that the turbulent eddy diffusivities K_H and K_W in equation (2.2a and b) are equal. Monin and Yaglon (1971) state that all empirical evidence indicates this equality is valid for neutral and unstable situations.

Using equation (2.34) equation (2.35) becomes

$$\phi_e = A\ \Delta T^{1/3}\ (e_s - e_a) \qquad (2.36)$$

where

$$A = \frac{0.622\ L}{P_a} (0.14)(c_{p_a} \rho_a\ \alpha)\left(\frac{\beta g}{\nu\alpha}\right)^{1/3}$$

and is a constant if average conditions are used to evalaute all the terms. The transfer coefficient $A\ \Delta T^{1/3}$ takes into account the buoyancy

effect induced by temperature differences. In general we might write it as

$$A'(\Delta b)^{1/3}$$

where A' is a constant and Δb is the buoyancy difference defined before. Now over a water surface both temperature and water vapor influence the density. To capture this effect Ryan and Harleman (1973) used $\Delta\theta_V = \theta_{V_s} - \theta_{V_a}$ instead of $\Delta T = T_s - T_a$ where θ_V is the virtual temperature

$$\theta_V = \frac{T}{(1-.378\ e/P_a)}$$

(T in absolute units). The virtual temperature is the temperature a dry parcel of air would have if it was at the same pressure and density of the moist air. The virtual temperature accounts for the buoyancy due to moisture and temperature. Thus equation (2.36) becomes

$$\phi_e = A(\Delta\theta_V)^{1/3}(e_s - e_a)$$

where A is defined before.

Goodling, Sill and McCabe (1976) use an anology between heat and mass transfer to derive

$$\phi_e \propto (\Delta e)^{1/3} \cdot \Delta e$$

The transfer coefficient is proportional to $\Delta e^{1/3}$ instead of $\Delta\theta_V{}^{1/3}$. Use of $\Delta\theta_V$ instead of Δe is more appropriate, however, because the mass transfer is due to buoyancy and $\Delta\theta_V$ captures the effect of both temperature and water vapor better than Δe.

Rimsha and Donchenko (1957) studied heat transfer from a thermally loaded stream and suggested that the free convection transfer coefficient, h_c, is directly proportional to ΔT. This does not have any theoretical basis like the $h_c \sim \Delta T^{1/3}$ relationship, but rather is entirely empirical. Another empirical attempt to capture the convection is just the constant "a" in $f(W_z) = a + bW_z$. For $W_z = 0$ evaporation will continue, the transfer coefficient "a" is a constant as opposed to some dependence on buoyancy.

All the above discussion is for a situation where $u_* = 0$. In reality the wind is rarely still and the question then is how to use these results for free convection in conjunction with forced convection. Typically what is done is to linearly sum the free and forced convection contributions:

$$\phi_e = (a(\Delta\theta_v)^{1/3} + bW_z)(e_s - e_z) \tag{2.38}$$

where bW_z represents the forced convection contribution and b is an empirically determined constant. The constant a in $f(W_z) = a + bW_z$ has thus been made a function of stability.

Strictly speaking this approach is not correct. The processes of free and forced convection are not independent but are related. This relationship is best given by z/L. In the extremes of $(z/L) \to \infty$ and $z/L \to 0$ free and forced convection become independent because the other process ceases to be important but for most cases they are both occurring. The wind causes forced convection which may be augmented by buoyancy considerations and the extreme temperature differences between air and water make buoyant free convection an important process.

2.1.2.3 Summary of Free and Forced Convection

The decision as to which is the best approach to compute evaporation (as represented by equation (2.30) and equation (2.38)) depends primarily on the measurement of the meteorological variables. Suppose that the water surface temperature is uniform but elevated over the ambient air temperature such that the boundary layer is unstable. If measurements of the meteorological conditions at a height z are available within the developed boundary layer [Hicks et al. (1977)] near enough to the water surface where $|z/L| < 1$ the forced convection approach, equation (2.30), is probably best. The meteorological variables are from a region where forced convection dominates. If the meteorological variables are measured outside the boundary layer, say at the pond edge or some nearby weather station (this is usually the case), the free convection correction, equation (2.38), or the empirical wind speed function $f(W_z) = a + bW_z$ is probably more applicable since measurements of the ambient conditions, say θ_{V_a}, are assumed in the development of equations similar in form to equation (2.38), although the forced part of equation (2.38) is often derived (or calibrated) from local windspeed measurements.

2.1.3 Fetch Dependence

Several investigators [Harbeck (1962), Goodling, Sill and McCabe (1976) and Resch and Selva (1979)] have shown both theoretically and experimentally that the evaporation rate, when averaged over the fetch length, decreases as the fetch increases. Cooling impoundments are of various sizes and shapes. Examples range from cooling lakes formed by

damming streams which tend to be irregular in shape, possibly with long side arms, and may have a surface area of 10^6 to 10^7 m^2, to small precooler or hotponds which are regular in shape with a surface area an order of magnitude less. As a result fetch dependence could be an important factor governing cooling pond evaporation.

A physical interpretation of this decrease in average evaporation with increased fetch is the water vapor discontinuity at the leading edge of the vapor boundary layer. See Figure 2.3. The discontinuity causes a larger vertical gradient in specific humidity (or vapor pressure) and thus higher evaporation at the upwind edge. Eventually, as the discontinuity is smoothed out by vapor boundary layer growth, a relatively uniform value of evaporation will result.

Experiments and theory imply $E \sim \ell^{-n}$, where ℓ is the fetch length and n is a constant. Several correlations of E vs. ℓ have been made and are summarized in Table 2.1. Data consists of both laboratory ($\ell \sim 0(10\ m)$) and field ($\ell \sim 0(1000\ m)$) measurements. Dependencies range from $n = 0.1$ to $n = 0.2$, with most being close to 0.1. Wengefeld and Plate (1977) using laboratory data showed some results outside of this range and also a dependence of n on windspeed.

The laboratory data were from wind-wave tanks on the order of 10 m long and the field data were from lakes varying from several acres area to several thousand acres. Evaporation pans are about 1-2 m in diameter (class A pans) and as such are even smaller than the laboratory situations. The pans usually overestimate lake evaporation. Lake evaporation ranges from 50 to 80% of the pan evaporation. This is not the same as the above dependencies would predict. The fetch of an impoundment is

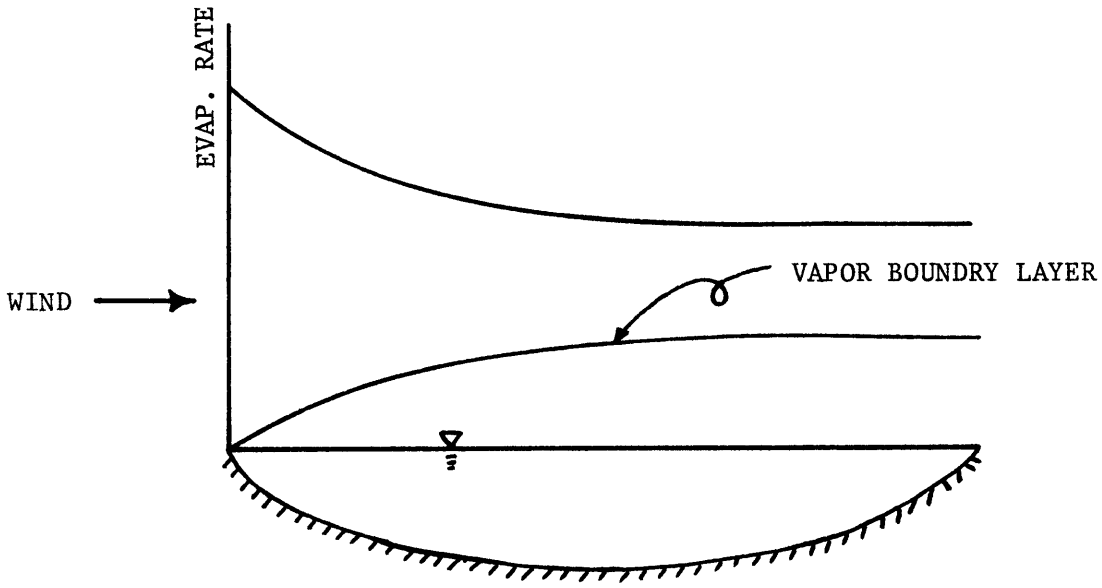

Figure 2.3: Evaporation vs. Fetch.

typically three or four orders of magnitude larger than that of a pan. For n = 0.1: $E(\ell = 10^3)/(E(\ell = 1) \approx 0.50$ and $E(\ell = 10^4)/(E\ell = 1) \approx 0.4$. The order of magnitude of the reduction of average evaporation from pan to lake is correct, but it is not the same as field measurements. This is most likely due to differences between pans and the laboratory experiments which are usually conducted in well controlled wind-wave facilities. Effects of the pan lip are not present in the laboratory experiments. Additionally the lab experiments are more dynamically similar to lakes. In both a boundary layer over the water must develop from the leading edge. The pans, on the other hand, are placed out in the open and are so small in comparison with the scale of the local boundary layer, that they do not cause any appreciable change in the boundary layer.

The result, n = 0.2, of Goodling, Sill and McCabe (1976) is deduced if one considers the water surface as a flat heated plate which is placed in a turbulent free stream flow so that the plate is parallel to the flow direction. McAdams (1954) gives

$$N_u \propto R_e^{0.8}$$

where $R_e = \frac{u_\infty \ell}{\nu}$ and u_∞ = free stream velocity, ℓ = plate length and ν = viscosity. Rearrangement gives

$$\phi_c \propto \frac{u_\infty \Delta T}{R_e^{0.2}}$$

The heat transfer is proportional to $\ell^{-0.2}$. Assumed similarity between heat and mass transfer gives $E \sim \ell^{-0.2}$. The above situation has air

flowing undisturbed which encounters a plate. A boundary layer must develop and the air speed near the plate slows down from its free stream (prior to plate) speed. In reality the air speeds up as it passes from land (where a boundary layer is already present) to water because of a drop in surface roughness. Thus the $E \sim \ell^{-0.2}$ result is questionable when applied to inpoundment evaporation.

Table 2.1: $E \sim \ell^{-n}$

Reference	n	Comments
Goodling, Sill and McCabe (1976)	0.2	semi-theoretical development
Wengefeld and Plate (1977)	0.13	laboratory and field data, $\ell = \sqrt{A}$
Gloyne (1971)	0.12 0.11	circular areas rectangular strips
Resch and Selva (1979)	0.1	laboratory data
Harbeck (1962)	0.1	field data from lakes and reservoirs, $\ell = \sqrt{A}$, A = water surface area

Incorporation of the fetch parameter for cooling impoundments poses some difficulty due to 1) large water surface temperature gradients and 2) the often irregular shape of cooling impoundments. Because of (1) the vapor boundary layer may constantly change characteristics with fetch. Given a specific wind direction (2) may result in different fetch lengths to be appropriate depending on location within the impoundment. Additionally the variability of wind direction also causes changes in appropriate fetch length.

One might also note that fetch effects, on weakly theoretical grounds, should be confined to the forced convection contribution (e.g., b in $f(W) = a + bW_z$). The free convection has no implied length scale as long as the situation is turbulent (see Section 2.1.2.2) and thus should not be affected by the impoundment size.

In this study several equations which depended on fetch were examined (see Section 2.4) to help determine if incorporation of this parameter improved evaporation estimates. To avoid problems associated with (2) above the fetch length was set equal to $A^{1/2}$.

2.1.4 Summary of Theory

Additional influences on evaporation such as wave height and spray (wave breaking) might in some cases (e.g., high wind speeds) become important [Mangarella et al. (1971)]. It is felt, however, that for cooling impoundments stability and fetch are more important. In summary, evaporation equations pertaining to heated water bodies might be of the form

$$E = E(W, T_s, T_a, \text{relative humidity, stability, fetch})$$

2.2 Empirical Equations

Presently, over 100 evaporation equations of various types have been identified. A complete listing of these equations would not be useful as many are slight variations of each other (i.e., they have different values of a and b in $f(W_z)$). For partial listings see Paily, Macagno and Kennedy (1974), Ryan and Harleman (1973) and Wunderlich (1972).

Based upon functional representation, usually the form of $f(W_z)$, it is possible to group the equations under several headings. Candidate groupings could include: type of data by which the equations were calibrated, whether or not they were for heated water bodies, etc. For the present purposes the equations were grouped into one of three categories: Dalton Law, Modified Dalton Law and Stability Dependent equations. A category for fetch dependence was also possible, but not chosen as an independent category.

2.2.1 Dalton Law Equations

These equations are of the form

$$E = (a + bW_z)(e_s - e_z)$$

where E = evaporative mass loss rate, a and b are empirically determined constants, e_s = saturation vapor pressure at water surface temperature, e_z = vapor pressure of the air at a given measurements height, W_z = wind speed at a given measurement height. This is the simplest and most common type of equation. Differences between equations in this group come in the values of a and b and vary significantly in the specified location and height of meteorological measurements.

2.2.2 Modified Dalton Law Equations

These are similar in appearance to the Dalton Law equations except that some dependence is added or changed. For example

$$E = (a + bW_z + cW_z^2)(e_s - e_z)$$

where c is another empirically determined constant. For c = 0 this equation reverts to the Dalton Law category. Another example is a set of equations that have the form

$$E = (a + bW_z)(e_s - e_z)^d$$

where d is some empirically determined constant.

2.2.3 Stability Dependent Equations

In this category are equations similar to the forced convection correction equation (2.30) where b = b(stability) or free convection equation (2.38) where a = a(stability). Again more differences come in measurement location and height.

2.3 Measurement Location of Meteorological Variables

As mentioned above one of the primary differences between evaporation equations concerns the location of measurements of relevant meteorological variables. Typically measurements are taken over the waterbody (on-pond) or adjacent to the water body (edge or off-pond). Sometimes no local data are available and remote (e.g., nearest NWS station) data must be used. This is a typical situation in cooling pond design. Another facet of the location question is the height at which the variables are measured. Evaporation equations typically employ finite difference approximations to compute the wind speed and vapor pressure gradients. The measurement height affects the computed gradient. Problems generally arise when an equation calibrated with a specific type of data (location and height), must be used with another type. The result will be an error in predicted evaporation.

Correction or translation of the data from one location and/or height to another is possible but is difficult to do with certainty. Figure 2.4 illustrates, in an idealized situation, some of the problems which arise in translating data. Location 1 is over land where the vapor pressure of the air e_{a_o} is assumed to be uniform with height (no evapotranspiration is occurring over the land). The boundary layer velocity profile is assumed to be longitudinally uniform and steady (i.e., established). Location 2 is over the upwind portion of the waterbody. The wind speed and vapor pressure at a given height (indicated by horizontal dashed line) have increased over the off-pond values. The wind has sped up because of an abrupt decrease in surface roughness z_o from land to water [Fraedrich (1971)] and the vapor pressure has increased because of the evaporation which is occuring over the water body. Further along the flow path at location 3 the vapor pressure at the specified height has increased still further as the vapor boundary layer develops. The windspeed may also increase as the velocity boundary layer develops. If at location 3 the boundary layers for both specific humidity and velocity are sufficiently developed so that the boundary layers are now approximately uniform, measurements at location 4 down the flow path from 3 would show little or no change.

Even from this idealized situation shown in Figure 2.4 it is obvious that on-pond data are dependent on both measurement height and position along the flow path. Pond surface shape, sheltering effects due to trees, terrain or buildings and changing wind directions

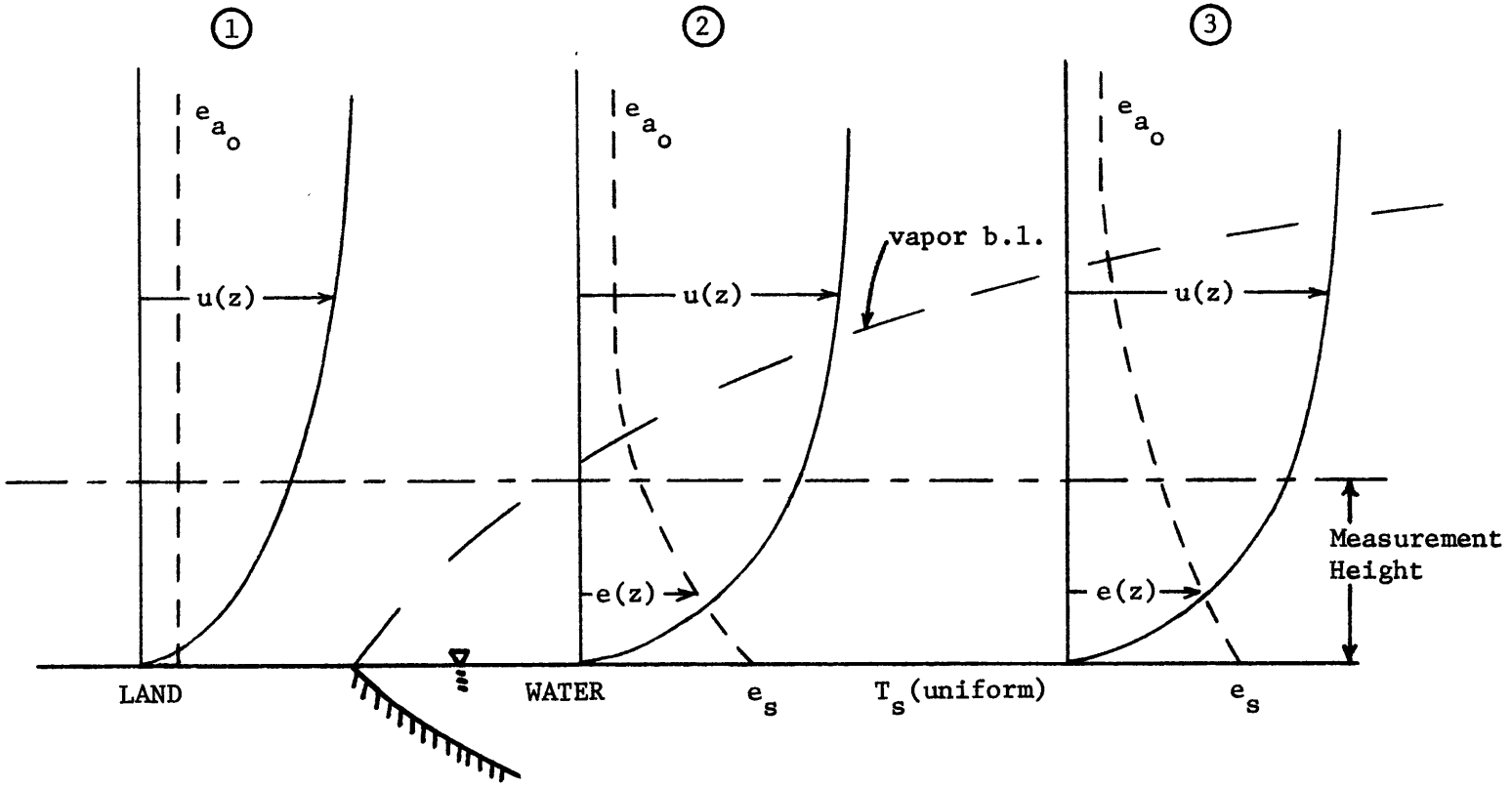

Figure 2.4: Change in Vapor Pressure and Wind Speed Profiles With Location.

complicate the situation. Off-pond data are also dependent on the pond shape and wind direction. If the met station is upwind of the pond, ambient conditions are measured. If it is downwind met conditions in the cooling pond plume are measured.

Translation of measurement height is the most common correction. Ryan and Harleman (1973) give

$$\frac{W_1}{W_2} = \frac{\ell n \frac{z_2}{z_o}}{\ell n \frac{z_1}{z_2}} \tag{2.39}$$

where W_1 = wind speed at height z_1, W_2 = wind speed at height z_2 and z_o = roughness height. Errors in using this relation occur because 1) it is derived based upon a neutral boundary layer 2) it requires specification of the roughness height z_o and 3) measurement of W_1 at one horizontal location to calculate W_2 at another location is not correct.

For a non-neutral atmosphere equation (2.39) should strictly be replaced, using equation (2.26), by

$$\frac{W_1}{W_2} = \frac{[\ell n(z_1/z_o) - \Psi_M(z_1/L)]}{[\ell n(z_2/z_o) - \Psi_M(z_2/L)]} \tag{2.40}$$

To illustrate the magnitude of error consider a case where z_1 = 10 m and z_2 = 2 m. As an estimate we will choose z_o = 0.0003 m (see below for typical values). A value of the Monin-Obukov length of L = -5 m is typical of unstable conditions over a cooling pond and $\Psi_M(z/L)$ will be computed following Hick's et al. (1977). Thus according to equation

(2.39) $W_1/W_2 = 1.18$ and from equation (2.40) $W_1/W_2 = 1.11$; an error of above 6% is incurred if the 2 m wind speed is estimated using equation (2.39). In view of the fact that measurement errors are likely to be as large as this and that a priori information on L is not usually available equation (2.39) should be adequate for most engineering work.

The roughness height z_o is important and should be specified correctly. Studies at Lake Hefner by Kohler (1954) found that over water $z_o = 0.0046$ m to 0.009 m. Lake Mead [Harbeck et al. (1958)] studies reported $z_o = 0.00015$ m, an order of magnitude less. The average wind speed at Lake Hefner was almost twice that experienced at Lake Mead; thus surface wave action may be the cause of the larger z_o values reported at Lake Hefner. Hicks et al. (1977) suggest, based on dimensional reasoning, that

$$z_o = \alpha u_*^2/g$$

where $\alpha = 0.008$ was determined from field measurements over Dresden cooling pond. Increased windspeed causes z_o to increase. Ryan and Harleman (1973) chose $z_o = 0.001$ m for wind speeds less than 2.25 m/s and $z_o = 0.005$ m for higher windspeeds. These are about an order of magnitude higher than suggested by the above equation. The order of error involved with an incorrect estimate of z_o is illustrated by using equation (2.39) assuming $z_o = 0.001$ m or $z_o = 0.0001$ m. Let $z_1 = 10$ m and $z_2 = 2$ m and assume that W_1 is the same for both cases; thus $(W_2|_{z_o = 0.001})/(W_2|_{z = 0.0001}) = 1.04$. Again considering possible measurement error this is small. For this study z_o values suggested by Ryan and Harleman were used.

A large potential error is encountered when measurements at one height z_1 and one location are translated to another height z_2 and location. Because of the decrease in surface roughness, z_o, from land to water the windspeed throughout the lower boundary layer can be expected to increase. Davenport (1967) says an increase up to about a factor of 2 is possible on large lakes. For cooling ponds this speedup is likely to be less, but no general correlation exists because of site specific parameters such as local topography, local ground cover, pond shape and changing wind directions. Use of off-pond windspeeds where on-pond values are needed for an empirical evaporation equation will probably result in an under-prediction of evaporation.

Vapor pressure may also be translated from one height to another by

$$\frac{e_1-e_s}{e_2-e_s} = \frac{\ell n\ z_1/z_W}{\ell n\ z_2/z_W} \tag{2.41}$$

where e_1 = vapor pressure at height z_1, e_2 = vapor pressure at height z_2, e_s = saturated vapor pressure at water surface and z_W = "roughness" height for water vapor. The same three sources of error--non-neutral boundary layer, incorrect specification of z_W and location translation that applied to windspeeds are relevant here. Stability aspects will give about the same error as illustrated for windspeeds and the same is true for an order of magnitude change in z_W. $z_W \simeq 0.000061$ m from the Lake Hefner study and $z_W \simeq 0.000003$ m from Lake Mead. Hicks et al. (1977) suggests $z_W \simeq D_W/\kappa u_*$ where D_W is the molecular diffusivity of water vapor. This formula gives results about the same as the Lake

Hefner and Lake Mead studies. A value of $z_w = 0.000061$ m was used when necessary in this study. Errors in translation from one location to another may be large because of the evolution of the water vapor boundary layer illustrated in Figure 2.4.

Use of an evaporation equation developed for on-pond data with off-pond data may involve some compensating errors because $W_{on} > W_{off}$ and $(e_s - e_{on}) < (e_s - e_{off})$. Just how much compensation is involved depends on the form of the evaporation equation and the measurement height of the variables. The higher the measurement height the less difference between on-pond and off-pond measurements. Evaporation equations of the form $f(W_z) = a + bW_z$ will not see any compensation in the $a(e_s - e_a)$ contribution because only the vapor pressure difference is involved.

Further field study on the errors associated with measurement location and height is necessary. Some of the error and certainly some of the differences between empirical evaporation equations could be reduced if a standard or preferred location is used consistently. The choices are essentially off-pond, but not a remote station, or on-pond. The former would have essentially undisturbed measurements of wind and vapor pressure (i.e., ambient air) and the latter would have conditions typical of those over the water surface. Of course, only off-pond data will exist prior to construction of a pond.

2.4 Evaporation Equations to be Tested

Ten equations, representing all three categories were selected in order to examine the variability of predicted evaporation from heated

water bodies. Table 2.2 lists these equations along with references and comments. Information most pertinent to this investigation includes whether or not a particular equation was developed for use on heated water bodies, what data if any it was originally calibrated with and what type of data (location, etc.) is needed to use the equation properly.

2.4.1 Lake Hefner Equation

Evaporation estimates by both bulk energy and water budgets from Lake Hefner, Oklahoma--an unheated lake of 2537 acres area surface area--were used to calibrate the Lake Hefner (denoted LH) equation [Kohler (1954)]

$$\text{English Units} \quad \phi_e = 17\, W_2\, (e_s - e_2)$$
$$\text{Metric Units} \quad \phi_e = 3.75\, W_2\, (e_s - e_2) \tag{2.42}$$

where the subscript 2 signifies a 2 meter measurement height. For this and all appropriate following equations the units are

English units: ϕ_e - BTU/ft^2-day

W - mph

e - mmHg

T - ^oF

A - acres

Table 2.2: Evaporation Equations

Name and Ref.	Equation*	Units	Calibration or Testing	Location of Met Variables	Comment
Lake Hefner (LH) [19]	$17W_2(e_s-e_2)$	BTU/ft^2-day mph mmHg	natural lakes	bulk of pond measurements at 2 meters height	Dalton Law
Ryan-Harleman (RH) [55]	$(22.4(\Delta\theta_v)^{1/3} + 14W_2)(e_s-e_2)$	BTU/ft^2-day mph mmHg	heated impoundments	bulk of pond measurements at 2 meters height	stability dependent
Rimsha-Donchenko (RD) [53]	$(61+1.47\Delta\theta+13.3W_2)(e_s-e_2)$	BTU/ft^2-day mph mmHg	thermally loaded streams	bulk of pond measurements at 2 meters height	stability dependent
Brady, Graves and Geyer (BGG) [4]	$(70+W_2^2)(e_s-e_2)$	BTU/ft^2-day mph mmHg	heated impoundments	bulk of pond measurements at 2 meters height	Modified Dalton Law
Harbeck (H) [22]	$\frac{24.2W_2}{A^{0.5}}(e_s-e_2)$	BTU/ft^2-day mph mmHg acres	natural lakes	bulk of pond measurements at 2 meters height	Dalton Law fetch dependence
Goodling, Sill and McCabe (GSM) [17]	$(25.1(\Delta e)^{1/3}+\frac{690W_z}{R_L^{0.2}})(e_s-e_2)$	BTU/ft^2-day mph mmHg	none	bulk of pond measurements at 2 meters height average fetch length	stability and fetch dependent
Weisman (W) [63]	$a(\frac{x_o}{z_o})^{-n} u_*(e_s-e_2)$	see ref.	none	Same as above	stability and fetch dependent
Argonne (ARG) [25]	$\frac{K^2W(q_s-q_a)}{(\ln(z/z_w)-\psi_m)(\ln(z/z_o)-\psi_m)}$	see ref.	heated impoundments	local boundary layer measurements for all variables. This study used bulk measurements at 2 meters.	stability dependent
Meyer (M) [39]	$(80+10W_2)(e_s-e_2)$	BTU/ft^2-day mph mmHg	natural lakes	bulk of pond measurements at 2 meters height	Dalton Law
Throne (T) [58]	$(67+17W_2)(e_s-e_2)$	BTU mph mmHg	heated impoundments	Same as above	Dalton Law

*see references for complete definition of variables

Metric units: ϕ_e - Watts/m^2 (W/m^2)

W - m/s

e - mbar

T - ^oC

A - hectare

This equation was originally calibrated with on-lake data from 8 meters measurement height and then correlated with measurements at 2 meters to give its present form. Although originally calibrated with on-lake data it has been used extensively with off-pond and remote data. The success of this simple equation may be due partially to the compensating errors of measurement location mentioned in Section 2.3.

2.4.2 Meyer Equation

The second Dalton Law equation tested was the Meyer (1942) equation (denoted M):

English units: $\phi_e = (80 + 10\ W_2)(e_s - e_2)$

Metric units: $\phi_e = (7.9 + 2.2\ W_2)(e_s - e_2)$ (2.43)

It was originally developed for unheated small lakes and reservoirs. Originally calibrated for meteorological measurements at 25 ft it was adjusted for measurements at 2 meters using equations (2.39) and (2.41) by Ryan and Harleman (1973).

2.4.3 Throne Equation

The only Dalton Law equation tested which was developed for heated water-bodies is the Throne equation [Throne (1951)]:

$$\text{English units:} \quad \phi_e = (67 + 17\ W_2)(e_s - e_2)$$

$$\text{Metric units:} \quad \phi_e = (6.6 + 3.75\ W_2)(e_s - e_2) \tag{2.44}$$

Data analyzed was from a small (120-210 acres) heavily loaded cooling pond. The Throne equation stems from an equation developed by Rohwer (1931) and was originally calibrated with data measured at 5 ft. and later adjusted for 2 meter data by Ryan and Harleman (1973). Note that it is similar to the LH equation in that both have b = 17 BTU/ft^2-day-mmHg-mpg (3.75 W/m^2-mb-m/s). The Throne equation has the additional term a = 67 BTU/ft^2-day-mmHg (6.6 W/m^2-mbar) which could account for the buoyancy enhanced evaporation expected over a heavily loaded water surface.

2.4.4 Harbeck Equation

The Harbeck equation (denoted H) [Harbeck (1962)],

$$\text{English units:} \quad \phi_e = \frac{24.2\ W_2}{A^{0.05}}(e_s - e_2)$$

$$\text{Metric Units:} \quad \phi_e = \frac{5.82\ W_2}{A^{0.05}}(e_s - e_2) \tag{2.45}$$

where A is the surface area of the waterbody, similar to the LH equation except for modification for fetch effects. Data was from several unheated lakes and reservoirs and included the Lake Hefner and Lake Mead [Harbeck et al. (1958)] studies. The areas ranged from several acres to several thousands of acres.

2.4.5 Brady, Graves and Geyer Equation

Another Modified Dalton Law equation is the Brady, Graves and Geyer equation (denoted BGG) [Brady et al. (1969)]:

$$\text{English units:} \quad \phi_e = (70 + W_2^2)(e_s - e_2)$$

$$\text{Metric units:} \quad \phi_e = (6.9 + 0.49\, W_2^2)(e_s - e_2) \qquad (2.46)$$

It was calibrated with data from three moderately loaded ($\sim$ 0.4 MW_t/acre) cooling ponds located in Texas and Louisiana using weekly bulk energy balances to deduce evaporation. The data collection location at each lake was different with one being on the lake, another at a lake edge and the third taken about 2 miles away from the pond. Additionally all three used different measurement heights and no attempt to correct for this was undertaken. Ryan and Harleman (1973) assumed a windspeed measurement height of about 8 meters and adjusted the BGG equation for a 2 meter measurement height. This result is shown above. Note the squared dependence on the windspeed which is not predicted on theoretical grounds and is a product of the best fit calibration to the original data. The BGG equation has been used quite extensively in heat loss

studies from cooling impoundments and is generally considered to give low values of evaporation.

2.4.6 Rimsha-Donchenko Equation

Rimsha and Donchenko (1957) developed an equation (denoted RD) using data at a thermally loaded river during the winter which reflects the influence of free convection through the temperature difference, $\Delta\theta$, between the air and water surface:

$$\text{English units:} \quad \phi_e = (61 + 1.47\ \Delta\theta + 14\ W_2)(e_s - e_2)$$

$$\text{Metric units:} \quad \phi_e = (6.0 + 0.26\ \Delta\theta + 3.1\ W_2)(e_s - e_2) \qquad (2.47)$$

where $\Delta\theta = \theta_s - \theta_2$. Weeks et al. (1971) used this equation with good success to determine heat loss from thermally loaded streams in the winter.

2.4.7 Ryan-Harleman Equation

Using the theoretical analysis summarized in Section 2.1.2.2, Ryan and Harleman (1973) developed an equation (denoted RH) which accounts for free convection:

$$\text{English units:} \quad \phi_e = (22.4(\Delta\theta_V)^{1/3} + 14\ W_2)(e_s - e_2)$$

$$\text{Metric units:} \quad \phi_e = (2.6(\Delta\theta_V)^{1/3} + 3.1\ W_2)(e_s - e_2) \qquad (2.48)$$

where $\Delta\theta_V$ is the virtual temperature difference between the water surface and air at 2 meters height. Original calibration was done with three years of monthly averaged energy balance estimates of evaporation from

the Hazelwood cooling impoundment in Australia. Meteorological data were taken at a pond edge station. The wind speed was measured at 1 ft. and converted to 2 meters using equation (2.39). Laboratory experiments were also performed to test the free convection formulation. Additional verification was done with the data of Brady et al. (1969). Work by Hicks and Wesely (1975) has suggested that the wind speed function predicts too much evaporation and should be reduced by a factor of 15%.

2.4.8 Goodling-Sill-McCabe Equation

The Goodling, Sill and McCabe equation (denoted GSM) [Goodling et al. (1976)]:

$$\text{English units:} \quad \phi_e = (25.1(e_s-e_2)^{1/3} + \frac{690\ W_2}{R_L^{0.2}})(e_s-e_2)$$

$$\text{Metric units:} \quad \phi_e = (2.25(e_s-e_2)^{1/3} + \frac{152\ W_2}{R_L^{0.2}})(e_s-e_2) \qquad (2.49)$$

where $R_L = \frac{W_2 \ell}{\nu}$, ℓ is the fetch length and ν is the viscosity of air, is similar to the RH equation except free convection is parameterized slightly differently and fetch effects are included per Section 2.13. The forced convection term can be reduced to

$$690(\frac{\nu}{\ell})^{0.2}\ W_2^{0.8} \qquad \text{(English units)}$$

which is not linear with windspeed as is usually the case. The original derivation of this equation on theoretical grounds required the meteorological data be taken in the free stream (i.e., W_∞, e_∞)as opposed to

2 meters height. Since the atmospheric boundary layer is of order 100 m thick use of 2 meter wind heights seemed more reasonable. Use of 2 meter values instead of some higher data should cause an underprediction of evaporation if the equation is correct. No verification of this equation is given by Goodling et al.

2.4.9 Weisman Equation

Weisman (1975) and Weisman and Brutsaert (1973) developed an equation (denoted W) which is based upon a numerical solution to the momentum, water vapor and sensible heat transport equations. They attempted to retain the non-linear interaction between shear induced and buoyancy induced turbulence. The equation is

$$\phi_e = a u_* \left(\frac{x_o}{z_o}\right)^{-n} (q_s - q_a) \tag{2.50}$$

where u_* = friction velocity, x_o = fetch length, z_o = roughness height, q_s = specific humidity at water surface temperature, q_a = specific humidity of the air and a,n = coefficients which are functions of stability. The coefficients a and n are functions of

$$A_* = \frac{\kappa g z_o}{u_*^2} \frac{T_s - T_a}{T_a}$$

and

$$B_* = -\frac{\kappa g z_o}{u_*^2} (q_s - q_a)$$

where κ = van Karman's constant, T_s is the water surface temperature and T_a is the air temperature which account for the buoyancy influences.

No specific measurement heights are specified so 2 meter values were used in this study. No verification of the equation was undertaken by Weisman, but for hypothetical conditions computed evaporative heat flux was shown to be similar to that predicted by the RH equation.

2.4.10 Argonne National Laboratory Equation

The last equation tested (denoted ANL) is one developed by Hicks et al. (1975) at Argonne National Laboratory. It accounts for atmospheric stability and is identical to equation (2.30). The stability dependent functions Ψ_W and Ψ_M are given in the reference. This equation was developed for use with measurements of the meteorological variables within the vapor boundary layer above a cooling pond and is therefore a prediction of point evaporation. Unlike all the other equations presented, it is meant to be used with met measurements well within the vapor boundary layer. It was also developed to give a point estimate of evaporation. Our studies used the equation to give an areal average evaporation. However, for the purposes of comparison of different equations under typical engineering situations the equation was used in this fashion. Verification of this equation was done using eddy flux measurements of point evaporation from Dresden cooling pond in Illinois. Agreement was excellent and Hicks and Wesely (1975) subsequently used this equation to generate synthetic evaporation rates against which to compare various empirical evaporation equations.

CHAPTER 3

HYDROTHERMAL MODELING

3.1 Methods of Measuring Evaporation

In order to understand the role of hydrothermal modeling in computing evaporation from field data it is useful to discuss some of the evaporation measurement schemes which have been employed previously with differing amounts of success. Table 3.1 lists several of these schemes along with pertinent information and comments. It should be noted that most of these methods were developed and first applied to natural waterbodies. Application of these methods to heated waterbodies which show large temporal and spatial variability in water temperatures and therefore evaporation, offer some problems not encountered in earlier studies of natural lakes.

Energy Balance

Probably the most common approach is the bulk energy balance. The entire waterbody is considered as a control volume. All inflows and outflows of energy over a given time period, with the exception of evaporation and conduction (related by the Bowen Ratio), are measured or computed with sufficient accuracy evaporative heat flux over that time period can be calculated as the remainder in the energy balance. Specifically

$$\phi_e = \frac{-\Delta S + \phi_{sn} + \phi_{an} + \phi_{ad} - \phi_{br}}{(1 + R)} \qquad (3.1)$$

Table 3.1: Evaporation Measurement Schemes

Technique	Measurement Type	Scope	Time Scale	Advantages	Disadvantages
Energy Budget	Field and Analytical	Whole Pond	∿7 day (minimum for bulk technique)	1. With good measurements it is usually quite accurate (< 10% error) 2. Applies to whole lake 3. Use of the hydrothermal model enables the effects of the non-uniform surface temperature to be retained. 4. Use of the hydrothermal model allows equations to be verified using short time steps.	1. Relies on Bowen Ratio concept (Some question as to whether it applies under highly unstable conditions.) 2. If analytical relationships for radiation terms are used (primarily atmospheric long wave) accuracy may be compromised. 3. If bulk technique is used equations developed from the results are limited to use with a time scale near that of calibration.
Water Balance	Field	Whole Pond	∿ monthly	1. Whole pond evaporation	1. Time scale problem with calibrated equations 2. Does not allow effect of non-uniform surface temperature to be investigated. 3. Several terms (i.e., groundwater loss, runoff) must be estimated or neglected, accuracy may therefore be compromised.

Table 3.1 Continued

Technique	Measurement Type	Scope	Time Scale	Advantages	Disadvantages
Vapor Budget	Field	Whole Lake	∿ 1 hour	1. Direct measurement of fluxes 2. Whole lake 3. Relatively short timescale	1. Shape of lake, temperature gradient and sonde location interactions must be considered. 2. Unsteady effects - the approach assumes no storage of vapor over the lake during time interval. Validity of this assumption is questionable. 3. Optical techniques for measuring water vapor are relatively new and untested.
Pan Measurement	Field	Single point extrapolated to whole	∿ day	1. Simple	1. Extrapolation of pan evaporation to pond is difficult due to scaling effects. 2. This method needs some site specific validation with one of the other methods. 3. For heated waterbodies the question of what temperature to keep the pan water must be answered. If the pan is immersed where should it be located?

Table 3.1 Continued

Technique	Measurement Type	Scope	Time Scale	Advantages	Disadvantages
Eddy correlation	Field	Point Measurement	∿ hourly	1. Measures flux directly 2. Time scale is more compatible w/use of desired equations	1. Gives only a point measurement 2. Instrumentation is expensive and sensitive.
Bulk Aerodynamic Technique	Field and Analytical	Point	Variable ∿ hour	1. Not a direct measurement of fluxes but potentially accurate results.	1. Question of relationship to use when atmosphere is unstable. 2. Detailed and precise measurements are necessary. 3. Gives only a point measurement.

where ϕ_e = evaporation heat loss, ΔS = change in stored energy, ϕ_{sn} = net incoming solar radiation, ϕ_{an} = net incoming atmospheric radiation, ϕ_{ad} = net advected energy, ϕ_{br} = back radiation and R = Bowen ratio. The above approach is termed the bulk energy balance and will give an average evaporation rate for the entire waterbody. This bulk approach has been used successfully to estimate evaporation on a weekly to monthly timescale. Examples include the USGS studies of Lake Hefner and Lake Mead [Kohler (1954) and Harbeck et al. (1958)]. An energy balance may also be computed using a hydrothermal model. By calibrating the evaporation component so that predicted and measured water temperatures agree, the model internally computes changes in the storage term and different evaporation rates over the water surface which are characteristic of heated impoundments. More on the use of hydrothermal models is discussed later in this chapter.

Water Balance

In a water balance approach, the water inflows, water outflows and changes in volume are measured over a period of time--typically monthly--in order to calculate a pond average evaporation as the remainder in

$$E = -\Delta V + (S_i - S_o) + P + R \pm G \qquad (3.2)$$

where E = evaporative volume loss, ΔV = lake water volume change, S_i = stream inflows, S_o = stream outflows, P = precipitation, R = overland runoff and G = groundwater inflow/outflows. Accurate estimation of evaporation on a short timescale (e.g., weekly-monthly) is very difficult due to large uncertainty in such terms as overland runoff and groundwater

flow. Winter (1981) gives an excellent discussion of the magnitudes of probable errors using this technique.

Vapor Budget

A method previously used for investigating water vapor plumes from cooling towers and ponds is a water vapor budget [West (1978)]. By measuring the flux of water vapor at the upstream end of a pond and at the downstream end the evaporation can be determined by the difference of the two. These measurements may be accomplished by ascending balloons which measure water vapor content and wind velocity with height and/or various optical techniques (e.g., Lidar/Raman scattering) which detect water vapor. Again a bulk or pond average evaporation is computed. Evaporation on a timescale of hours is computed but three dimensional effects and unsteady vapor storage over the pond are potential drawbacks to this technique.

Pan Measurement

Another technique is to place a carefully monitored pan in or near the cooling impoundment [Nystrom and Hecker (1975) and Moy and Sanghani (1977)]. It then can be easily monitored to obtain evaporation from the pan using an energy balance. This provides a local value of evaporation which then must be extrapolated to infer total pond evaporation. Due to edge and length scale effects evaporation from the pan and the pond are not equal and a relation between evaporation from the pan and waterbody is needed. While many empirical correlations (pan coefficients) have been suggested for natural waterbodies, this is not the case for heated impoundments so calibration under similar heat load conditions is necessary.

Eddy Correlation

Probably the most accurate measure of local (point) evaporation can be obtained with the eddy correlation method. In Chapter 2 evaporation was defined as

$$E = \rho_a \overline{w'q'} \tag{2.1}$$

Sensitive instruments are able to measure both w' and q', obtain their correlation,and thus compute this flux directly on a timescale of several minutes to an hour. Several such measurements may be necessary to evaluate total cooling impoundment evaporation.

Bulk Aerodynamic Profile

The bulk aerodynamic profile technique is a method often used by meteorologists and atmospheric scientists. It involves accurate measurement of $\partial\bar{u}/\partial z$ and $\partial\bar{q}/\partial z$ and analytical computation of evaporation with a relationship similar to equation (2.4). Alternatively,relationships such as equation (2.30) have been derived in order to calculate evaporation using boundary layer meteorological measurements and represent a type of aerodynamic approach. These techniques give evaporation on a timescale of an hour and produce estimates of evaporation at a point.

3.2 Need for Hydrothermal Models

Evaluation of evaporation formulae performance on cooling impoundments is more difficult than for natural water bodies. This is due primarily to the larger spatial and temporal variability in water temperatures caused by plant loading and complicated hydraulic characteristics.

Natural lakes by comparison exhibit less of these variabilities in water temperatures. For these reasons the bulk energy and water budget approaches often used in calibration/verification of evaporation equations are not very useful. The bulk approaches are typically used on time-scales longer ($\tilde{\sim}$ weekly at the shortest) than cooling impoundment fluctuations. Also the bulk approaches do not consider spatial variations in water surface temperatures and therefore evaporation. The point measurements such as eddy correlation can give information on spatial and temporal variability but logistics and economics limit their applicability to short term studies. Hydrothermal models, on the other hand, provide a useful tool for indirectly "measuring" evaporation and for calibrating formulae while taking into account temporal and spatial variability. A hydrothermal model performs these functions by means of an energy budget. Just as is done in bulk energy budgets solar, atmospheric and back radiation have to be measured or computed, conduction is estimated using the Bowen ratio and advective fluxes have to be measured. The hydrothermal model differs from a bulk budget in that storage term (water temperatures) are predicted on space and time scales that the bulk budget cannot accommodate. Predicted water temperatures, both in pond (storage term) and pond outflow (advected energy) are matched with measurements by adjusting the evaporative heat flux. Thus when the storage and outward advected energy terms match the measured values the evaporation must be correct to have a closed energy balance. Jobson (1975), Mitry and Sill (1978) and Octavio et al. (1980) give examples of hydrothermal models used for these goals. Additionally, these models are necessary to accurately predict future evaporation from cooling impoundments.

3.3 Types of Hydrothermal Models

With hydrothermal models it is possible, in principle, to define the thermal structure of a pond in up to three spatial dimensions and in time. A recent survey of such numerical models was performed by Pagenkopf and Fong (1980). Because of ponds' widely varying spatial and temporal structures, a general purpose cooling pond model must be 3-D and transient. However, except for short periods of computation (order of hours) computer costs for such models are prohibitive. And while short time steps (order of minutes or less) are necessary from a numerical point of view, it is doubtful that such short term output is of much physical significance since cooling ponds possess a certain thermal inertia which suppresses short term fluctuations. Time scales which are of the most physical significance are of the order of one day or longer. Furthermore, for assessing water consumption it is necessary to consider much longer time frames (order of 10 years) in order to capture seasonal and annual variability in meteorological and hydrological (e.g., make-up water supply) parameters.

At the other end of the spectrum, a number of simple, usually steady-state models exist [Edinger and Geyer (1965) and Littleton Research (1970)]. The plug flow and well-mixed type are the most common. While these are useful as preliminary design tools, they clearly shortcut consideration of many of the physically relevant characteristics of cooling ponds such as transient meteorology and station loading, or spatial detail associated with thermal stratification, circulation and mixing.

Clearly an intermediate level of sophistication is necessary - one which embodies the relevant spatial and temporal scales of interest and

meets computational efficiency objectives. For this study the model MITEMP [Octavio et al. (1980)] was chosen. It facilitates the modeling of cooling impoundments in a numerically one-dimensional framework yet at the same time preserves the essential spatial structure and transient response characteristic of a cooling impoundments. Use of the full non-linear surface heat transfer formulations is also possible.

3.4 Hydrothermal Structure Classification Scheme

Because of the wide variety of shapes, sizes and other features which define cooling impoundments it was necessary to develop a classification scheme which would bring out the important hydrothermal characteristics. This scheme was developed by Jirka et al. (1978) and depends upon three parameters:

1) thermal loading ϕ (MW_t/acre)
2) relative pond depth expressed by the pond number $\mathbb{P}$
3) horizontal aspect ratio, L/W

Thermal Loading

The thermal loading is defined as the amount of artificial heat put into the impoundment per unit of surface area. The artificial heat source is usually a point or local source such as a plant discharge. Thus the higher the thermal loading the more horizontal variability in water temperatures one should expect. The following distinction between natural impoundments and cooling ponds was proposed:

Natural Impoundment: $\phi < (0.1 \text{ to } 0.2) MW_t/\text{acre}$

Cooling Impoundment: $\phi > (0.1 \text{ to } 0.2) MW_t/\text{acre}$

In a cooling impoundment the artificial source causes significant horizontal temperature variability over the entire impoundment and the temperature distribution is determined by both natural and artificial heat loading. For low loadings (ϕ < 0.1 to 0.2 MW_t/acre) the horizontal variability is limited to the artificial source region and the temperature distribution is determined primarily by natural influences.

Pond Number

The pond number is defined as

$$\mathbb{P} = \left(\frac{f_i Q_o^2}{4\beta \Delta T_o g H^3 W^2} D_v^3 \frac{L}{H}\right)^{1/4} \tag{3.3}$$

where L = pond length along flow path, W = flow path width (W = A/L), A = pond surface area, Q_o = condenser flow rate, ΔT_o = condenser temperature rise, D_v = volumetric dilution produced by vertical entrance mixing, f_i = interfacial friction factor, β = coefficient of thermal expansion = $-\frac{1}{\rho}\frac{\partial \rho}{\partial T}$ and g = acceleration due to gravity. $\mathbb{P}$ is essentially the ratio of the heated surface layer h_s (of a deep lake) to the total pond depth H. h_s is the depth of heated water necessary to drive the condenser flow across the pond by gravitational convection against interfacial friction. It is derived (see Jirka et al. (1978)) assuming steady two layer flow with a linear horizontal density (temperature) gradient in the surface layer. The total depth is assumed to be large enough so that return flow in the lower layer has negligible velocity and that the lower layer is uniform in density. The density at the down-

stream end of the upper layer is also assumed to equal that in the lower layer.

Comparison with laboratory and field data showed for $\mathbb{P} \lesssim 0.3$ the above assumptions are valid and the computed pond number matches measured conditions. For $\mathbb{P} > 0.3$ the assumptions are no longer valid and significant horizontal stratification and flow velocities are present in the lower layer. In fact a distinct lower layer may no longer be present. In this situation the pond number can only be used in an empirical fashion to delineate vertical hydrothermal structure. Figure 3.1 emphasizes its usefulness in classifying the vertical structure of a cooling impoundment. At one extreme are the vertically fully mixed ponds ($\Delta T_v = 0$, $\mathbb{P} \geq 1$) and at the other are the ponds with a distinct surface layer ($\mathbb{P} \lesssim 0.3$). In the region $0.3 < \mathbb{P} < 1$ no distinct surface layer is evident and vertical temperature gradients may be important.

Horizontal Aspect Ratio

For shallow ponds ($\mathbb{P} \gtrsim 0.3$) the throughflow current is more important than the surface density currents which characterize the deep ponds. The horizontal aspect ratio L/W plays an important part in defining the flow structure. For L/W > 3 to 5 horizontal recirculation (large scale eddy formation) usually does not occur and the flow pattern is predominently dispersive in one horizontal direction (see Figure 3.4). When L/W < 3 to 5 large scale horizontal eddies take up a major portion of the pond area and horizontal recirculation becomes the most important flow characteristic (see Figure 3.5).

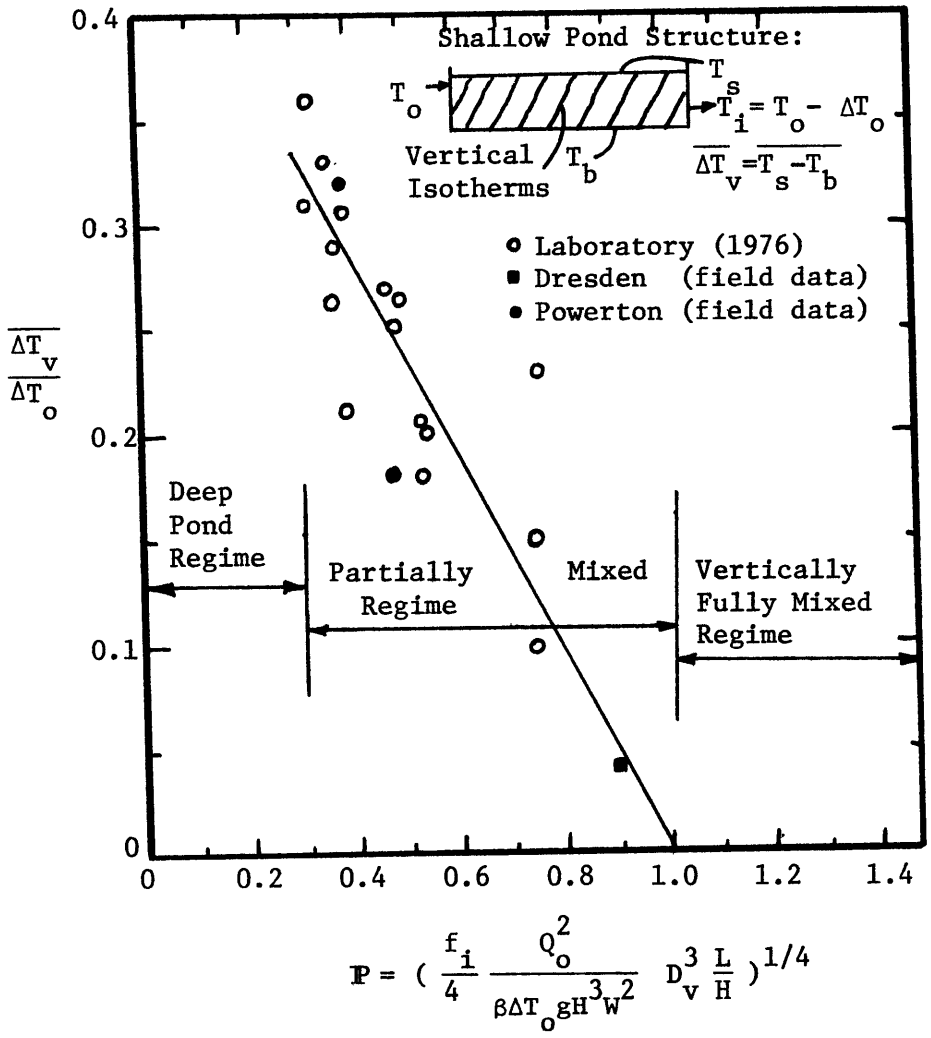

Figure 3.1: Relationship Between Pond Number, $\mathbb{P}$, and Vertical Temperature Gradient, $\overline{\Delta T_v}/\Delta T_o$.

3.5 Cooling Impoundment Model MITEMP

3.5.1 MITEMP Classification Scheme

Figure 3.2 shows the classification scheme upon which MITEMP is based and the role of the three parameters discussed in the previous section in defining the appropriate modeling technique. Four categories of pond structure are available. For this work on evaporation from cooling impoundments only the three pertaining to heat loaded conditions (ϕ > 0.1 to 0.2 MW_t/acre) are of interest. When $\mathbb{P}$ < 0.3 the impoundment is modeled as two layers with the Deep Stratified Cooling Pond Model which is shown schematically in Figure 3.3. When $\mathbb{P}$ > 0.3 there is usually no distinct two layer structure and the one layer or "shallow" cooling pond models are employed. For 0.3 < $\mathbb{P}$ < 0.5, however, the deep model may be used if individual situations indicate it applies. Further distinction between the shallow models is based upon the horizontal aspect ratio. If L/W > 3 to 5 the dispersive model is used and if L/W < 3 to 5 a recirculating model is used.

In terms of modeling complexity the Deep Stratified Model is first followed by the shallow recirculating model then the shallow dispersive model. Only the two one-layer models will be discussed because of their use in later calibration/verification studies of evaporation equations. Further details of all model formulations and example applications can be found in Jirka et al. (1978) and Octavio et al. (1980).

3.5.2 Shallow Cooling Pond Model with Longitudinal Dispersion

The shallow cooling pond with longitudinal dispersion ($\mathbb{P}$ > 0.3 and L/W > 3 to 5) is schematized in Figure 3.4. Representation of the

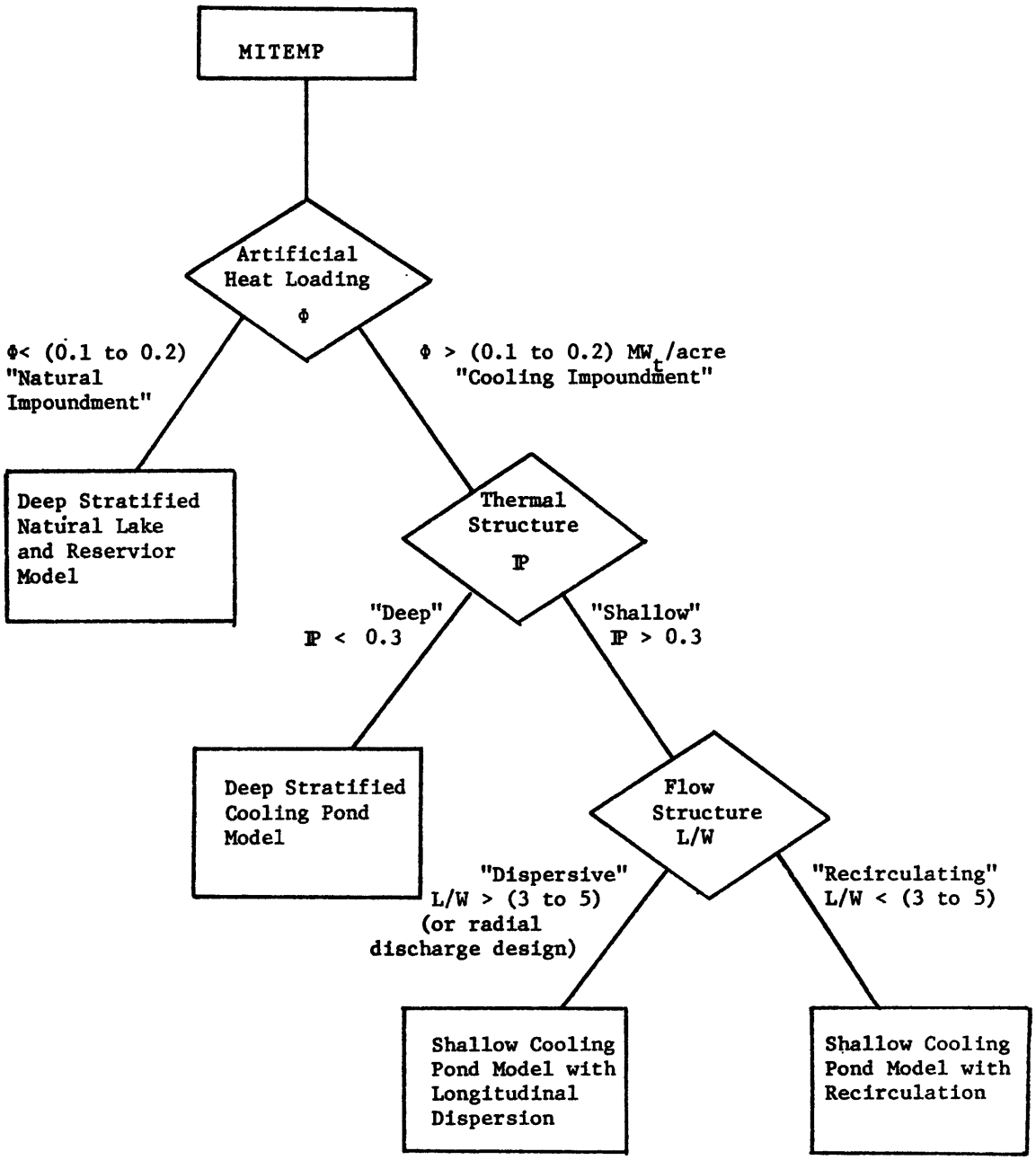

Figure 3.2: MITEMP Classification Scheme

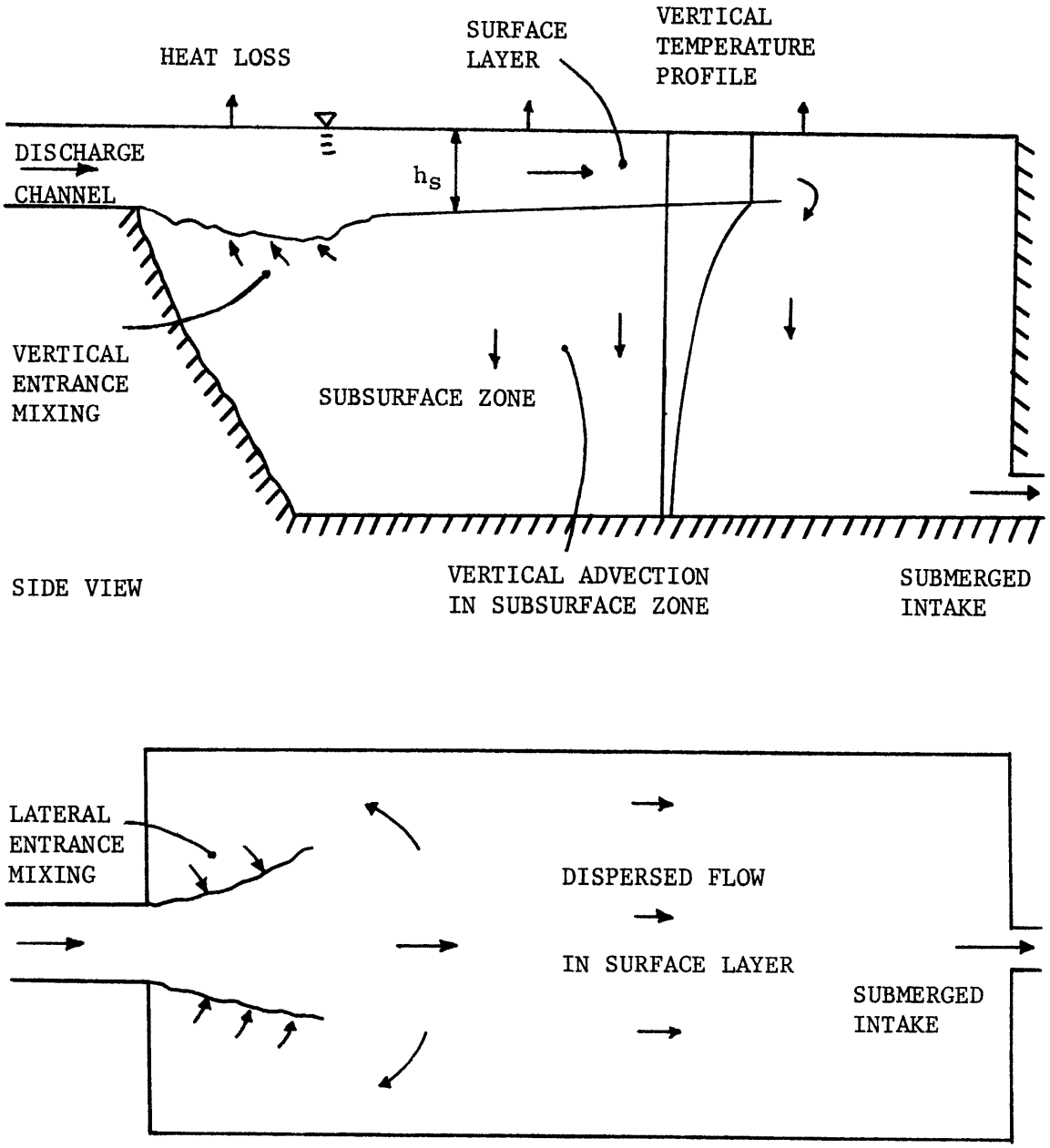

Figure 3.3: Schematic View of Deep Stratified Cooling Pond.

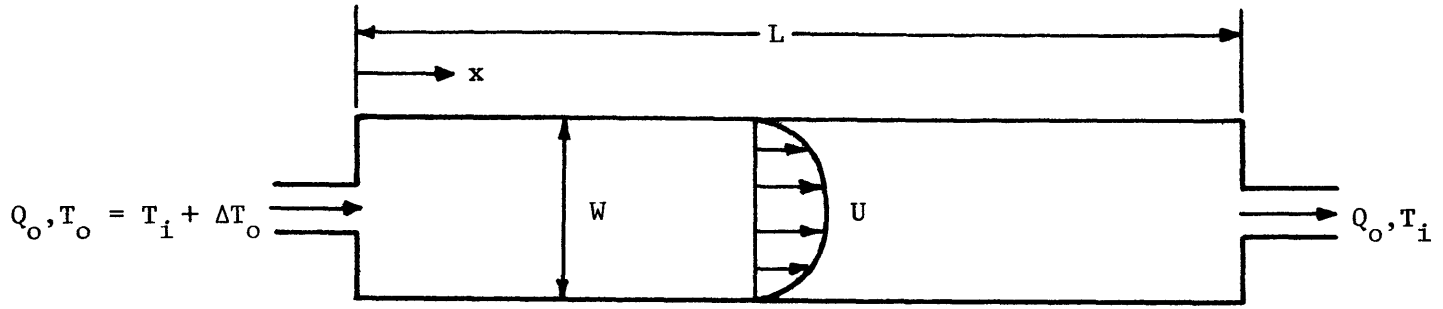

Figure 3.4: Plan View of Shallow Cooling Pond with Longitudinal Dispersion (Depth = H)

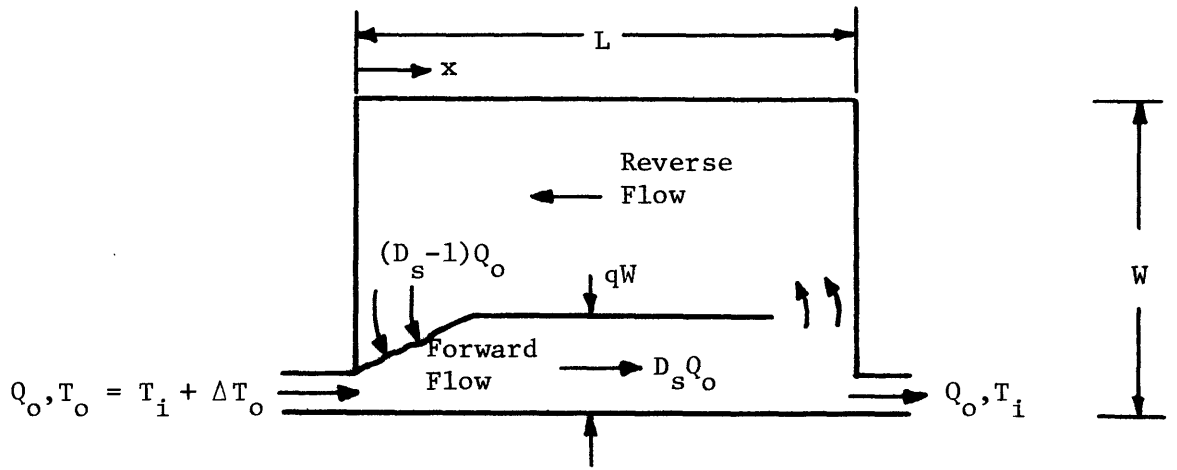

Figure 3.5: Plan View of Shallow Cooling Pond with Lateral Recirculation (Depth = H)

pond is given by the flow path length L, average depth H, average width W, flow rate Q_o and temperature rise across the plant condensers ΔT_o. For open cycle operation the inflow temperature $T_o(t)$ is specified. There is a jet entrance mixing region which is a small fraction of the total pond area such that the major through flow portion of the pond can be characterized by a regular longitudinal dispersion process. The governing equation for the pond temperatures is the one-dimensional bulk-dispersion equation:

$$\frac{\partial T(x,t)}{\partial t} + U \frac{\partial T(x,t)}{\partial x} = E_L \frac{\partial^2 T(x,t)}{\partial x^2} - \frac{\phi_n(x,t)}{\rho c H} \tag{3.4}$$

with boundary conditions

$$UT(0,t) - E_L \frac{\partial T}{\partial x}(0,t) = UT_o(t) \qquad \text{at } x = 0$$

and (3.5)

$$\frac{\partial T(L,t)}{\partial x} = 0 \qquad \text{at } x = L$$

where $T(x,t)$ = cross-sectionally averaged temperature, U = cross-sectionally averaged velocity Q_o/WH, x = longitudinal distance, t = time, $T_o(t)$ = inflow temperature, E_L = longitudinal dispersion coefficient, $\phi_n(x,t)$ = net surface heat transfer to the atmosphere comprised of net solar radiation, net atmospheric radiation, back radiation, evaporation and conduction (non-linear analysis), ρ = density of water and c = specific heat of water. The boundary conditions are specified to insure conservation of thermal energy. The main parameter required to describe the hydrothermal structure is the dispersion co-

efficient, which may be estimated approximately from Fischer's analysis [Jirka et al. (1978) and Fischer (1969)]

$$E_{L_F} = \frac{0.3\sqrt{f_o/8}\ U(\frac{W}{2})^2}{\kappa^2 H} \tag{3.6}$$

where κ is van Karman's constant and f_o is a bottom friction factor. Fine tuning of E_L in accordance with temperature measurements can be made to help eliminate uncertainty in predicted evaporation caused by incorrect modeling of the hydrothermal structure.

The equation is solved with an implicit numerical scheme and the model formulation allows the analysis of several compartments in series. Each compartment is treated individually according to equations (3.4) and (3.5) with inflow temperature $T_o(t)$ equal to the outflow temperature of the preceeding pond.

3.5.3 Shallow Cooling Pond Model with Lateral Recirculation

Shallow cooling ponds with low horizontal aspect ratios ($L/W < 3$ to 5) are characterized by a complex eddy flow pattern. The hydrothermal characteristics are shown in Figure 3.5 and are schematized by a forward (jet) zone and a return (entrainment or recirculating flow) zone. Additional variables of representation are the jet surface area function $q(\sim .25 - .4)$ and the lateral entrance dilution $D_s(> 1)$, which is assumed to be concentrated at the beginning of the jet zone. Each flow zone is governed by the same equation (3.4) and boundary conditions (3.5) as the longitudinally dispersive case although longitudinal dispersion is of secondary importance in view of the bulk recircula-

tion. Correct specification of D_s and q is necessary to reduce uncertainty in predicted temperature and therefore evaporation.

3.6 Vertical Temperature Gradients in Shallow Ponds

MITEMP, in order to capture relevant physical space and time scales and at the same time to be computationally efficient, models a cooling impoundment in a numerically 1-D framework. Given that all ponds exhibit at least some degree of three-dimensionality modeling in 1-D fashion does pose some shortcomings. In the cases of the shallow or one-layer ponds of interest in this work, vertical temperature gradients (i.e., incomplete vertical mixing) present the most trouble.

For $0.3 < \mathbb{P} < 1.0$ or impoundment was termed partially mixed (see Figure 3.1). The decision criteria for MITEMP says that when $\mathbb{P} > 0.3$ the shallow one-layer models should be used to predict impoundment temperatures. These models transport the depth-averaged temperature and as such disregard any vertical temperature structure. This is a serious drawback because it is the surface temperature, not the depth averaged temperature, which drives the evaporation conduction and back radiation. A first order correction to this problem is found using Figure 3.1. A pond average vertical temperature difference $\overline{\Delta T}_v/\Delta T_o$ can be found as a function of the pond number (solid line in Figure 3.1). Considering the vertical temperature gradient to be linear the basic heat transport equation (3.4) is not altered except that the net surface heat flux ϕ_n is evaluated at a temperature $\overline{\Delta T}_v/2$ above the depth-averaged temperature calculated by the model.

In reality the vertical temperature gradient usually exhibits some variation along the flow path. It is likely to be largest near the plant discharge and smallest near the plant intake. The above correction pond average $\overline{\Delta T}_v$ does not account for this and obviously some error could result. If the pond is modeled as one compartment no further correction, other than a pond average $\overline{\Delta T}_v$, can be made in the present model framework. For a pond that consists of several compartments in series it is possible to compute a pond number for each compartment and thus a $\overline{\Delta T}_v$ for each compartment. In initial design stages it is best just to compute a pond average $\overline{\Delta T}_v$. If field data is available it may be used to help decide the correct route to take.

CHAPTER 4

EMPIRICAL TESTING OF EVAPORATION EQUATIONS

4.1 Variability of Evaporation Equation Predictions

In Chapter II ten evaporation equations were introduced. The purpose in selecting such a group is to obtain a sample of different types of equations and investigate their applicability for predicting evaporation from heated water bodies. All three categories of evaporation equations - Dalton Law, Modified Dalton Law and Stability Dependent - are represented. A second motivation for examining these equations is to demonstrate the variability of their predictions. That the variability might be large is suspected both from the variety of forms of equations and from the differences in data sets (in terms of heat loading, climate, time period, etc.) used in calibrating or verifying them.

Variability of equations is illustrated in Figure 4.1 where the evaporative heat flux predicted by the different equations is plotted against several sets of water surface temperatures and atmospheric conditions which are realistic for cooling impoundments. Condition 3, which might be typical of a region near the plant discharge during a summer day, exhibits a large range of evaporative heat flux values - variations of about $\pm$ 40% from the mean. Condition 8, typical of late fall or early winter conditions, shows more consistency in predictions than the rest, yet variation is still about $\pm$ 20% from the mean value. Condition 5 represents the average of conditions during the 50-day period in September and October 1975 at Dresden Pond which will be discussed later in connection with model calibrations.

Symbol	Equation
1	LH
2	RH
3	RD
4	BGG
5	H
6	GSM
7	W
8	ARG
9	M
10	T

Condition	T_s (^oF)	T_a (^oF)	Rel Hum	W (mph)	Area (acres)
1	90	80	.8	20	400
2	100	85	.85	10	1500
3	105	80	.85	3	1500
4	70	50	.3	10	1500
5	78	55.5	.68	6.9	1250
6	85	65	.6	3	1500
7	80	70	.6	8	3000
8	65	50	.6	12	400

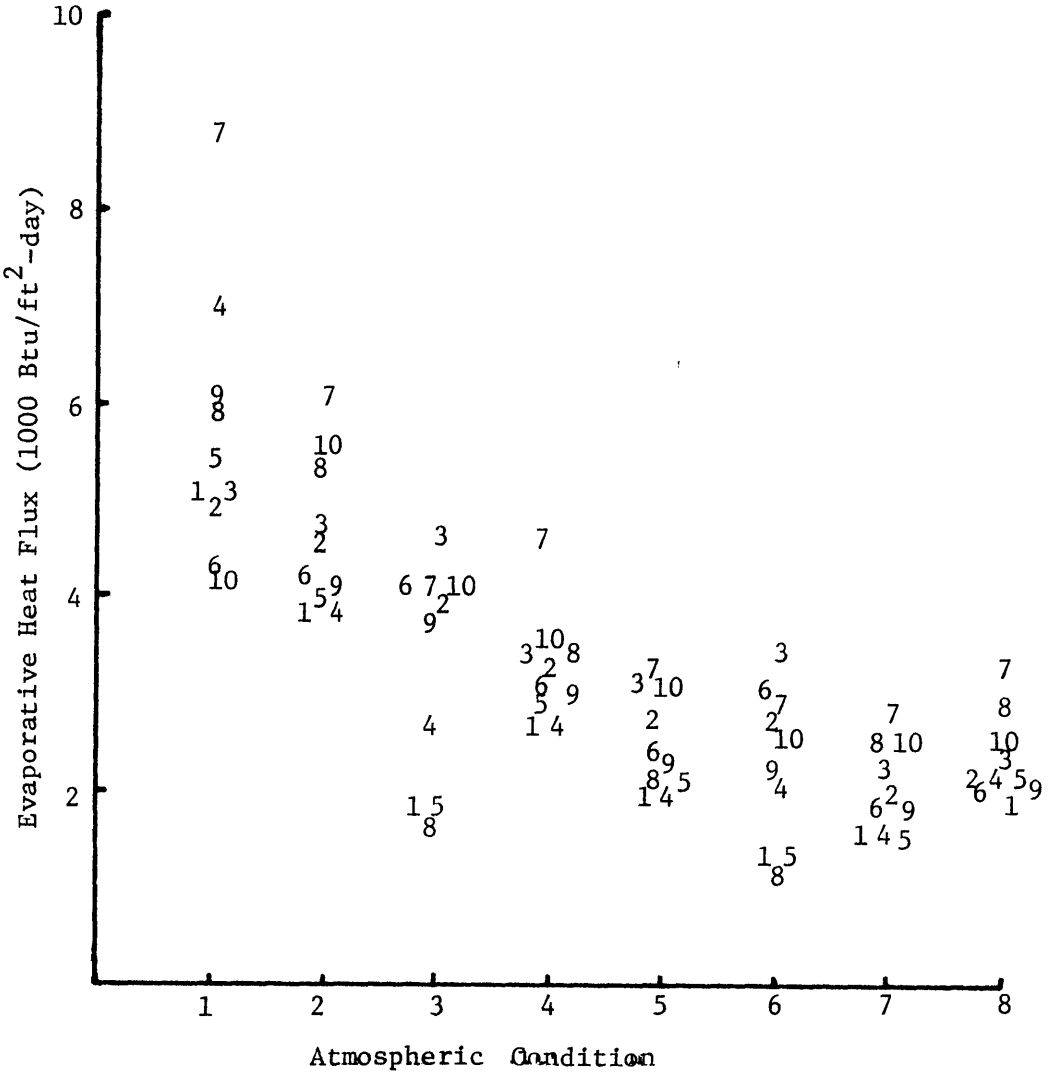

Figure 4.1: Evaporative Heat Flux vs. Various Atmospheric Conditions.

Figure 4.1 is not an absolute statement regarding the variation in predicted evaporation resulting from the different formulae. In practice, the water surface temperatures indicated on Figure 4.1 as independent parameters will be computed along with the evaporation rate. The negative feedback between evaporation and water temperature will result in generally less variation in predicted evaporation than indicated in these comparisons. Also, in realistic applications, the formulae will be applied over an extended period of time and thus will face a variety of atmospheric conditions. This last effect could result in either more or less variation among formulae than that indicated in Figure 4.1.

4.2 Data Sets Available for Testing of Equations

In order to further examine the predictive ability of the equations, adequate sets of data had to be found and assessed. Primary emphasis was placed on data sets which would allow computation of evaporation by the energy budget technique as opposed to the several other methods discussed in the previous chapter. Additionally, the use of a hydrothermal model for computing surface temperatures and the changes in thermal storage is advantageous due to the temporal and spatial variability of water temperatures in most cooling impoundments. Typically bulk energy budgets rely on one average measured value for water surface temperature and therefore omit the effects of the changing evaporation rate along the pond length.

Table 4.1 lists appropriate data sets which have been identified The following characteristics of the data sets are listed: data taken,

Table 4.1a: Data Sets - Site Physical Characteristics

Pond and Location	Gen'l. Description	A (acres)	$\overline{H}$ (ft)	Φ (MW_t/acre)	Pond No.	L/W
Hazelwood; Australia						
Hot Pond	Rectangular	70	12	2.70	0.4	2.8
System	Oblong	1250	18.4	0.72	0.11 (main lake)	2
Brady, Graves & Geyer						
Site 3; Louisiana	dammed Bayou Side arm present	605	6.7	0.43	0.49	6.4
Site 7; Texas	Oblong	2500	7.6	0.32	0.33	1
Site 11; Texas	long flow path	650	15.4	0.36	0.06	4.3
Lake Trawsfyngdd, Wales	Two small hot ponds	140	11.5		0.5	3.5
	in series	86	11	1.0	0.8	5
	Main lake	1009 (variable)	18 (variable)	for whole system	0.25 (rough estimate)	3
Dresden, Illinois	3 long narrow compartments	1275	10	1.40	0.9	19.5 (whole system)
Powerton, Illinois	3 compartments L/W $\approx$ 2-3	1442	10.9	1.69	0.5	7 (whole pond)
L. Anna, Virginia						
Hot Ponds	3 ponds, side arms present	3400	18	1.1	Distinct two-layer flow due to side arms.	6
Main lake		9600	25	0.15	0.3	$\sim$5
L. Belews, North Carolina	dammed stream side arms present	3860	47	0.72	0.1	$\sim$8
L. Norman	dammed stream side arms present	32,500	60	0.07	Complex - Three Generating Stations on Lake	

Table 4.1a: Continued

Pond and Location	Gen'l. Description	A (acres)	$\bar{H}$ (ft)	Φ (MW_t/acre)	Pond No.	L/W
Gentleman Station, Nebraska						
Canal		25	9.5			
Hot Pond	Rectangular	100	8	2.7	0.5	4
Hot Pond	Rectangular	200	8			1.4
Main lake	Round	2700 (variable)	17	0.4	0.36	1
East Mesa Geothermal Test Facility, California	Square lined pond	0.8	5	very high	1	1
Raft River Geothermal Test Facility, Idaho	Square lined pond	0.7	5	very high	1	1

Table 4.1b: Data Sets - Data Characteristics

Pond	Water Temp. Data	Met Tower Location	Met Data Recorded	Duration of Records
Hazelwood	periodic temp. surveys several thermographs throughout both ponds	on edge of hot pond	dry bulb air temp. (3 hr) wet bulb air temp. (3 hr) wind speed (1') (1 hr) solar radiation cloud cover (daily ave.)	Jan. 1967 to Dec. 1969
Brady, Graves & Geyer Site 3	several thermographs in take weekly ave. surface temp. reported	at power plant ∿ 2 mi. from lake	air temperature dew point wind speed (5' & 49') solar radiation 4 hr. taken - weekly ave. reported	July 1966 to Aug. 1968
Site 7	same as above	on lake edge	same as above except wind speed at 18'	Intermittently from Nov. 1966 to Sept. 1968
Site 11	same as above	lake edge	same as above except wind speed at 22'	Intermittently from Sept. 1966 to April 1969
Lake Trawsfynydd	hourly averages of temp. at various locations and depth in impoundment	several met stations. Main one on baffeling between hot ponds and lake	air temperature wet bulb temp. wind speed solar and total radiation all 1 hour averages	1963 through 1969 Jan. - March and July - Dec., 1969 may still be acquired for de- tailed study
Dresden	4 continuous thermographs and periodic temp. surveys	on lake edge except solar radiation and cloud cover recorded from remote locations	air temperature relative humidity wind speed (2m) wind direction solar radiation cloud cover all 1 hr. averages	Sept. 12 to Oct. 31, 1975

Table 4.1b: Continued

Pond	Water Temp. Data	Met Tower Location	Met Data Recorded	Duration of Records
Powerton	4 continous thermographs and periodic temperature surveys	NWS station Peoria, Ill. (9 miles away) except solar rad on-site	same as Dresden	Aug. 1 to Aug. 31, 1976
L. Anna	several continuous thermographs monthly temp. surveys	on main lake edge	same as Dresden	Aug. 1974 to present
L. Belews	several thermographs (vertical temp. profile) throughout lake	on island in lake	air temperature dew point temperature (2 & 8m) wind speed (2 & 8m) incident and net solar radiation daily averages for all	all 1976
L. Norman		similar to L. Belews		
Gentleman Station	daily average inflow and outflow temperatures periodic temp. surveys	on reservoir edge	air temperature relative humidity wind speed cloud cover all 3 hr. averages	Several periods between July 1972 and Dec. 1974
East Mesa		individual heat loss experiments - data for energy and water budgets		
Raft River		individual heat loss experiments - data for energy and water budgets		

frequency of acquisition, length of record, etc. Also listed are characteristics of the pond hydrothermal structure: heat loading, surface area, pond number, horizontal aspect ratio, etc. This latter information is included because it helps define the hydrothermal structure and thus indicates how the impoundment should be modeled (per Chapter III) if the approach using the hydrothermal model is to be taken.

Three of these data sets have been used previously to develop evaporation equations. The first set is from the Hazelwood cooling impoundment in Australia. These data were used by Ryan and Harleman (1973) to calibrate their equation (2.48). Hazelwood consists of two separate compartments. The first is a 70 acre hot pond which is connected to the main pond by a long narrow outlet channel. The total surface area is 1250 acres. The original analysis was done using the bulk energy budget approach with mean monthly data from 1967, 1968 and 1969. Balances were applied to both the total cooling impoundment and the hot pond individually. Meteorological and water temperature data on a one-day time step for the same period is also available. It was not used in this study, however, because of the quality of some of the essential data and the relative complexity of the hydrothermal structure, which would involve modeling of a deep stratified cooling impoundment.

The second previously analyzed heated impoundment data set is that used by Brady, Graves and Geyer (1969). They studied three ponds, two in Texas and one in Louisiana. All three ponds were lightly loaded

thermally ($\sim$ 0.4 MW_t/acre). At all three sites water temperatures and meteorological data were originally recorded in 4-hour averages, but weekly averages were used to estimate evaporation by way of bulk energy balances because time steps shorter than this produced unrealistic values of evaporation. Duration of the records, though incomplete, is about three years. These ponds were not used in this study because of the unavailability of the necessary data for use with a hydrothermal model.

The third previously analyzed data set is from Lake Trawsfynydd, Wales [McMillan (1973)] and was used to develop several evaporation equations. Lake Trawsfynydd consists of three compartments: two small hot ponds in series and a main impoundment. The total surface area is about 1235 acres maximum, but varies (up to 19%) due to lake level fluctuations. Data was recorded from 1963 through 1969. Water temperatures (with depth) were recorded at numerous locations throughout the impoundment. Several met stations were also situated throughout the impoundment measuring variables at several heights. The original analysis was performed using a bulk energy budget approach with averaging periods between 8 hours and one month. These data were not used in this study because high frequency data (3 hour averages) was not immediately available. Some data for periods of 1969 may still be available for future study. In terms of hydrothermal modeling the variable water level and the deep stratified structure of the main lake could cause some difficulties and might induce significant uncertainty in the predicted evaporation rates.

Water temperature and meteorological data form six cooling impound-

ments not previously studied in relation to evaporation were available. They were from the Dresden Pond, Powerton Pond, Lake Anna, Lake Belews, Lake Norman and Gentleman Station cooling impoundments. The first two were of excellent quality and were used in this study. They are discussed in more detail below. Although the meteorological and water temperature data was generally adequate for use with a dynamic model, the last four sites were not studied because of the complex nature of their hydrothermal structure. Inability to model the water temperature field accurately could lead to significant uncertainty in predicted evaporation rates.

Lake Anna, located in Virginia, consists of three hot ponds in series connected to a main lake created by a dam. Long dendritic sidearms, important in the surface heat transfer process were also present. The difficulty in modeling this impoundment accurately is caused by two layer flow evident in the hot ponds, deep stratified conditions in the main impoundment and the sidearm flow.

Lake Belews and Lake Norman, both in North Carolina, were also created by damming river reaches. As such their structure is highly irregular and they contain sidearm flow sections. These lakes also show strong vertical stratification in the lower layer and a heated surface layer. Lake Norman has three generating stations which adds difficulty to an already complex situation. These types of lakes are difficult to model and significant uncertainty in results could be expected.

Gentleman Station (Sutherland Reservoir) in Nebraska consists of a 14,700 ft canal which leads into two hot ponds in series, 100 acres and 200 acres in area. The water then goes into the main reservoir.

These data were not used in this study because of the complicated hydrothermal structure associated with the main lake. It is operated such that the water level and therefore volume and surface area are variable.

The last sites where data are available to assess evaporation from heated waterbodies are from the East Mesa Geothermal Test Facility in California and the Raft River site in Idaho [Hadlock and Abbey (1981)]. Individual heat loss experiments were carried out by filling the ponds at each site (East Mesa: area = 0.8 acres, depth ≈ 5 ft., Raft River: area = 0.7 acres, depth ≈ 5 ft.) with hot geothermal source water and recording the drop in water level to deduce evaporation. Detailed water temperature, soil temperature and meteorological measurements were also carried out. Godbey (1981) has analyzed initial experiments at these two sites using water and energy budgets and has compared these results with predictions using several evaporation equations. Recently (summer 1981) more experiments have been carried out at the East Mesa site using more detailed data collection procedures. At this time the data have not been analyzed.

4.2.1 Dresden Pond Data Set

The Dresden Pond was chosen as the first site at which to investigate the predictive accuracy of the evaporation equations. Reasons for this choice are 1) the data set is complete enough to allow calculations on a short time step, in this case 3 hours and 2) the thermal structure is better defined in terms of a mathematical model than the other candidate ponds. Thus, uncertainty in computed evaporation is less likely to result from inability to model the hydraulics properly.

As indicated in Table 4.1 the Dresden Pond, located in Illinois, has a total surface area of 1275 acres. It is a perched impoundment designed specifically for waste heat disposal and consists of three compartments separated by internal diking and constrictions. See Figure 4.2.

The data set used for this study [NUS (1976a)] was for the 50-day period of 9/12/75 to 10/31/75 and contained detailed information on plant operating characteristics (i.e., flow rate, etc.), pond temperatures and meteorological conditions. Water temperatures at four locations - pond inflow and outflow and at the two constrictions - were measured continuously and reported in one-hour averages. In addition to these continuous measurements intensive water temperature surveys were conducted approximately daily. This information was particularly useful in regards to correct modeling of the hydrothermal structure as will be discussed in Section 4.3.1.

Meteorological measurements for the same 50-day period were made on-site except for solar radiation which was measured at the Argonne National Laboratory ($\sim$ 40 miles away) and cloud cover which was reported from O'Hare International Airport ($\sim$ 100 miles away). The met data was reported in 1-hour averages and converted to 3-hour averages for use in MITEMP.

4.2.2 Powerton Pond Data Set

Powerton Pond also located in Illinois was chosen as the second site for this study for the same reasons as Dresden Pond: complete data set and moderately well defined thermal structure. It is also a

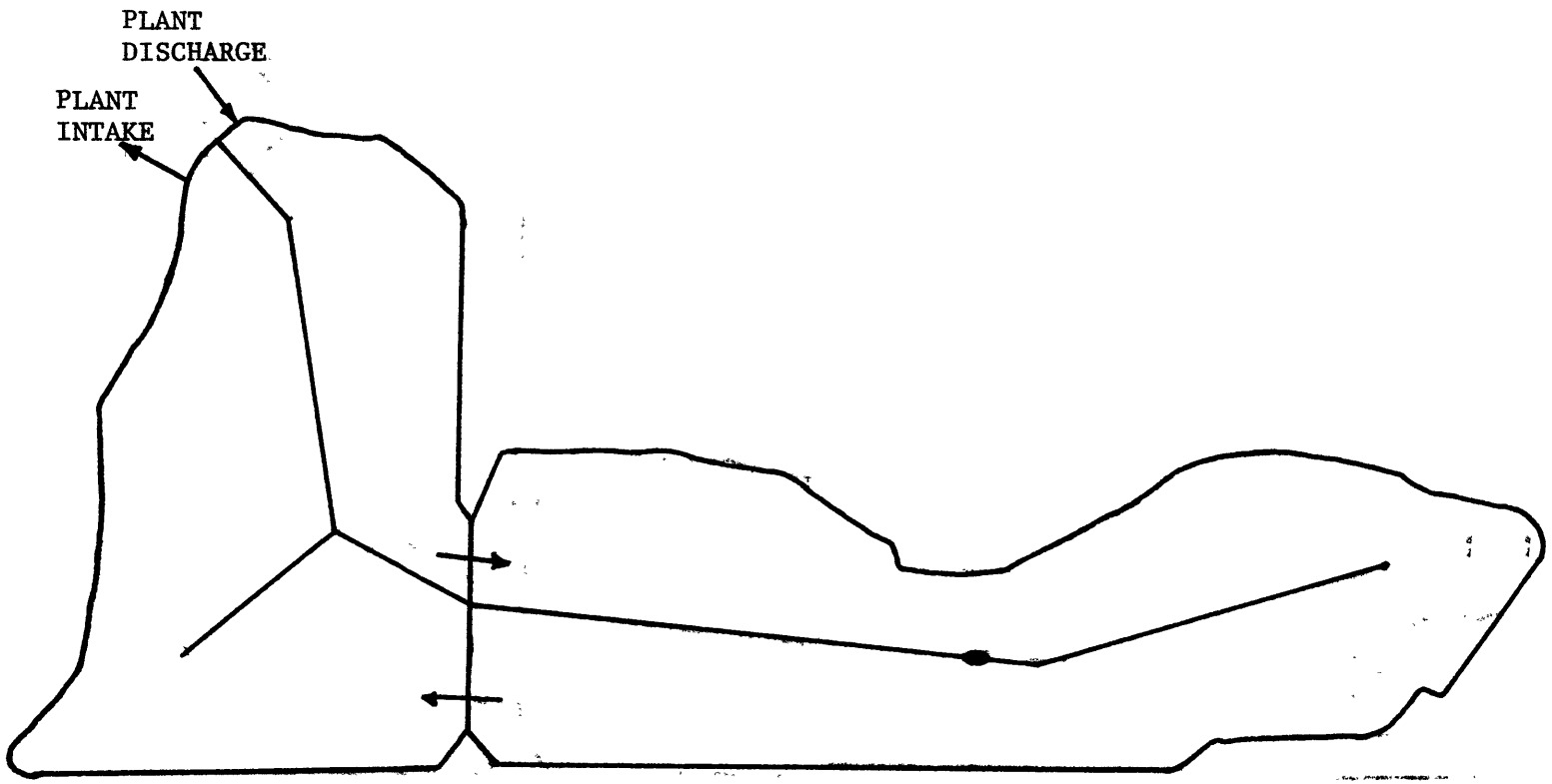

Figure 4.2: Dresden Cooling Pond.

perched pond designed for waste heat disposal and as such it is generally regular in shape. See Figure 4.3. It consists of three compartments in series, though in terms of hydrothermal structure it is quite different from Dresden Pond as will be discussed in Section 4.4.1.

The data set [NUS (1976b)] covers the 30-day period 8/1/76 to 8/31/76. The water temperature data is similar to Dresden data with pond inflow and outflow temps reported in 1-hour averages. Several other in-pond temperatures were also reported. Water temperature surveys were conducted approximately daily as was done with Dresden. The met variables were measured at the NWS station in Peoria, Illinois (9 miles away) with the exception of solar radiation which was measured on-site. Remote measurements of met conditions is not ideal in view of the discussion in Section 2.3 but had to be accepted because of the lack of other adequate data sets from other cooling ponds.

4.3 Evaluation of Equations with Dresden Data

The predictive ability of the ten evaporation equations was tested first with the Dresden Pond data. The deviation of predicted station intake temperatures (pond outlet temperatures) from the corresponding measured temperatures is a measure of the predictive accuracy of each equation assuming the pond hydraulics are well modeled and that all other energy inputs or outputs are accurately represented. The energy input from the plant is specified using measured station discharge temperature and flow rate (termed open-cycle operation). Two measures of the deviation between the model and measurement were computed. One was the mean error of the predicted vs. measured intake temperatures.

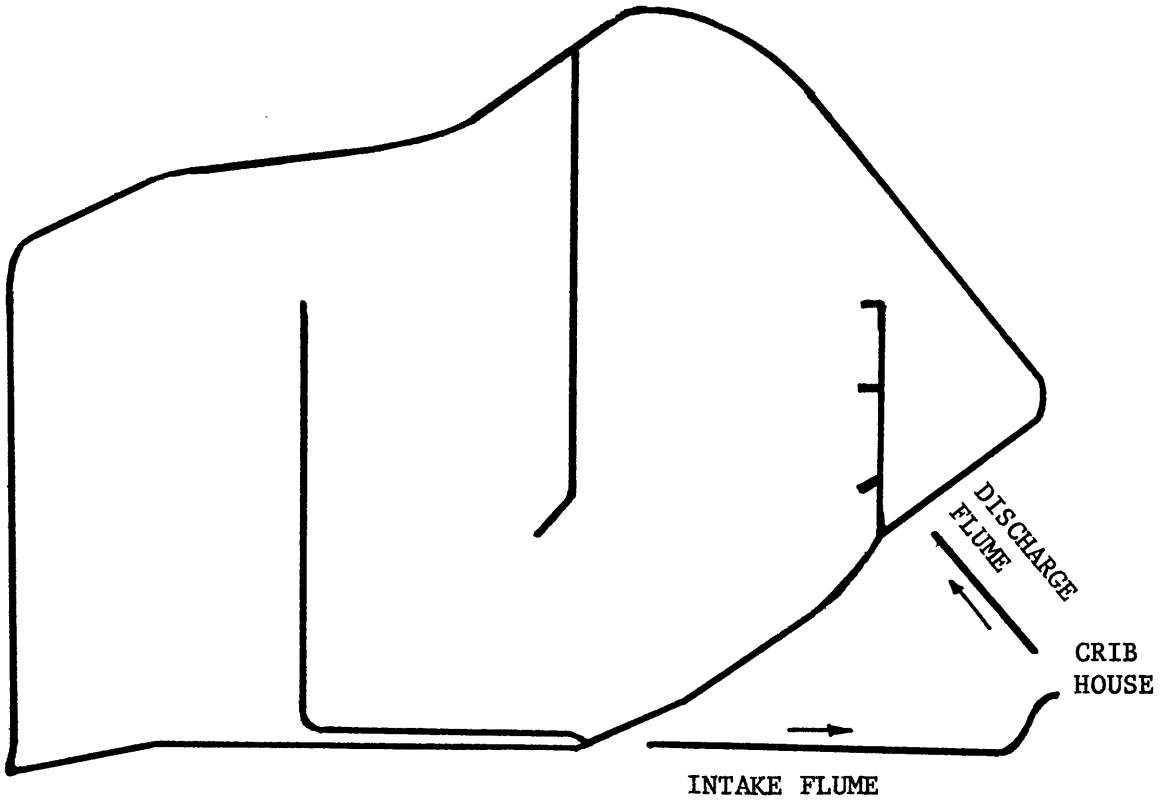

Figure 4.3: Powerton Cooling Pond.

The other was the variance (or standard deviation) of the predicted vs. measured intake temperature about the mean error. The mean error indicates if too much or too little total heat loss is occuring and the standard deviation indicates, to some degree, how well the formulae respond to shorter term variations in meteorological conditions. After computing the mean error, standard deviation and total predicted water loss, each equation was calibrated to the Dresden data by adjusting the factor α in

$$E = \alpha f(W_z)(e_s - e_z) \tag{4.1}$$

until the mean error was zero.

4.3.1 Hydrothermal Structure and Modeling

As mentioned Dresden Pond has a total surface area of 1275 acres. See Figure 4.2. It consists of three compartments separated by internal diking and constrictions. The flow path is about 33,000 ft. and the average depth is 10 ft. The plant condenser flow rate and temperature rise are nearly constant at 1800 cfs and 15^{o}F during the period of investigation. The pond number at Dresden is calculated to be 0.9. Along with large horizontal aspect ratios for each compartment the hydraulics are predominently vertically fully mixed and dominated by a longitudinal dispersive process. The NUS (1976a) field measurements verify this assessment. Figure 4.4 shows a typical surface isotherm pattern measured during the investigation pattern. Except for obvious jet structure near the constrictions between the compartments the flow is unidirectional. Thus Dresden was modeled as three shallow longitudinally dispersive ponds in series using MITEMP. No correction for vertical temperature gradients

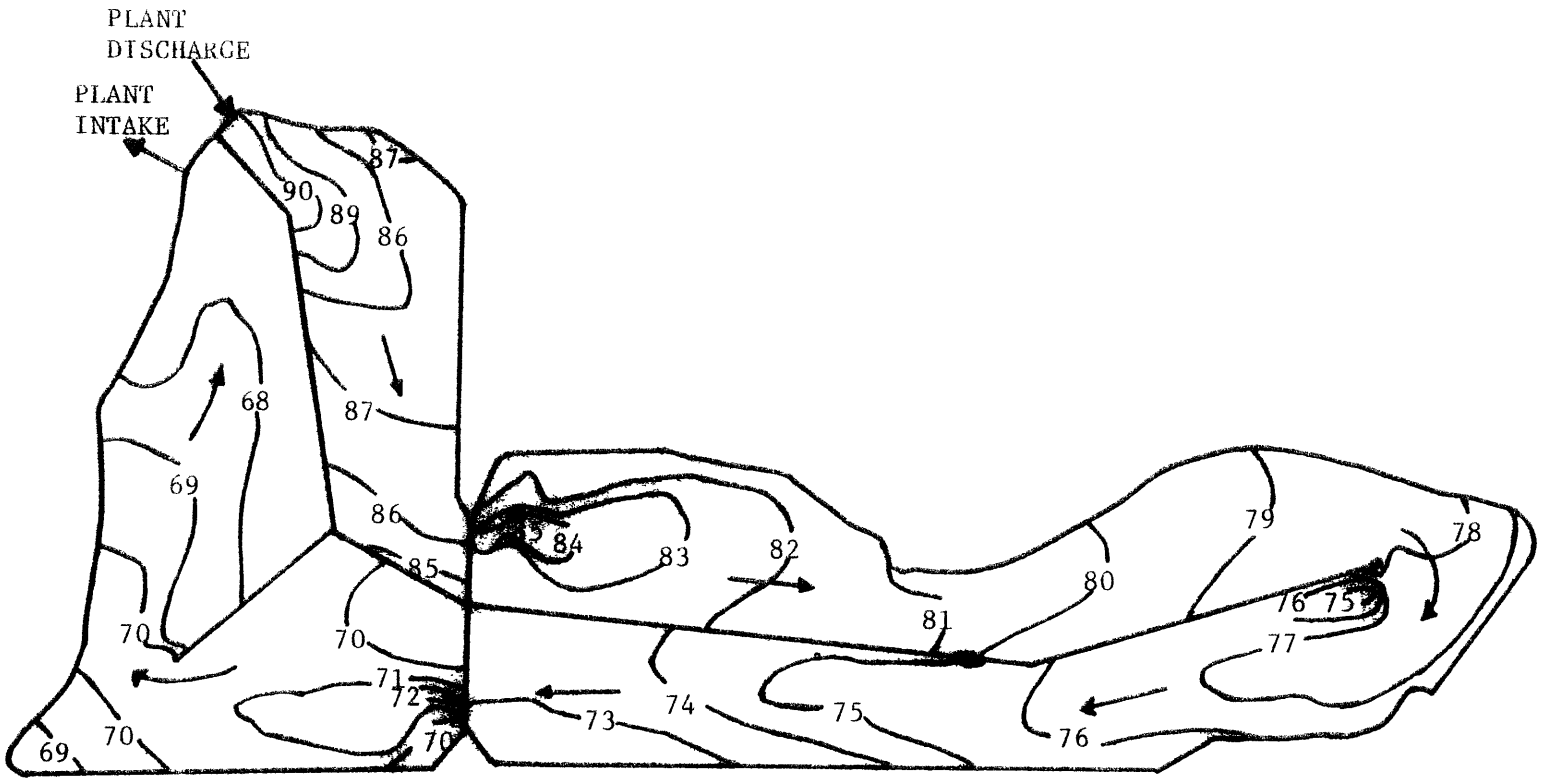

Figure 4.4: Surface Isotherm Pattern for Dresden Cooling Pond, 10/21/75 (NUS, 1976a).

(see Section 3.5.1) have been undertaken as the field data indicated very slight gradients ($\overline{\Delta T}_V \lesssim 1^oF$) on a pond average basis. Table 4.2 contains the details of the model geometry.

Table 4.2: Dresden Model Geometry

Compartment	Length(ft)	Width(ft)	Area(acres)	Depth(ft)
1	5,030	1,470	170	14.0
2	18,130	1,660	692	7.3
3	9,760	1,840	413	13.0

If one is to judge the accuracy of an evaporation equation by comparison of predicted and measured end temperatures, the hydraulic structure must be accurately represented. In the case of Dresden Pond, the main hydraulic parameter is the dispersion coefficient, E_L (see Equation (3.4)). Initial estimates of the dispersion coefficients were made for each pond compartment based upon Fischer's (1967) analysis, equation (3.6). Then, using the Lake Hefner equation, the dispersion coefficients were changed by a constant factor of the Fischer value (E_{L_F}) until the shape of the predicted longitudinal temperature profiles match the shape of the measured cross-sectionally averaged profiles. Figure 4.5 shows a typical result. This procedure was used because the shape of the temperature profile is predominently a function of the dispersion coefficient, while the actual water temperatures are predominently a function of the surface heat transfer (e.g., evaporation). With this approach a value of 0.25 times the Fischer relationship was determined to best represent the hydraulic characteris-

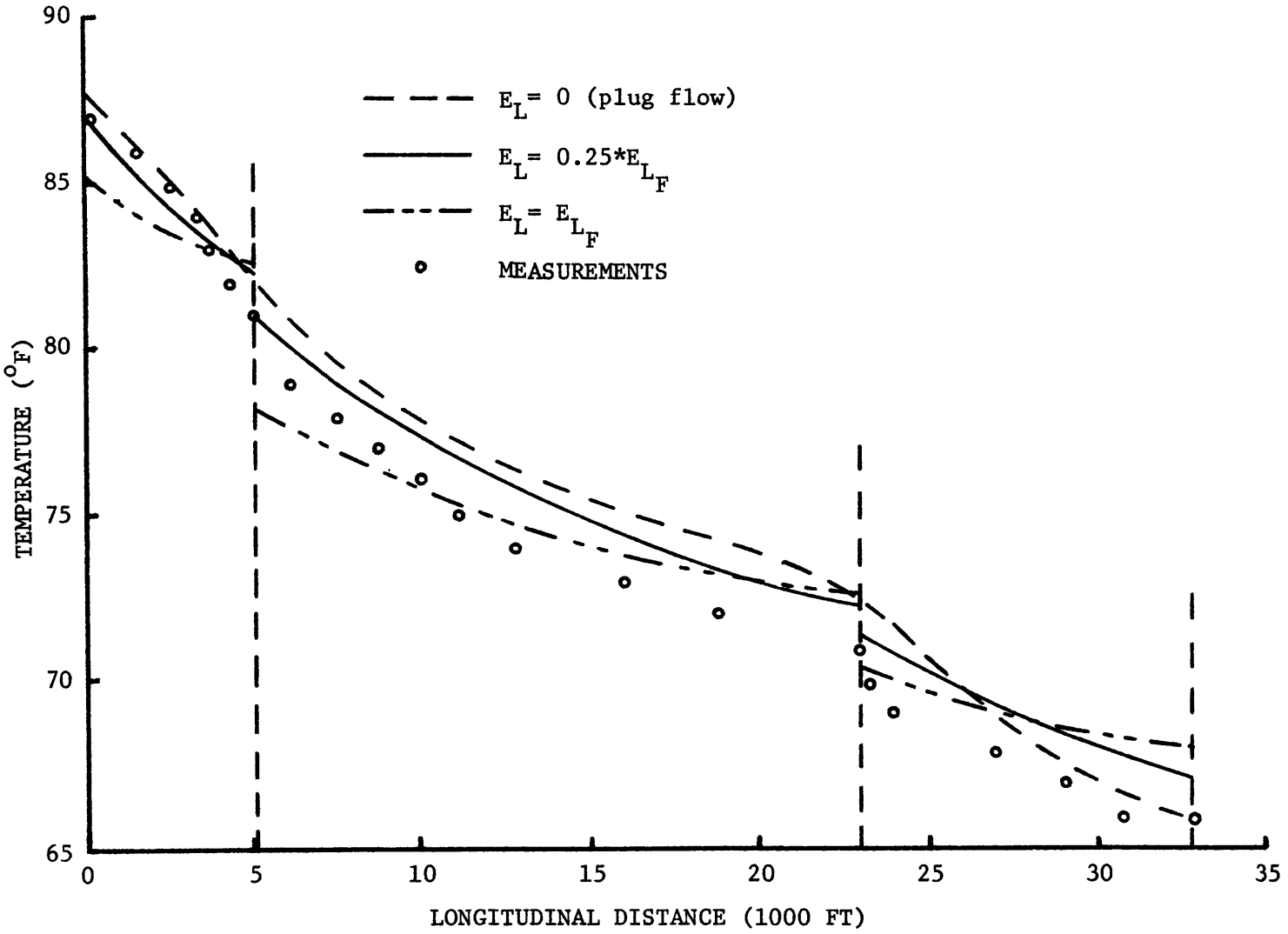

Figure 4.5: Temperature Distribution for Dresden Cooling Pond 10:00am 10/20/75.

tics of Dresden Pond and was used in subsequent evaporation model calibration/verification.

Due to the range in values of E_L (between 0 and 0.5 E_{L_F}) which gave satisfactory longitudinal temperature profiles when compared to the measured data, some uncertainty is associated with the chosen value of E_L. For a range of values of the dispersion coefficient (fraction of E_{L_F}) the Lake Hefner equation was calibrated by adjusting the factor α until there was zero mean error between predicted and measured end temperatures. Table 4.3 shows these results. The uncertainty in the dispersion coefficients (0 to 0.5 E_{L_F}) translated to an uncertainty of about $\pm$ 3.5% in α calibrated for zero mean error or $\pm$ 1.5% in predicted water loss if α is set constant and the dispersion coefficient varied. These results are representative of all ten equations.

Table 4.3: Sensitivity of Evaporation Calibration to the Dispersion Coefficient (Dresden Data, Lake Hefner Equation)

E_L/E_{L_F}	α
0	1.06
0.25	1.11
0.50	1.14
1.00	1.17
5.00	1.23

4.3.2 Equation Predictions with Dresden Data

Table 4.4 contains the equation predictions for the 50 days of data from Dresden Pond. The average water loss rates and mean errors

Table 4.4: Equation Predictions at Dresden

Equation	Mean Intake Error α=1.0 (^{o}F)	Std. Dev. (^{o}F)	Water Loss Rate (cfs)	Calibrated α for Dresden	Mean Intake Error (^{o}F)	Std. Dev. (^{o}F)	Water Loss Rate (cfs)
1 (LH)	0.94	0.91	18.7	1.11	0	0.95	20.1
2 (RH)	-2.22	1.11	23.0	0.79	0	1.07	19.8
3 (RD)	-3.58	1.28	25.0	0.69	0	1.20	19.8
4 (BGG)	0.01	0.94	20.1	1.00	0	0.94	20.1
5 (H)	0.98	0.92	18.7	1.11	0	0.95	20.1
6 (GSM)	-1.44	1.28	21.9	0.86	0	1.31	19.9
7 (WB)	-2.56	1.06	23.6	0.76	0	0.95	19.9
8 (ARG)	-0.46	1.34	21.0	0.95	0	1.29	20.3
9 (M)	-1.57	1.28	22.0	0.85	0	1.33	19.8
10 (T)	-3.68	1.12	25.3	0.69	0	1.07	19.9
Average =	-1.36^{o}F		21.9 cfs	0.88			20.0 cfs
Spread =	$\pm$ 2.33^{o}F		$\pm$ 15%	$\pm$ 0.21			$\pm$ 1.3%

between predicted and measured intake temperatures ranges from 18.7 cfs to 25.3 cfs and -3.68°F to +0.94°F (α = 1.0 for all equations). The average predicted water loss rate was 21.9 cfs. The spread, 0.5* (High-Low)/average, was about $\pm$ 15%.

The equations were then calibrated by adjusting α. The appropriate values of α are also shown in Table 4.4. There is some slight variability (spread = $\pm$ 1.3%) in the predicted water loss rates for the calibrated equations. This is to be expected since we are calibrating to temperature measurements not water loss rates. It should also be noted that for all the equations, both calibrated and uncalibrated, there is only slight variability in the standard deviation of intake temperature predictions and therefore distinction between equations on this basis is not possible.

4.4 Evaluation of Equations with Powerton Data

To assess the consistency of the calibrations performed with the Dresden data a similar analysis with the Powerton data was performed.

4.4.1 Hydrothermal Structure and Modeling

Powerton Pond presented a more difficult modeling job than Dresden. It has a surface area of 1442 acres and consists of three compartments of approximately equal size. See Figure 4.3. Based upon the average plant flow rate of 1540 cfs and condenser temperature rise of 23°F and the physical characteristics of the impoundment a pond number of 0.5 (whole pond) was computed. The horizontal aspect ratio for each compartment was less than 3 to 5 suggesting recirculating flow in each compartment. Figure 4.6 shows surface isotherm patterns derived from an infrared survey during the investigation period. This figure tends to confirm

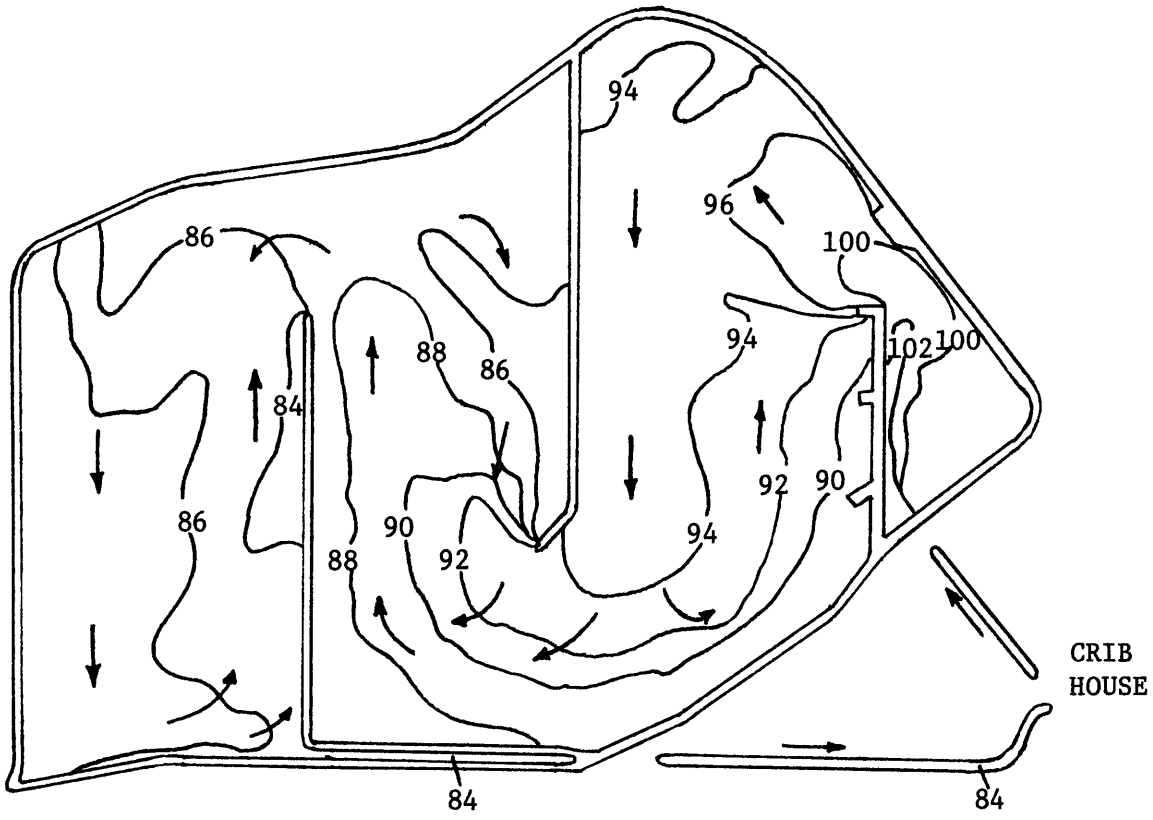

Figure 4.6: Infrared Temperature Survey for Powerton Cooling Pond, Indicating Sturcture of Surface Currents

the assumption of recirculating flow in each compartment. Thus Powerton was modeled as three shallow recirculating compartments in series using MITEMP (see Figure 3.2). Previous modeling of Powerton Pond [Jirka et al. (1978)] had treated the small entrance zone as a separate (fourth) compartment. In this study it was considered as part of the jet or forward flow zone in the first compartment.

The fairly low pond number of 0.5 indicated that some vertical stratification would be present. Analysis of the field data confirmed this suspicion. It also indicated that the bottom water was flowing in the same direction as the surface water and thus a shallow or hydraulically one-layer model was appropriate. From Figure 3.1 an average value of $\overline{\Delta T_V} = 4^oF$ was computed which agreed well with the field data on a pond average basis.

Further specification of the hydraulic structure was possible using the dilution, D_s, and area, q, factors defined in Figure 3.5. The dispersion coefficient was set equal to 0.25 x E_{L_F}. Sensitivity analysis showed both α calibrated for zero mean error and water loss predictions were not very sensitive to E_L ($< \pm$ 1% variation in both water loss and calibrated α). Instead, mixing characteristics in a recirculating pond is primarily dependent upon D_s and q.

These factors were set by comparing initial simulations with field data and using results of previous studies of Powerton [Jirka et al. (1978)]. Sensitivity studies showed that a $\pm$ 10% change in D_s values caused a $\pm$ 4.5% in α calibrated for zero mean error (with LH equation).

Correspondingly a ± 10% uncertainty in D_s produced just ± 1% uncertainty in predicted water loss for a constant α. These results give slightly more uncertainty in the calibrated α's (± 4.5% vs. ± 3.5%) due to hydraulic characteristics than Dresden and about the same uncertainty in water loss predictions. Details of the model geometry for Powerton are given in Table 4.5.

Table 4.5: Powerton Model Geometry

Compartment	Length(ft)	Width(ft)	Area(acres)	Depth(ft)	D_s	q
1	7892	3000	540.1	10	1.8	1/3
2	7100	2800	456.5	11	1.5	1/3
3	6967	3000	445.4	12	1.5	1/3

4.4.2 Equation Predictions with Powerton Data

The results for the uncalibrated (α = 1.0) and the Dresden-calibrated equations are shown in Table 4.6. As would be expected all ten calibrated equations performed much better when compared to the uncalibrated results at either Dresden or Powerton. The spread of the water loss estimates was ± 3.7% about a mean of 27.0 cfs. By comparison the non-calibrated equations had a spread of ± 14% about a mean of 29.1 cfs. The average (of the ten equations) of the mean station intake error decreased slightly from + 0.91°F for the non-calibrated equations to + 0.44°F for the calibrated equations. The spread of predicted mean intake error did decrease drastically, from ± 2.69°F to ± 0.79°F.

The calibrated equations which performed best (measured by mean

Table 4.6: Equation Predictions at Powerton

Equation	Mean Intake Error α=1.0 (^{o}F)	Std. Dev. (^{o}F)	Water Loss Rate (cfs)	Calibrated α for Dresden	Mean Intake Error (^{o}F)	Std. Dev. (^{o}F)	Water Loss Rate (cfs)
1 (LH)	1.90	0.97	24.9	1.11	0.91	0.94	26.5
2 (RH)	-1.99	1.09	30.7	0.79	0.17	1.10	27.4
3 (RD)	-3.28	1.17	32.7	0.69	0.16	1.18	27.3
4 (BGG)	0.60	1.06	26.7	1.00	0.60	1.06	26.7
5 (H)	1.99	0.97	24.8	1.11	1.22	0.94	26.3
6 (GSM)	-1.86	1.17	30.6	0.86	-0.46	1.18	28.3
7 (WB)	-1.67	1.01	30.4	0.76	0.84	1.03	26.5
8 (ARG)	0.31	0.98	27.5	0.95	0.81	0.98	26.7
9 (M)	-1.66	1.14	30.1	0.85	-0.05	1.17	26.7
10 (T)	-3.39	1.00	33.0	0.69	0.29	1.03	27.2
Average =	0.91^{o}F		29.1 cfs	0.88	0.44^{o}F		27.0 cfs
Spread =	$\pm$ 2.69		$\pm$ 14%	$\pm$ 0.21	$\pm$ 0.79^{o}F		$\pm$ 3.7%

error) were the Meyer equation, the Ryan-Harleman equation, the Rimsha-Donchenko equation and the Throne equation. The last three equations were developed specifically for heated water conditions while the Meyer equation was originally developed for natural situations.

4.5 Hierarchy of Predictions - Feedback Between Water Temperature and Evaporation

Reference back to Table 4.4 and condition 5 on Figure 4.1 shows an interesting result concerning the variability in predicted evaporative loss rates. In Figure 4.1, condition 5, the evaporative mass loss rate was computed for each equation (α = 1.0) using the average meteorological conditions and average measured water temperature at Dresden during the 50-day period. (T_s = 78°F, T_a = 55.5°F, relative humidity = 68%, W_2 = 6.9 mph.) Using this single set of conditions (referred to as a static calculation) the spread about an average mass loss rate is $\pm$ 23%. The dynamic open cycle calculations, where pond inflow rate and water temperature (i.e., energy advected in) were specified, gave a spread of $\pm$ 15%. Similar analysis with the Powerton data showed a reduction in the spread from 27% for the static calculations to $\pm$ 14% for the dynamic open cycle calculations.

When the calibrated equations were reapplied to the static conditions the spread about the average value was reduced to $\pm$ 6.3% for Dresden and $\pm$ 10.6% for Powerton (note that equations were calibrated to the Dresden data). The reduction in the variability of water loss predictions between dynamic open cycle calculations ($\pm$ 15% Dresden,

$\pm$ 14% Powerton) and static calculations ($\pm$ 23% Dresden, $\pm$ 27% Powerton) can be attributed to two factors: feedback between water temperatures and evaporation and the effect of averaging over variable atmospheric conditions.

Along similar lines it is noted that with the Dresden data (Table 4.4), on average, a $\pm$ 1% change in calibration (i.e., factor α) caused a $\pm$ 0.67% change in water loss and a $\overline{+}$ 0.10°F change in mean station intake error. Correspondingly the Powerton results showed a $\pm$ 0.55% change in water loss and a $\overline{+}$ 0.10°F change in mean error for a $\pm$ 1% change in calibration. Thus a change in the magnitude of an evaporation equation causes a smaller change in water loss because of the water temperature-evaporation feedback inherent in a dynamic model.

To further characterize the feedback between evaporation and water temperature associated with the dynamic model we ran some hypothetical cases using the Dresden Pond configuration and meteorological conditions in a closed cycle mode of station operation. In a closed cycle mode the station condenser temperature rise ΔT_o and flow rate were specified rather than the measured plant discharge temperatures and flow rates as was done in the open cycle tests. In this situation the predicted water loss rates for all non-calibrated equations (α = 1.0) exhibited a spread about the average value of $\pm$ 2.6%, much lower than the previous two cases ($\pm$ 23% static and $\pm$ 15% open cycle dynamic). The calibrated equations produced a spread of $\pm$ 1.4% in the closed cycle simulation. These results suggest a hierarchy of probable uncertainty in water consumption estimates. Static calculations based on fixed

meteorological and water temperature data give the most uncertainty whereas calculations using a dynamic model in a closed cycle mode are quite consistent regardless of the evaporation equation being used. Results for the Powerton data are similar and all results are summarized in Table 4.7.

Table 4.7: Variability of Water Loss Predictions

Situation	Spread About Average Value	
	Uncalibrated	Calibrated at Dresden
Static Calculation at Dresden	± 23 %	± 6.3%
Static Calculation at Powerton	± 27 %	± 10.3%
Dynamic Open Cycle Simulation at Dresden	± 15 %	− 1.3%
Dynamic Open Cycle Simulation at Powerton	± 14 %	± 3.7%
Dynamic Closed Cycle Simulation at Dresden	± 2.6%	± 1.4%
Dynamic Closed Cycle Simulation at Powerton	± 5.2%	± 1.2%

It should be noted that although the variability in water loss rates for uncalibrated equations using a dynamic model in closed cycle mode are small the predicted water temperatures may be quite variable. As an example for the Dresden data closed cycle simulation the average plant intake temperature was 73.5°F for all ten equations but values ranged ± 4.5°F about this average. From a regulatory or plant efficiency point of view it is often the water temperatures which are most important. Thus the water loss results, which imply that similar

results are obtained for any of the ten equations, could be misleading if accurate water temperature predictions are also desired results.

The strong feedback between evaporation and water temperatures is a major reason for reduced variability suggesting additional motivation for the use of dynamic hydrothermal model to compute evaporation. Even if only approximate water loss estimates are required, the coupling suggests that these estimates should be based on anticipated water temperatures which reflect the evaporation equation used to compute water loss.

4.6 Additional Uncertainty in Dynamic Energy Budget Results

It is important to recognize that the variabilities reflected in Table 4.8 and the calibration/verification results in Tables 4.5 and 4.7 represent the relative accuracy of the various equations under different predictive conditions and not the absolute accuracy of the equations. Any uncertainty in the latter is a function of uncertainty in the measured meteorolgoical and water temperature data and uncertainty in the other heat flux terms (measured or computed).

4.6.1 Meteorological and Water Temperature Data

For both data sets studied the water temperature data is considered excellent and virtually no uncertainty should be attributed to the above results due to inaccurate measurement. Measurement of the meteorological variables, primarily location, might have introduced some uncertainty into the results. As mentioned all the Dresden met data except solar radiation and cloud cover were recorded on-site.

Inasmuch as the measurement instruments would allow it was assumed that the on-site measured data; air temperature, relative humidity and wind speed, were representative of the bulk atmospheric conditions which were occuring over the cooling pond. The fact that 3-hour averages were used (derived from continuous records) probably eliminates most uncertainty that these values were not representative of the driving meteorological conditions over the whole pond. Additionally, all the evaporation equations tested except the Argonne National Laboratory equation (ARG) were meant to be used with bulk meteorological measurements. The possible error associated with remote measurement of solar radiation and cloud cover are discussed in Section 4.6.2.

All of the meteorological measurements used in the Powerton Pond work, except solar radiation, were recorded at a remote site (NWS station 9 miles away). This undoubtedly adds some uncertainty to the results. However, because the separation is only 9 miles and there are no significant topographic influences there is no reason to expect major differences between on-site met conditions and those measured at the NWS station.

4.6.2 Other Heat Flux Terms

In addition to evaporation correct specification of the remaining heat flux terms - conduction, advected energy, back radiation, atmospheric radiation, and solar radiation - is necessary to insure absolute accuracy of the equation claibrations. Conduction, related to evaporation by the Bowen ratio, has been discussed in Section 2.1.1. The energy advected into the ponds is assumed well known. Accurate

measurements of the plant condenser flow rate and pond inlet temperature were measured at both sites. By adjusting the predicted pond out-flow temperatures to match the measured temperatures this term is accounted for accurately on the mean.

The remaining heat flux terms are all radiation terms. The solar radiation has a short wavelength ($\lesssim$ 2.8 - 3.0μ). The back radiation and atmospheric radiation are the result of the fact that any body (e.g., atmosphere or water surface) above $0^{o}K$ will radiate energy. This radiation is distinguished by a long wavelength ($\gtrsim$ 3.0μ). Spectral measurements of radiation over all wavelengths typically show a drop in energy near 3.0μ which serves as the distinction between the long-wave and short-wave components.

Long-wave radiation may be measured with radiometers which are specially designed to block out wavelengths shorter than a specified limit. It is unusual, however, to have measurements of back and atmospheric long-wave radiation. The radiation is temperature dependent and therefore the back radiation may change dramatically over the water surface due to large spatial temperature gradients experienced in cooling impoundments. Both these terms may be computed using the Stephan Boltzmann relation

$$\phi_{LW} = \varepsilon\sigma T^{4} \qquad (4.2)$$

where ϕ_{LW} = long-wave radiation flux, ε = emissivity, σ = Stephan Boltzmann constant and T = temperature (absolute) of either the water surface or air.

Back Radiation

The back radiation is usually the largest term in the energy budget. It is, however, computed quite accurately because the emissivity of water is known within precise limits. In this study it was taken to be constant at 0.97 (the water is radiating almost as a black body, $\varepsilon = 1.0$). The accuracy of this relationship is assumed to be within several percent.

Atmospheric Radiation

The atmospheric long-wave radiation is less well predicted and probably represents the largest possible source of error in this study. Reasons for this inability to accurately predict long-wave atmospheric radiation are primarily the influence of atmospheric moisture, dust and cloud cover on incoming long-wave radiation.

For clear skies (no cloud cover) several relations exist to predict the emissivity of the atmosphere. In this study we used the relation of Swinbank (1963)

$$\varepsilon_{ac} = 0.936 \times 10^{-5} T_a^{\,2} \quad \text{(with } T_a \text{ in } {}^{o}K\text{)} \qquad (4.3)$$

where ε_{ac} = emissivity of the atmosphere under clear skies to compute the clear sky long-wave radiation. Other forms for ε_{ac} which depend on T_a and/or the vapor pressure of the air have been suggested by several investigators [Idso and Jackson (1969), Burtsaert (1975) and Idso (1981)]. Aase and Idso (1978) compared the relation of Brutsaert and the Idso-Jackson formula. They determined that for clear skies there was little or no difference between the two formulae for air temperatures

above freezing. Below freezing both deviated from measured values with one overestimating and the other underestimating. Comparison of equation (4.3) with the other two forms using the Aase and Idso data showed that for temperatures above freezing equation (4.3) also performed as well as the other two relations. Idso (1981) presents a formula for ε_{ac} which corrects the deficiency of the other formulas for air temperatures below freezing. For this study, though, equation (4.3) was used because the air temperature never went below freezing at Dresden or Powerton during the periods of interest.

Further corrections to the computed atmospheric long-wave radiation must be made because of cloud cover. Cloud cover, by far, is the most difficult correction to make. Clouds darken the atmosphere and therefore tend to increase the emissivity. In this study the relation given by Geiger (1965)

$$\varepsilon_a = \varepsilon_{ac}(1 + 0.17\ C^2) \qquad (4.4)$$

where ε_a = emissivity of the atmosphere and C = fractional cloud cover in tenths, was used. It is known that the altitude and the density (type) of the clouds significantly affect the emissivity. However, because of the lack of data and good correlation formulae, no account could be made for these factors. Review of the current literature turned up no viable alternatives for equation (4.4). A definite lack of good data exists and points to the need for more work in this area.

The last correction to be made is for reflectance. 3% reflectance is generally accepted as representative of water surfaces. For land

the reflectance is nearly 0%. Thus the net incoming long-wave atmospheric radiation is given by

$$\phi_{atm} = 0.97 \cdot (1 + 0.17C^2)\varepsilon_{ac}\ \sigma T_a^4 \qquad (4.5)$$

Ryan and Harleman (1973) state that the accuracy of equation (4.5) for clear skies (C = 0) is $\pm$ 5%. This figure corresponds with our results using the data of Aase and Idso (1978). For cloudy conditions it is estimated that the accuracy is probably within $\pm$ 15% at most.

This uncertainty could definitely be reduced if long-wave radiation was measured as opposed to computed. Instrumentation is nearly identical to the solar radiation measurement which is performed regularly. The calculations could be improved if better relations for the cloud cover effect were developed. Additionally, better measurements of cloud cover could improve these calculations. Cloud cover is usually "measured" by visual observation and therefore significant personal bias may be introduced. Use of whole sky cameras would help. The best answer, though, is to measure the atmospheric radiation.

In this study of the Dresden and Powerton cooling impoundments measurements of cloud cover were taken at remote locations ($\sim$ 100 miles away from Dresden, 9 miles away from Powerton). Considerable error might have been introduced, particularly in the case of Dresden. It is estimated, though, that for both cases the error in computed net atmospheric long-wave radiation is within the $\pm$ 15% mentioned above and on average below this.

Solar Radiation

Solar radiation flux is made up of a direct component and a diffuse or scattered component. Empirical relationships [Wunderlich (1972)] are available to estimate the solar radiation but direct measurements are quite common and more accurate. Measurements are made with a pyranometer which generally measures radiation in the 0.28 to 2.8-3.0μ wavelength band. These measurements are typically of total downward solar radiation and therefore reflected radiation must be estimated. Ryan and Harleman (1973) suggest an average value of 6% reflectance based upon work done at Lake Hefner.

On-site measurements were available for the Powerton study and are considered to be quite accurate (± 3-5%). The Dresden results relied on solar radiation measurements made about 40 miles away. Differences in cloud cover, which affect the total incoming solar radiation, at the measurement site and at Dresden Pond could cause slightly more uncertainty in the solar radiation than expected with the Powerton data.

4.6.3 Sensitivity of Calibration and Water Loss Results to the Radiation Heat Flux Terms

Table 4.8 shows the results of sensitivity studies of the Lake Hefner and Ryan-Harleman equation calibrations and water loss predictions to the radiation heat flux terms. The results for these two equations are nearly identical and are thus considered representative of all ten equations. The results showed the most sensitivity to the back radiation term. This is not surprizing since it is larger in

Table 4.8: Sensitivity of Calibration and Water Loss Predictions to Radiation Heat Flux Terms (Dresden Pond Data, Open Cycle Runs)

Radiation Heat Flux Term	Change in Heat Flux Term	Evaporation Equation	Change in Calibration (α) for Zero Mean Error	Change in Predicted Water Loss (α set at Dresden Calibration Value)
Back Radiation	$\pm$ 5%	LH	$\mp$ 6.3%	$\mp$ 1.7%
		RH	$\mp$ 6.3%	$\mp$ 1.9%
Atmospheric Radiation	$\pm$ 15%	LH	$\pm$ 13.5%	$\pm$ 3.6%
		RH	$\pm$ 13.4%	$\pm$ 3.9%
Solar Radiation	$\pm$ 10%	LH	$\pm$ 5.4%	$\pm$ 1.2%
		RH	$\pm$ 5.0%	$\pm$ 1.4%

magnitude than the other two terms. Also note that the equation calibrations are much more sensitive to a constant percentage change in the radiation heat flux terms than the predicted water loss rates are. This is attributed to the coupling between evaporation and water temperature discussed in Section 4.5.

4.7 Effect of Using Averaged Meteorological Variables

A main objective of this study was to explore the use of evaporation formulae to predict water loss. Knowing that a primary concern is with long time scales, on the order of years, the effect of data averaging was investigated. Experience with evaporation from unheated reservoirs [Jobson (1972)] suggests that averaging data up to one month results in a generally acceptable error (5% or less). However, the non-linearities associated with several formulations appropriate for heated ponds implies that in this case the error might be significantly greater. Questions to be addressed were:

1) What effect will averaging have on consumptive water loss predictions?
2) What effect will averaging have on MITEMP's predictions of pond temperatures?
3) Do some of the evaporation equations respond with more sensitivity to data averaging?

4.7.1 Analysis Method

In order to investigate the effects of averaging on thermal performance and consumptive water loss predictions at least one year of

met and water temperature data from a cooling impoundment was needed. As mentioned in Section 4.2 no data of this duration were available. To get by this problem a hypothetical pond, identical in structure to the Dresden Pond, was used in conjunction with one year of meteorological data (3-hour averages) collected at Moline, Illinois (located on the Mississippi River 75 miles NE of Powerton and 110 miles W of Dresden).

The analysis was carried out as follows. The pond was modeled in a closed cycle mode with the condenser flow rate and temperature rise specified and constant (1800 cfs and $20^{o}F$). For each equation tested the program was first run for a period of thirteen months with the set of 3 hourly data points to generate reference plant intake (pond end) temperatures as a function of time and a reference cumulative water loss for that equation. (Note: the first month was for warm up and the comparisons are based on the last 12 months.) Then the program was run with an averaged data set and the station intake temperatures and the average water loss rate were compared to the reference values. The comparison resulted in a mean error and variance between the two temperature sets.

The averaging periods were daily, weekly, monthly and yearly. To avoid step changes in meteorological conditions, which would unrealistically affect the model results, central running averages were used. For example, consider an averaging period of one day and a 3-hour model time step (chosen for computational stability). The model input value at a certain time was comprised of the average of the four previous data

points, the present point, and the three points to follow. This type of procedure was carried out for all averaging periods. The result was a smooth curve for each meteorological variable which was increasingly damped (smoothed) as the averaging period increased.

4.7.2 Data Averaging Results

Three evaporation equations were tested:

1) Lake Hefner (LH)

2) Brady, Graves and Geyer (BGG)

3) Ryan-Harleman (RH)

Thus all three categories of evaporation equation type were examined. Results of the simulations are shown in Tables 4.9 a,b,c. The water consumption results (Table 4.9 a) are interesting in that they show very little change in water consumption predictions as the averaging period is increased from 3 hours to one year. The maximum change is -4.8% from the BGG equation when annual averages are used. (Note that the BGG equation has a quadratic dependence in wind speed which would produce greater sensitivity to averaging.) The LH and RH equations show lower maximum errors with the LH maximum error occuring for one month averages. Results for all three equations are within the 5% error found by Jobson (1972). The reason for this modest error is the use of a dynamic model which allows the feedback between water temperature and evaporation to take place as discussed earlier. Jobson used bulk or static calculations to arrive at his result and thus should expect more error.

Table 4.9: Data Averaging Results

Eqn.	Data Averaging Period				
	3 hour	1 day	1 week	4 weeks	1 year
LH	23.39	23.05	22.89	22.82	23.05
BGG	25.20	24.85	24.64	24.56	24.00
RH	26.06	25.76	25.63	25.57	25.02

a) Annual Average Water Loss Rate (cfs)

Eqn.	Data Averaging Period			
	1 day	1 week	4 weeks	1 year
LH	-0.36	-0.74	-0.96	-0.70
BGG	0.29	0.33	0.30	0.85
RH	-0.21	-0.45	-0.53	-0.13

b) Mean Station Intake Error (^{o}F)

(predictions with averaged data-predictions with 3-hr data)

Eqn.	Data Averaging Period			
	1 day	1 week	4 weeks	1 year
LH	0.33	1.61	2.96	16.00
BGG	0.37	1.12	2.07	14.40
RH	0.36	1.36	2.61	15.60

c) Standard Deviation of Intake Temperature (^{o}F)

The temperature results are shown in Tables 4.9b and c. For all three equations the mean error did not exceed $\pm$ 1.0°F (relative to 3-hour reference values) for any averaging period. The standard deviations, however, became large for averaging periods of one month or longer. This leads to the obvious conclusion that the correct transient temperature response can only be modeled using a transient model with transient meteorological input data. Further sensitivity of transient cooling pond response to averaged data is given by Adams and Koussis (1980).

Finally, these three equations were not significantly different in their response to using averaged meteorological conditions. Thus the results presented should be representative of all ten evaporation equations presented in this study.

4.8 Summary of Empirical Testing of Equations and Uncertainty

In this chapter calibration/verification studies of ten evaporation equations using data sets from two cooling ponds, Dresden and Powerton, were undertaken. The calibration/verification results in Tables 4.4 and 4.6 indicated that four equations performed quite well: Meyer, Ryan-Harleman, Rimsha-Donchenko and Throne equations. Note that all but the Meyer equation were developed for heated waterbodies. For this reason, it is suggested in future evaporation studies from cooling impoundments either the calibrated versions of the Ryan-Harleman, Rimsha-Donchenko, or Throne equations be used.

The calibrations performed in this study are not absolute calibrations. Some uncertainty in the hydrothermal modeling, the meteorological

data and computation of the long-wave atmospheric and back radiation terms limit the confidence of the calibrations and water loss predictions. Results from the dispersion sensitivity tests (Section 4.3.1) suggest that uncertainty in hydraulic structure leads to a $\pm$ 3.5% uncertainty in calibrated α and a corresponding uncertainty of $\pm$ 1.5% in evaporation. Assuming that the uncertainites associated with hydraulic structure and the three radiation terms are independent (and thus that combined uncertainty equals the square root of the sum of the squares of the individual uncertainties), the results from Table 4.8 can be used to estimate a combined uncertainty in calibrated α of 16% ($16^2 = 3.5^2 + 6.3^2 + 13.5^2 + 5.2^2$) and a corresponding uncertainty in evaporation of $\pm$ 4.6% ($4.6^2 = 1.5^2 + 1.8^2 + 3.8^2 + 1.0^2$). Because several of the error terms are expected to be negatively correlated, and hence not independent, the above estimates are conservative.

Further studies incorporating data from other cooling ponds (as these become available), preferably in different geographic and climatic conditions than Dresden and Powerton, should help to verify and further reduce uncertainty in these results.

Additionally it was found that a hierarchy in variability of water loss predictions exists. The most variability among the ten equations occurred for static calculations (i.e., when evaporation was calculated from fixed meteorological and water temperature conditions) and the least occurred when a hydrothermal model was used in a closed cycle mode. The feedback between water temperature and evaporation is responsible for the reduced variability. Table 4.7 summarizes these results.

Lastly it was shown that the effects of using averaged meteorological data with a hydrothermal model to estimate long term water consumption were minimal. The most error observed was an underestimate in annual average evaporation by 4.8% when yearly averaging period results were compared to 3-hour averaging period results. Water temperature predictions, on the other hand, were compromised by averaging periods much over a week in length.

CHAPTER 5

FORCED EVAPORATION DIAGRAMS

5.1 Harbeck Diagram for Forced Evaporation

The results of Section 4.7 indicate that consistent estimates of long term water consumption may be made using averaged data. This is dependent upon having an evaporation equation which accurately predicts evaporation. Given such an equation it would be useful if there were some way to predict water loss using long term averaged data without using a dynamic model. The Harbeck Diagram [Harbeck (1964) and Ward (1980)] for estimating forced evaporation due to artificial heat input was an attempt to do this.

This model, based on what is essentially a linearization of the surface heat loss terms, postulates that the relative proportion of evaporative heat loss to evaporative, conductive and back radiative heat loss is independent of the excess temperature rise $\Delta T = T_h - T_n$. Here T_h is the water surface temperature under heated conditions and T_n is the water surface temperature under natural conditions. Assuming that all waste heat input to the impoundment from the power plant is rejected to the atmosphere by a combination of evaporation, conduction and back radiation (i.e., steady state conditions - no change in heat storage) the fraction lost by evaporation can be estimated and converted to water consumption.

There are several shortcomings with this technique and they will be discussed later. It is useful, however, to derive the Harbeck

Diagram (following Ward (1980)) in order to help understand the improvements to this technique suggested later.

Excess evaporation due to a waste heat input is given by

$$\Delta E = E_h - E_n = f(W)(e_s(T_h)-e_a)-f(W)(e_s(T_n)-e_a)) \tag{5.1}$$

where E_h = evaporative mass loss rate from heat loaded conditions, E_n = evaporative mass loss rate under natural conditions, $f(W)$ = some empirical wind speed function not dependent upon water temperature, e_a = vapor pressure of the air and $e_s(T)$ saturated vapor pressure at temperature of the water surface (hot or natural). Rearranging equation (5.1) leaves

$$\Delta E = f(W)(e_s(T_h)-e_s(T_n)) \tag{5.2}$$

Expanding $e_s(T_h)$ in a Taylor series about T_n gives

$$e_s(T_h)-e_s(T_n) \simeq \frac{\partial e_s}{\partial T}\bigg|_{T_n} \cdot \Delta T + O(\Delta T^2) \tag{5.3}$$

where $\partial e_s/\partial T\big|_{T_n}$ is the derivative of the saturated vapor pressure function evaluated at T_n and ΔT is assumed small so that the second order and higher terms are neglected (following both Harbeck and Ward). Finally excess evaporation is given by

$$\Delta E = f(W) \frac{\partial e_s}{\partial T}\bigg|_{T_n} \cdot \Delta T$$

Excess evaporative heat flux is

$$\Delta\phi_e = L\, f(W) \left.\frac{\partial e_s}{\partial T}\right|_{T_n} \cdot \Delta T \tag{5.4}$$

where L = latent heat of vaporization of water.

Excess conductive heat flux is simpler and given by

$$\Delta\phi_c = \gamma L f(W)(T_h - T_a) - \gamma L f(W)(T_n - T_a) \tag{5.5}$$

where $\gamma = (0.61 \times 10^{-3}\ ^oC^{-1})P_a$ (see Equation (2.13)), P_a = atmospheric pressure (units are consistent with f(W)) and T_a is the air temperature. Equation (5.5) reduces to

$$\Delta\phi_c = \gamma L f(W) \cdot \Delta T \tag{5.6}$$

The excess back radiative heat flux is

$$\Delta\phi_{br} = 0.97\sigma[(T_h + 273)^4 - (T_n + 273)^4] \tag{5.7}$$

using the Stephan-Boltzmann relationship and where σ = Stephan-Boltzmann constant and the temperatures are in ^oC. Ward linearized Equation (5.7) to

$$\Delta\phi_{br} = 0.97\sigma\, g(T_n)\Delta T \tag{5.8}$$

where

$$g(T_n) = 8.14 \times 10^7 + 8.94 \times 10^5\, T_n \tag{5.9}$$

in units of $^oK^3$ (T_n in ^oC). Ward estimates the total error in this linearization to be 5% for $T_n = 30^oC$ and $\Delta T = 5^oC$ and decreasing as T_n and ΔT decrease.

Combining Equations (5.4), (5.6) and (5.9) the ratio of excess evaporation to excess total heat loss, $\Delta\phi_e/\Delta\phi_\ell = \Delta\phi_e/(\Delta\phi_e + \Delta\phi_c + \Delta\phi_{br})$, is

$$\frac{\Delta\phi_e}{\Delta\phi_\ell} = \frac{Lf(W)\left.\frac{\partial e_s}{\partial T}\right|_{T_n}}{Lf(W)\left\{\left.\frac{\partial e_s}{\partial T}\right|_{T_n} + \gamma\right\} + 0.97\sigma\, g(T_n)} \tag{5.10}$$

Note that any dependence on the excess temperature, ΔT, has been eliminated. This was possible because of two assumptions: 1) small ΔT so that $O(\Delta T^2)$ terms in expansions could be dropped and $\partial e_s/\partial T$ could be evaluated at T_n and 2) that f(W) does not depend upon the water surface temperature.

As an example, take $f(W_2)$ to be 1.11 times the Lake Hefner evaporation equation (2.42). Figure 5.1 shows Equation (5.10) plotted vs. T_n using this evaporation equation and is referred to as a Harbeck Diagram. The slope of the vapor pressure curve is given by

$$\left.\frac{\partial e_s}{\partial T}\right|_{T_n} = \frac{5278.2}{(T_n+273)^2} \cdot e_s(T_n) \quad \left(\frac{\text{mbar}}{^oC}\right) \tag{5.11}$$

where T_n is in ^oC and e_s is in mbar. Also P_a = 1000 mbar, L = 597 cal/gm and $\sigma = 1.171 \times 10^{-7}$ cal/cm^2-day-$^oK^4$. To use the diagram one must have an estimate of T_n, which along with T_h must be assumed uniform over the entire water surface, and one must know the plant heat rejection rate, H,

$$H = \rho c Q \Delta T_o \tag{5.12}$$

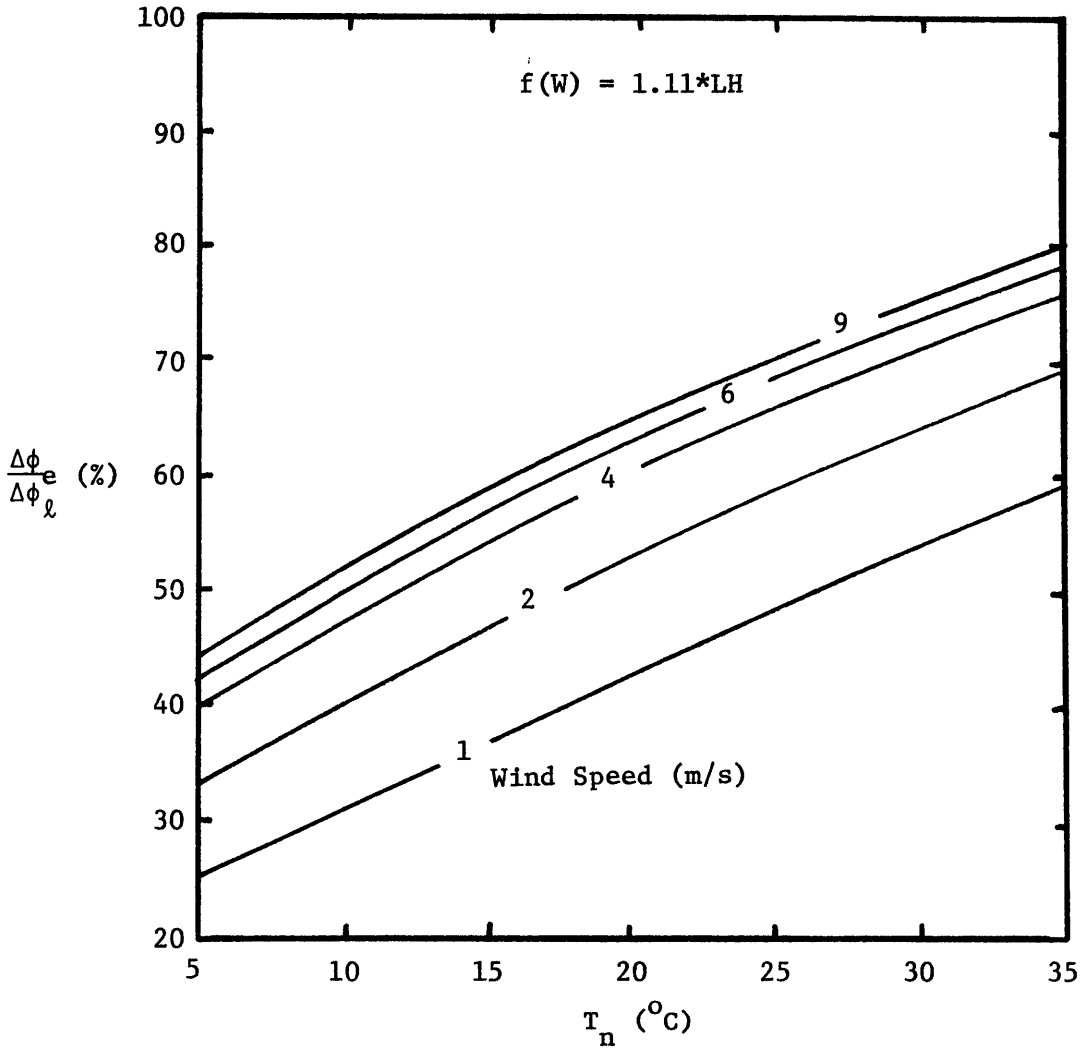

Figure 5.1: Harbeck Diagram for Forced Evaporation (1.11*LH Equation).

where ρ = density of water, c = specific heat of water, Q = condenser flow rate and ΔT_o = temperature rise across the condensers. Since T_n is not always known a priori it may be estimated from either the equilibrium temperature, T_e (discussed in Section 5.3), or the air temperature T_a. With an estimate for T_n one can then get from the Harbeck Diagram the fraction of heat input lost as evaporation, $\Delta\phi_e/\Delta\phi_\ell$. Multiplying this number by H and converting to water mass or volume one then has an estimate for the forced evaporative loss due to the heat input.

5.2 Weaknesses of Harbeck Diagram

The Harbeck Diagram is a simple tool for estimating water loss by forced evaporation, but it has several shortcomings already mentioned. One is that ΔT is small enough so that the expansion of $e_s(T_h)$ around T_n and subsequent truncation (dropping of $O(\Delta T^2)$ terms) did not introduce much error. Based upon Ward's (1980) results ΔT must be less than about 5^oC so that the error between the Harbeck diagram and result one would get using the full non-linear formulae (Equation (5.2), (5.6) and (5.7)) is less than about 5%. For ΔT around 10^oC the error is 10% or greater. Typically ΔT for a modern cooling facility is on the order of 10^oC or more for the majority of the year. Thus significant "intrinsic" error due to the linearization and truncation could result.

Secondly, in order to insure that any dependence upon the excess temperature, ΔT, is eliminated no evaporation equation with a windspeed function which depends on the water surface temperature could be used. Only simple functions of the Dalton Law type are permissible. Thus one

cannot use the Ryan-Harleman equation (2.48) or Rimsha-Donchenko equations (2.47) which were suggested for use in cooling impoundment studies in Chapter IV.

In the next two sections an improvement upon the Harbeck Diagram which will take into account these two shortcomings will be suggested.

5.3 Linearized Surface Heat Transfer

The Harbeck Diagram concept linearizes the surface heat transfer and as such is a version of the linearized surface heat transfer formulations developed by Edinger and Geyer (1965) and improved by Ryan, Harleman and Stolzenbach (1974). The net surface heat transfer from a water surface, ϕ_n, is given by

$$\phi_n = \phi_r - \phi_\ell$$

where

$$\phi_\ell = \phi_e + \phi_c + \phi_{br} \tag{5.13}$$

and ϕ_r = net incident shortwave solar and longwave atmospheric radiation.

Following Ryan et al. (1974) we define the surface heat transfer coefficient, K, as

$$K = -\frac{\partial \phi_n}{\partial T_s} = \frac{\partial \phi_\ell}{\partial T_s}$$

where T_s = water surface temperature. Given the definitions

$$\phi_e = Lf(W)(e_s(T_s)-e_a),$$

$$\phi_c = \gamma Lf(W)(T_s-T_a)$$

and

$$\phi_{br} = 0.97\sigma(T_s{}^a)^4$$

where T^a signifies absolute units of temperature, we can determine K to be

$$K = 3.88\sigma {T_s}^{a^3} + Lf(W)\left[\frac{\partial e_s}{\partial T_s}\bigg|_{T_s} + \gamma\right] + \frac{\partial f(W)}{\partial T_s}\bigg|_{T_s} \cdot L \cdot [e_s(T_s)-e_a + \gamma(T_s-T_a)] \tag{5.14}$$

A general windspeed function which may depend upon the water surface temperature has been allowed and therefore the last term involving $\frac{\partial f(W)}{\partial T_s}$ must be kept. Figure 5.2 illustrates the relation between K and T_s. An incremental change in the water surface temperature will cause an incremental change in ϕ_n.

Net surface heat transfer can be estimated by

$$\phi_n = -K(T_s-T_e) \tag{5.15}$$

where T_e is the equilibrium temperature. T_e is defined as the water surface temperature at which net surface heat transfer is zero and is found by iteratively solving

$$\phi_n = 0 = \phi_r - Lf(W)(e_s(T_e)-e_a) - L\gamma f(W)(T_e-T_a) - 0.97\sigma {T_e}^{a^4} \tag{5.16}$$

for T_e for a given set of atmospheric conditions.

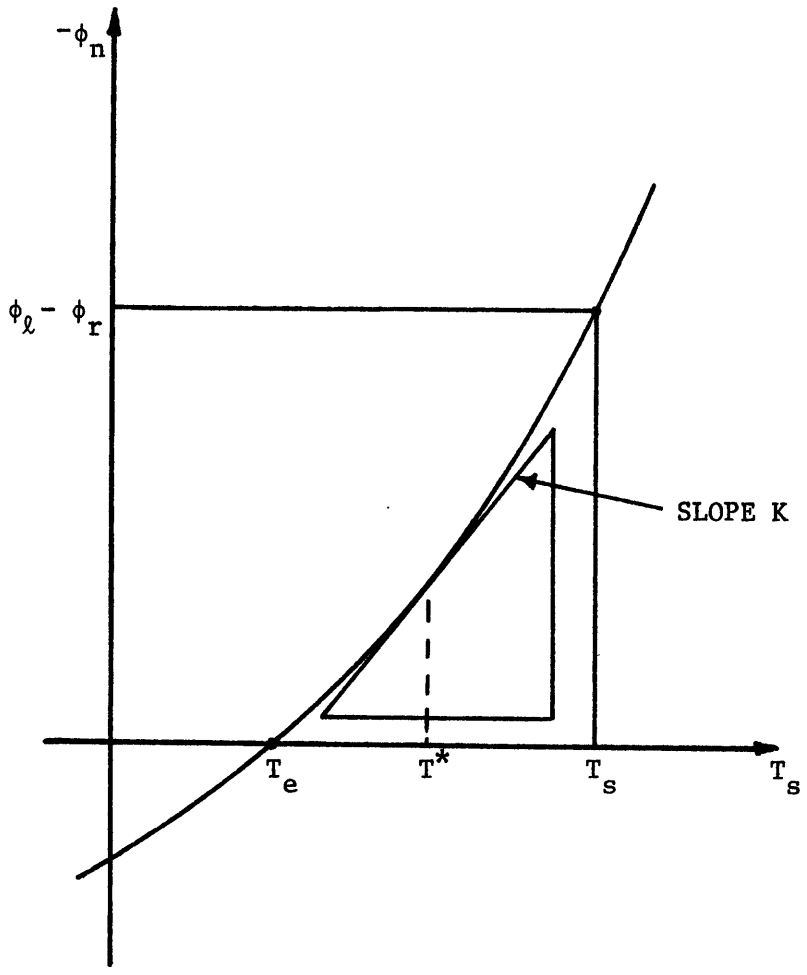

Figure 5.2: Relationship Between ϕ_n, K and T_s.

When computing K from Equation (5.14) Ryan and Harleman (1973) suggest that K be evaluated at

$$T^* = (T_s + T_e)/2 \tag{5.17}$$

This helps reduce errors associated with the non-linearity of the ϕ_n vs. T_s curve.

Figures 5.3, 5.4 and 5.5 show plots of K vs. wind speed at 2 meters and T^* for several values of T_s-T_a. The wind speed function was taken to be 0.79 times the RH wind speed function (equation (2.48)) based on the results of Chapter IV. It was necessary to make several figures because the dependence upon the surface temperature and the air temperature could not be eliminated. The relative humidity used in making these plots was 75%. An error of less than 7% occurs if the relative humidity is between 50 and 100%.

These figures may also be used to estimate the excess temperature rise, $\Delta T = T_h-T_n$, a fully mixed body of water will incur for a given artificial heat input rate, H (Equation (5.12)). Assuming steady-state conditions, Ryan et al. (1974) give

$$-\Delta\phi_n = \frac{H}{A} \tag{5.18}$$

Here $\Delta\phi_n$ is the excess surface heat transfer caused by a temperature rise above natural conditions and A is the water surface area. The excess heat transfer is given by

$$\Delta\phi_n = -K(T_h-T_n) \tag{5.19}$$

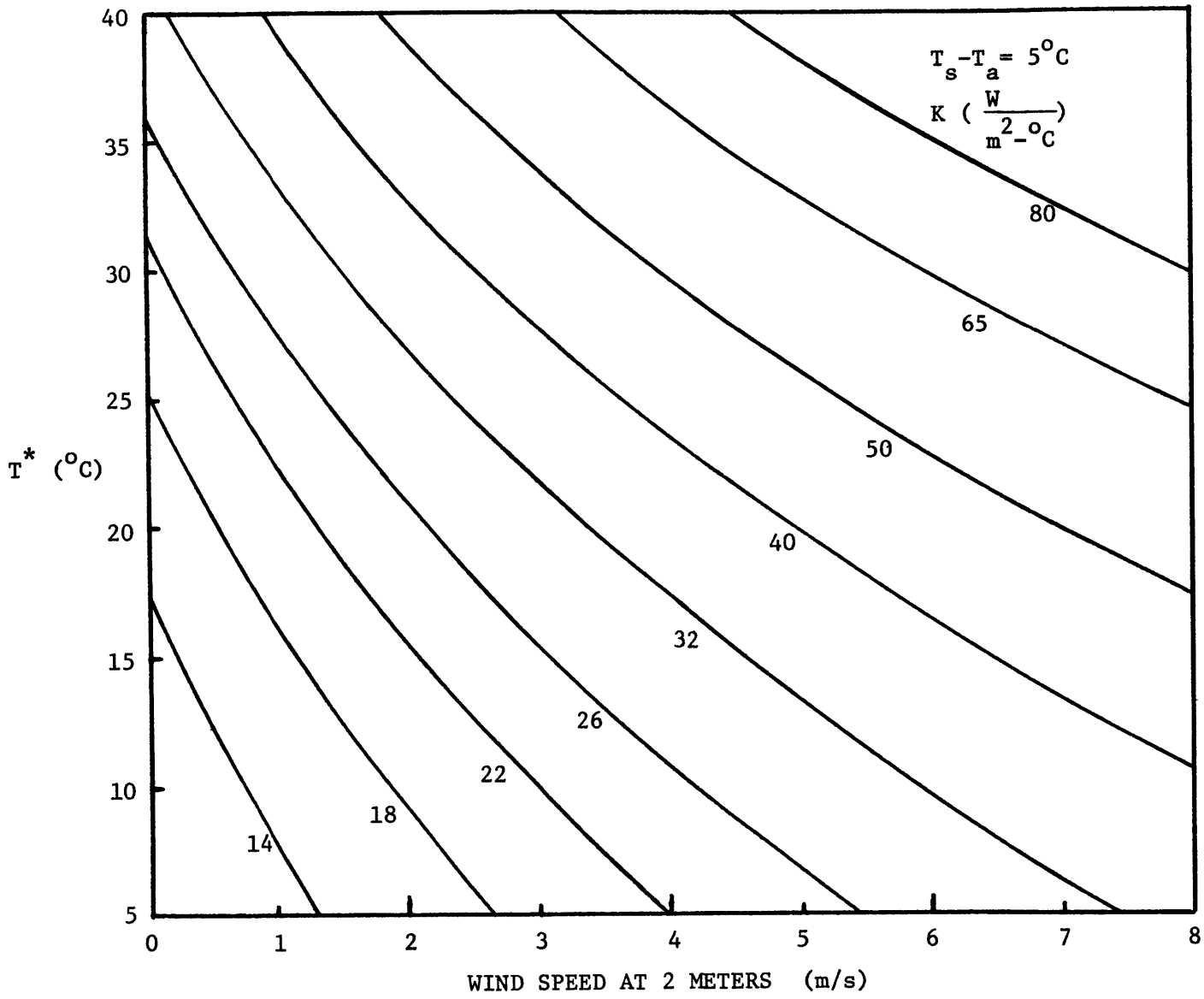

Figure 5.3: Heat Exchange Coefficient, K, for Heated Water Surface ($T_s - T_a = 5^oC$). f(W)=0.79*RH. Relative Humidity = 75%.

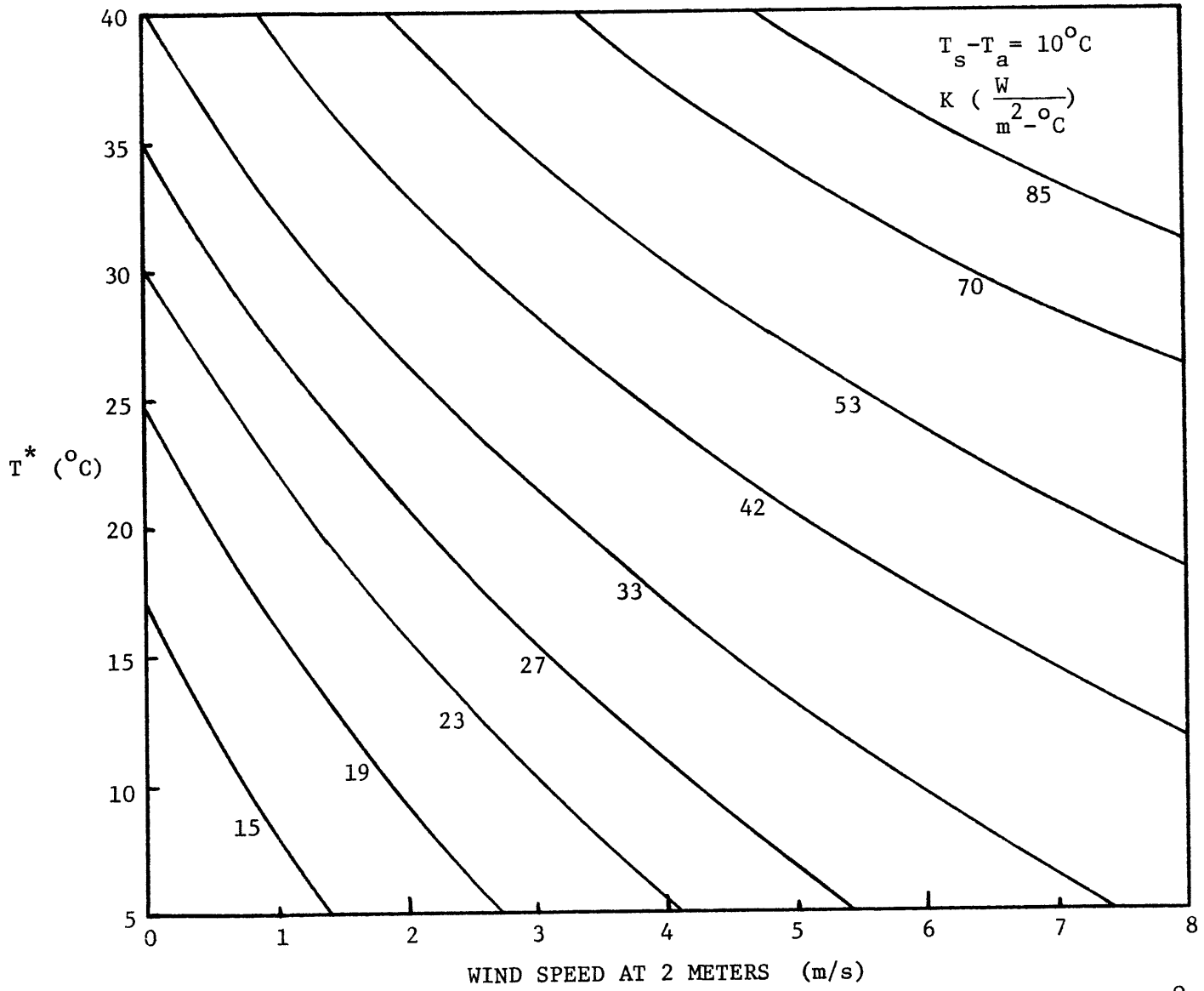

Figure 5.4: Heat Exchange Coefficient, K, for Heated Water Surface ($T_s - T_a = 10^oC$). f(W)=0.79*RH. Relative Humidity = 75%.

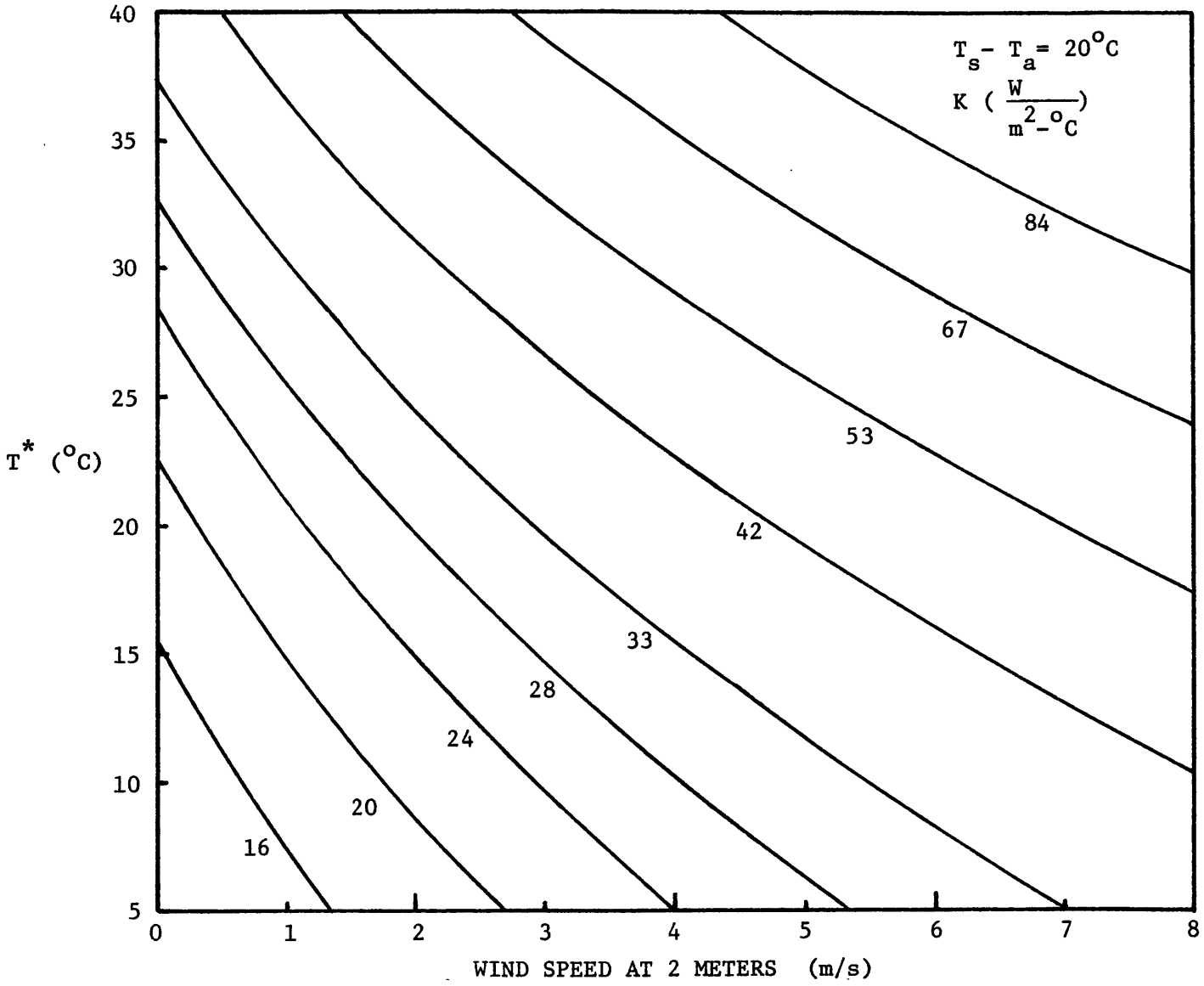

Figure 5.5: Heat Exchange Coefficient, K, for Heated Water Surface ($T_s - T_a = 20^oC$) f(W)=0.79*RH. Relative Humidity = 75%.

where K is evaluated at $T^* = (T_h - T_n)/2$. With Equation (5.19) we have

$$\Delta T = \frac{H}{KA} \tag{5.20}$$

Given H, W_2, T_a and T_n (may be assumed equal to T_e or T_a if not available) ΔT is found iteratively as follows:

1) Assume a value for ΔT
2) Calculate $T^* = T_n + \Delta T/2$
3) Enter figure which corresponds closest to

$$T_s - T_a = T_n - T_a + \Delta T$$

and find value for K.

4) Use Equation (5.20) to calculate new ΔT
5) Compare new ΔT to old value and return to (2) until desired accuracy is achieved.

5.4 Improved Forced Evaporation Diagrams

In Section 5.2 some weaknesses of the Harbeck Diagram were pointed out. Improvement can be made using the concepts of the last section. Notice that the denominator of Equation (5.10)

$$\Delta\phi_\ell = \{Lf(W)\ [\frac{\partial e_s}{\partial T}\Big|_{T_n} + \gamma] + 0.97\ \sigma g(T_n)\}\Delta T$$

is a version of the linearized excess heat loss given in Equation (5.19) with $\Delta\phi_n = -\Delta\phi_\ell$ and the heat loss coefficient, K, given by the quantity in braces. This K is very similar to Equation (5.14) except that (5.14) is more complicated and retains a dependence upon the water surface temperature.

One may easily define a heat transfer coefficient for evaporation as

$$K_e = \frac{\partial \phi_e}{\partial T_s} \tag{5.21}$$

From the Harbeck Diagram results it is easily shown that K_e is just the numerator of Equation (5.10). An improvement is made, though, if one defines K_e using the method of Section 5.3. Thus

$$K_e = Lf(W)\ \frac{\partial e_s}{\partial T_s}\Big|_{T_s} + L\ \frac{\partial f(W)}{\partial T_s}\Big|_{T_s} (e_s(T_s)-e_a) \tag{5.22}$$

For excess evaporative transfer caused by a temperature rise above natural we have

$$\Delta\phi_e = K_e(T_h-T_n) \tag{5.23}$$

where K_e is evaluated at $T^* = (T_h+T_n)/2$.

Using Equation (5.19) and (5.23) the fraction of evaporative heat loss to evaporative, conductive and back radiative heat loss is simply

$$\frac{\Delta\phi_e}{\Delta\phi_\ell} = \frac{K_e}{K}$$

or

$$\frac{\Delta\phi_e}{\Delta\phi_\ell} = \frac{Lf(W)\left.\frac{\partial e_s}{\partial T_s}\right|_{T^*} + L\left.\frac{\partial f(W)}{\partial T_s}\right|_{T^*}(e_s(T^*)-e_a)}{3.88\sigma T^{a^{*3}} + Lf(W)\left[\left.\frac{\partial e_s}{\partial T_s}\right|_{T^*} + \gamma\right] + \left.\frac{\partial f(W)}{\partial T_s}\right|_{T^*} L\,[e_s(T^*)-e_a + \gamma(T^*-T_a)]} \tag{5.24}$$

This version is an improvement over the Harbeck Diagram (Equation (5.10)) because it allows the use of a windspeed function which depends upon water temperature and because the error associated with truncation on linearization is reduced by evaluating $\partial e_s/\partial T_s$ at T^* instead of T_n.

Because of these improvements it was necessary to construct several forced evaporation diagrams for different values of T_h-T_n. Figure 5.6, 5.7 and 5.8 are the diagrams for $\Delta\phi_e/\Delta\phi_\ell$ vs. T_n using 0.79 times the Ryan-Harleman evaporation equation. For low wind speed these improved diagrams show significantly higher forced evaporative fractions than the Harbeck Diagram (Figure 5.1). This is due to the influence of buoyant free convection accounted for with the RH equation but not in the LH equation. One might also note the near linearity of the curves for a given wind speed. This implies results obtained by these diagrams should be insensitive to the averaging period used.

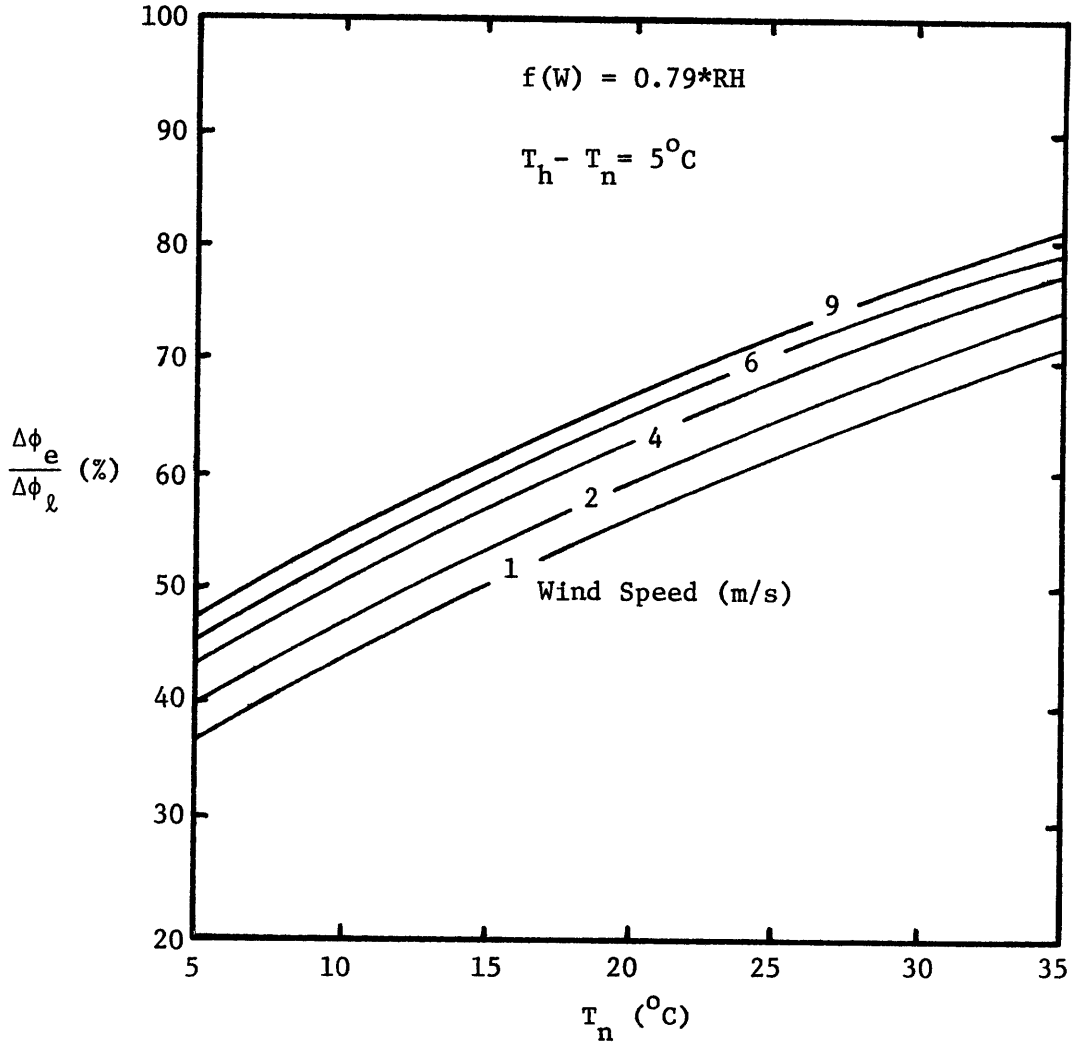

Figure 5.6: Forced Evaporation Diagram (T_h-T_n=5°C). f(W)=0.79*RH Equation.

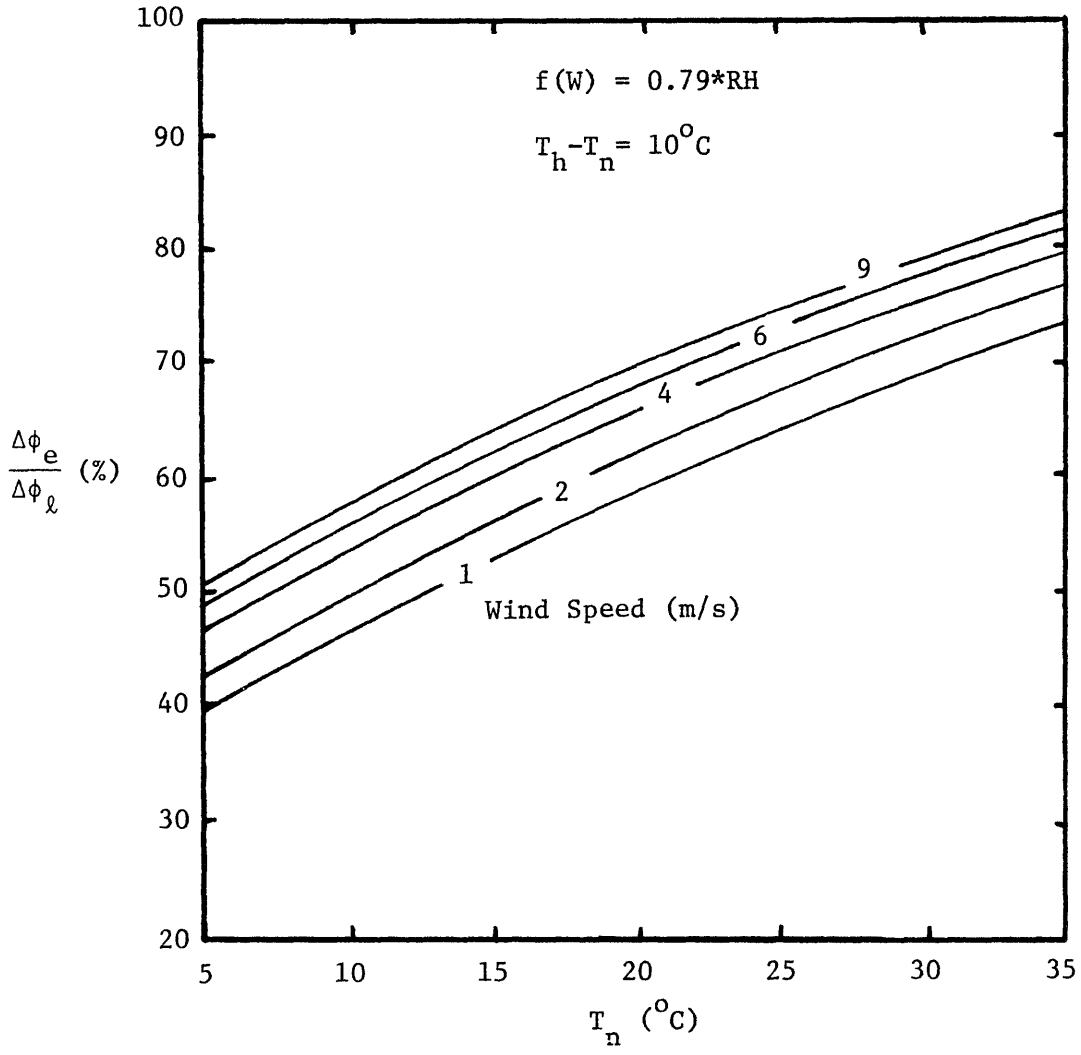

Figure 5.7: Forced Evaporation Diagram ($T_h - T_n = 10^oC$). f(W)=0.79*RH Equation.

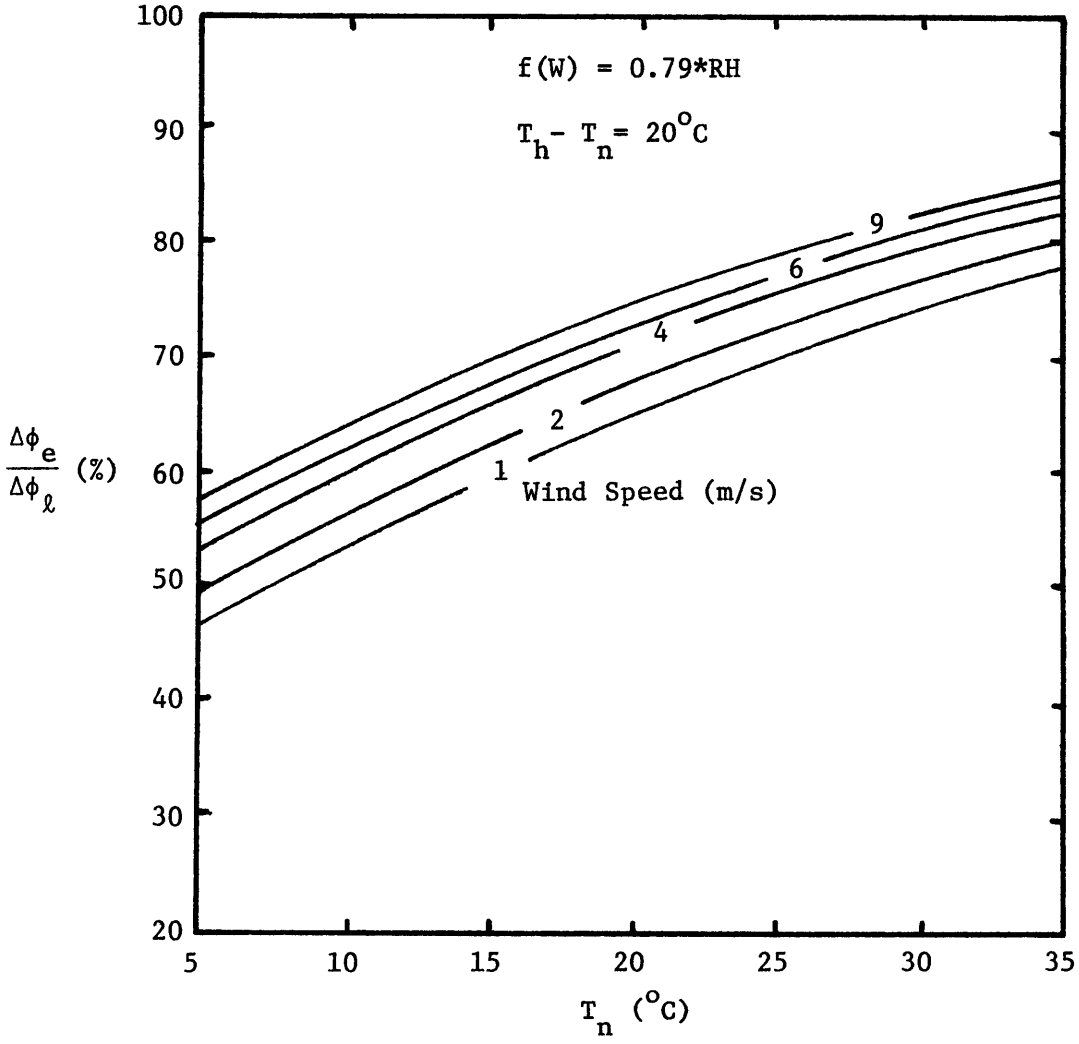

Figure 5.8: Forced Evaporation Diagram (T_h-T_n=20°C). f(W)=0.79*RH Equation.

5.5 Example Application of Improved Forced Evaporation Diagrams

Using the Moline, Illinois meteorological data and the hypothetical pond structure (Dresden Pond) of Section 4.7 an application of the improved forced evaporation diagrams (Figure 5.6, 5.7 and 5.8) is shown in Table 5.1. These results are obtained with the improved diagram using the Moline data for three month averaging periods and for the annual average met conditions. The pond characteristics are: A = 516 hectares (1275 acres), Q = 51 m^3/s (1800 cfs) and ΔT_o = 11.1°C (20°F). Thus H/A = 459 W/m^2. These results were obtained as follows:

1) Determine ΔT as discussed in Section 5.3 using $T_n = T_a$ and W_2 given in the met data.
2) Use appropriate diagram (Figure 5.6, 5.7 or 5.8) based upon ΔT calculated in (1) along with $T_n = T_a$ and W_2 to determine $\Delta\phi_e/\Delta\phi_\ell$.
3) Forced evaporative water loss, ϕ_e, is given by

$$\phi_e = H \frac{(\Delta\phi_e/\Delta\phi_\ell)}{100} \frac{1}{L\rho}$$

It should be noted that the forced water loss rate of 0.53 m^3/s determined by averaging the four three-month period results is only slightly less ($\sim$ 5%) than the result obtained by using the annual average met conditions (0.56 m^3/s). The near linearity of the forced evaporation curves is the reason for this. In the following section, these estimates, based on the diagrams, are compared with evaporation estimates obtained with the dynamic hydrothermal model.

Table 5.1: Forced Evaporative Loss Rate Results Using the Improved Diagrams and Moline, Illinois Meteorological Data

3-month Period	T_a(°C)	W_2(m/s)	ΔT(°C) (From Fig. 5.3,5.4 & 5.5)	$\Delta\phi_e/\Delta\phi_\ell$(%)	Forced Evap. Water Loss Rate (m^3/s)
JFM	-4.3	1.87	27	34	0.34
AMJ	17	1.81	15	63	0.62
JAS	21.2	1.36	14	68	0.67
OND	4.8	1.70	15	49	0.48
Average of above Results			17.75	54	0.53
Annual Average of Met Data	9.9	1.71	20	55	0.56

5.6 Comparison of Improved Diagrams with Harbeck Diagram and Dynamic Model Predictions

Table 5.2 compares the results obtained using the Harbeck Diagram, the improved diagrams and the dynamic model. The dynamic results were determined assuming a Dresden Pond type configuration (see Section 4.3.1). Forced Evaporation was computed as the difference between total water consumption for runs of $\Delta T_o = 11.1^oC$ (heat loaded) and $\Delta T_o = 0$ (no station loading). For both cases the evaporation equation was 0.79 times the Ryan-Harleman Equation.

On an annual average basis the improved diagrams predicted nearly

Table 5.2: Comparison of Harbeck Diagram, Improved Diagrams and Dynamic Model Estimates of Forced Evaporation

3-month Period	Forced Water Loss Rate (m^3/s)		
	Harbeck Diagram*	Improved Diagrams**	Dynamic Model***
JFM	0.18	0.34	0.41
AMJ	0.46	0.62	0.68
JAS	0.51	0.67	0.70
OND	0.32	0.48	0.49
Average of 3-Month Results	0.37	0.53	0.57
Annual Average Met Data Results	0.38	0.56	----

*f(W) = 1.11 LH; no dependence on ΔT

**f(W) = 0.79 RH; dependence on ΔT retained through iteration

***f(W) = 0.79 RH; numerical time step of 3-hr used

the same forced water loss rate as the dynamic model (0.56 m^3/s vs. 0.57 m^3/s). The Harbeck Diagram, using the LH equation calibrated for evaporation for heated impoundments, gave results significantly below the dynamic model (0.38 m^3/s vs. 0.57 m^3/s). The reason for this poor result is that the Harbeck Diagram retains no dependence upon the water surface temperature. From the results of Chapter IV it was shown that the feedback between water surface temperature and evaporation is very strong. The improved diagrams retain this dependence. The excess temperature rise, ΔT, is a function of the evaporation and had to be found iteratively before the forced evaporative fraction could be determined.using the improved diagrams.

In summary, it is felt that the new technique for estimating forced evaporation, while requiring slightly more effort, will give more accurate results because the water temperature-evaporation feedback is retained. Additionally this new technique allows the use of wind speed functions which depend upon the water surface temperature. It is not necessary, however, to use a wind speed function which depends on water temperature. Figures similar to 5.3, 5.4 and 5.5 may be generated with any f(W) using equation (5.14) and corresponding forced evaporation diagrams, Figures 5.6, 5.7 and 5.8, from equation (5.20) can be produced. Because of the feedback,low variability of forced evaporation predictions made using the new technique with several different wind speed functions is expected.

CHAPTER 6

CONCLUSION

Despite many advantages of cooling ponds over cooling towers their use is somewhat limited because of a lack of confidence in the ability to predict various aspects of their hydrothermal performance and consumptive water use. This report focussed upon evaporation, which is related to both pond performance and consumptive water use as illustrated in Figure 1.1. The objective was to improve the understanding and quantification of cooling pond evaporation.

Theoretical and empirical considerations were discussed in an effort to improve, or at least bring forth, several important aspects of the underlying physics of evaporation. Key among them was the role of buoyancy enhanced heat and mass transfer. Buoyancy influences are particularly important with respect to cooling impoundments because of the elevated water surface temperatures which characterize them. It is primarily for this reason that evaporation equations developed for natural waterbodies in general perform poorly when applied to cooling ponds. Further study on the buoyancy effect, specifically the interaction of free and forced convection, is warranted since present parameterizations are lacking a solid theoretical basis.

Because of the functional dependence of evaporation upon water surface temperature any attempt to assess cooling impoundment evaporation must employ hydrothermal models. The commonly used bulk energy or water budget techniques to estimate evaporation do not capture the relevant spatial and temporal scales of impoundment water temperature

and therefore evaporation which are characteristic of cooling impoundments. Use of such models either in interpretation of existing field data on evaporation (as was done in this report) or in predicting evaporation at future sites is seen as an improvement in our ability to quantify evaporation.

Analysis of the predictive ability of ten evaporation equations, representing three categories of functional dependence: Dalton Law, Modified Dalton Law and Stability Dependent, with data sets from Dresden Pond and Powerton Pond was undertaken. The calibration/verification and water consumption results are shown in Tables 4.4 and 4.6. Four equations performed quite well: Meyer, Ryan-Harleman, Rimsha-Donchenko and Throne. The last three were developed specifically for evaporation from heated waterbodies and therefore the calibrated versions of these three are recommended for future use in cooling impoundment studies. In terms of their theoretical basis the Ryan-Harleman equation is the most satisfactory. The confidence of the calibrations (values of α in equation 4.1 as given in Table 4.4) is estimated at about 15%. Corresponding water consumption estimates are estimated to be within $\pm$ 5%.

These numbers were arrived at partially by assessing the sensitivity of the calibration and water consumption results (Table 4.8) to uncertainty in the pond hydraulic structure and the remaining surface heat flux terms of which long-wave atmospheric radiation is the most questionable. Improvement upon the calibration/verification results would most likely occur 1) if studies utilizing data from other cooling ponds (as

these becomes available) were undertaken and 2) if uncertainty due to the long-wave atmospheric radiation component was reduced by using direct measurements instead of calculations.

It was also shown that a hierarchy of variability in water consumption estimates exists (see Table 4.7) due to the feedback between water temperature and evaporation. The most variability among equation estimates is found when evaporation was calculated from fixed meteorological and water temperatures (i.e., no feedback permitted) and the least variability occured when a hydrothermal model was used in a closed cycle mode (i.e., most feedback allowed). However, corresponding water temperature predictions using a closed hydrothermal model in a closed cycle mode still exhibited significant variability.

Use of long-term average meteorological conditions was shown to only cause a small error (< 5%) in water consumption estimates compared to results obtained using more dynamic meteorology (see Table 4.9). Water temperature estimates, of course, are compromised by using averaged data.

Lastly,an improved method similar to the Harbeck Diagram [Harbeck (1964) and Ward (1980)] for estimating forced evaporation was developed in order to retain the important water temperature-evaporation feedback. Comparison with a dynamic model utilizing full non-linear surface heat transfer relations showed excellent agreement on an annual average basis. The Harbeck Diagram performed quite poorly and the new technique is suggested for future use in order to obtain first cut estimates of annual forced water consumption.

REFERENCES

1. Aase, J.K. and Idso, S.B., "A Compariosn of Two Formula Types for Calculating Long-Wave Radiation From the Atmosphere," Water Resour. Res., Vol. 14, p. 623, 1978.

2. Adams, E.E. and Koussis, A.D., "Transient Analysis for Shallow Cooling Ponds," Journal of the Energy Division, ASCE, Vol. 106, No. EY2. October 1980, pp. 141-153.

3. Bowen, I.S., "The Ratio of Heat Losses by Conduction and by Evaporation From Any Water Surface," Physical Rview, Vol. 27, p. 779-87, June 1926.

4. Brady, K.D., Graves, W.L. and Geyer, J.C., "Cooling Water Studies for Edison Electric Institute, Proj. No. RP-49- Surface Heat Exchange at Power Plant Cooling Lakes," The Johns Hopkins University, 1969.

5. Brocard, D.N., Jirka, G.H. and Harleman, D.R.F., "A Model for the Convective Circulation in Side Arms of Cooling Lakes," R.M. Parsons Laboratory, Technical Report No. 223, MIT, March 1977.

6. Brutsaert, W., "On a Deriveable Formula for Long-Wave Radiation from Clear Skies," Water Resour. Res., Vol. 11, p. 742, 1975.

7. Businger, J.A. et al., "Flux-Profile Relationships in the Atmospheric Surface Layer," Jour. of the Atmos. Sciences, Vol. 28, p. 181-189, 1971.

8. Davenport, A.G., "The Dependence of Wind Loads on Meteorological Parameters," Proc. of Internat. Research Seminar on Effects of Winds on Buildings and Structures, Vol. 1, Ottawa, Canada, September 1967.

9. Dyer, A.J., "A Review of Flux-Profile Relationships," Boundary Layer Meteorology, Vol. 7, p. 363-372, 1974.

10. Dyer, A.J. and Hick, B.B., "Flux-Gradient Relationships in the Constant Flux Layer," Quart. J. Roy. Meteorol. Soc., Vol. 96, p. 715-721, 1970.

11. Edinger, J.R. and Geyer, J.C., "Cooling Water Studies for Edison Electric Institute, Project No. RP-49-Heat Exchange in the Environment," The Johns Hopkins University, 1965.

12. Fischer, H.B., "The Mechanics of Dispersion in Natural Streams," Journal of the Hydraulics Div., ASCE, Vol. 93, No. HY6, 1967.

13. Fraedrich, K., "On the Evaporation from a Lake in a Warm and Dry Environment," Tellus, Vol. 24, p. 116-121, 1972.

14. Geiger, R., The Climate Near the Ground, Harvard University Press, Cambridge, Mass., 1965.

15. Gloyne, R.W., "A Note on the Measurement and Estimation of Evaporation," Meteorological Magazine, Vol. 100, No. 1189, p. 322, 1971.

16. Godbey, A.L., "Evaporation Determined from Energy and Water Balances at Two Heated Ponds," M.S. Thesis, Department of Civil Engineering, MIT, June 1981.

17. Goodling, J.S., Sill, B.L. and McCabe, W.J., "An Evaporation Equation for an Open Body of Water Exposed to the Atmosphere," Water Resources Bulletin, Vol. 12, No. 4., p. 843-853, 1976.

18. Hadlock, R.K. and Abbey, O.B., "Thermal Performance and Water Utilization Measurements on Ultimate Heat Sinks--Cooling Ponds and Spray Ponds," prepared for Division of Reactor Safety Research, Office of Nuclear Regulatory Research, U.S. Nuclear Regulatory Commission, draft report, January 1981.

19. Harbeck, G.E., "The Lake Hefner Water Loss Investigation," USGS Circular 229, 1952.

20. Harbeck. G.E., "A Practical Field Technique for Measuring Reservoir Evaporation Utilizing Mass-Transfer Theory," USGS Prof. Paper No. 272-E, 1962.

21. Harbeck, G.E., "Estimating Forced Evaporation from Cooling Ponds," Journal of the Power Division, ASCE, Vol. 90, No. PO3, pp. 1-9, 1964.

22. Harbeck, G.E. et al., "Water Loss Investigations: Lake Mead Studies," USGS Prof. Paper 298, 1958.

23. Hicks, B.B. and Hess, G.D., "On the Bowen Ratio and Surface Temperature at Sea," Journal of Physical Oceanography, Vol. 7, p. 141-145, 1977.

24. Hicks, B.B. and Wesely, M.L., "An Examination of Some Bulk Formulae Used for Assessing the Performance of Industrial Cooling Ponds," in 1974 Annual Report of Radiological and Environmental Research Division, Argonne National Lab., ANL-75-60 Part IV, 1975.

25. Hicks, B.B., Wesely, M.L. and Sheih, C.M., "Eddy-Correlation Measurements over a Cooling Pond with Limited Fetch," in 1974 Annual Report of Radiological and Environmental Research Division, Argonne National Laboratory, ANL-75-60, Part IV, 1975.

26. Hicks, B.B. et al., "A Study of Heat Transfer Processes Above a Cooling Pond," Water Resources Research, Vol. 13, No. 6, Dec. 1977.

27. Idso, S.B., "A Set of Equations for Full Spectrum and 8- to 14-μm and 10.5- to 12.5-μm Thermal Radiation from Cloudless Skies," Water Resour. Res., Vol. 17, p. 295, 1981.

28. Idso, S.B. and Jackosn, R.D., "Thermal Radiation from the Atmosphere," Jour. Geo. Res., Vol. 74, p. 5397, 1969.

29. Jirka, G.H. et al., "Mathematical Predictive Models for Cooling Ponds and Lakes Part A: Model Development and Design Considerations," R.M. Parsons Laboratory, Technical Report. 238, MIT, December 1978.

30. Jirka, G.H. and Watanabe, M., "Thermal Structure of Cooling Ponds," Journal of the Hydraulics Division, ASCE, Vol. 106, No. HY5, May 1980.

31. Jobson, H.E., "Canal Evaporation Determined by Thermal Modeling," Symposium of Modeling Techniques, Waterways, Harbors and Coastal Engr. Div., ASCE, p. 729, September 1975.

32. Jobson, H.E., "Effect of Using Averaged Data on the Computed Evaporation," Water Resour. Res., Vol. 8, p. 513, 1972.

33. Kohler, M.A., "Lake and Pan Evaporation in Water Loss Investigations - Lake Hefner Studies, Technical Report," USGS Prof. Paper 269, 1954.

34. Littleton Research and Engineering Corp., "An Engineering Economic Study of Cooling Pond Performance," EPA-14-12-521, 1970.

35. Mangarella, P.A. et al., "Energy and Mass Transfer Through an Air-Water Interface," Dept. of Civil Engr., Stanford Univ., Technical Report No. 134, May 1971.

36. McAdams, W.H., Heat Transmission, McGraw-Hill Book Company, New York, 3rd Edition, 1954.

37. McMillan, W., "Cooling from Open Water Surfaces: Final Report Part 1: Lake Trawsfynydd Cooling Investigation, NS/SSD/RR/1204/73, North Western Region Scientific Services Division, CEGB, Sept. 1973.

38. McNaughton, K.G., "Evaporation and Advection I: Evaporation from Extensive Homogeneous Surfaces," Quart. J. Meteorol. Soc., Vol. 102, p. 181-191, 1976.

39. Meyer, A.F., "Evaporation from Lakes and Reservoirs," Minnesota Resources Comm., St. Paul, Minn., June 1942.

40. Mitry, A.M. and Sill, B.L., "A Model for Prediction of Evaporative Heat Flux in Large Bodies of Water," Proc. of the Second Conf. on Waste Heat Mgmt. and Util., P. VII-B-109, December 1978.

41. Monin, A.S. and Yaglom, A.M., Statistical Fluid Mechanics: Mechanics of Turbulence, Vol. 1, MIT Press, Cambridge, Mass. 1971.

42. Moy, H.C. and Sanghani, "Experimental Evaluation of Water Surface Heat Exchange," presented at AIChE-ASME Heat Transfer Conference, Salt Lake City, Utah, August 1977.

43. NUS Corporation, "Temperature Distribution in Dresden Pond," 1976a.

44. NUS Corporation, "Temperature Distribution in Powerton Pond," 1976b.

45. Nystrom, J.B. and Hecker, G.E., "Experimental Evaluation of Water to Air Heat Transfer Equations," paper presented at ASCE Annual Convention, Denver, CO, 1975.

46. Octavio et al., "Mathematical Predictive Models for Cooling Ponds and Lakes Part B: User's Manual and Applications of MITEMP," R.M. Parsons Laboratory, Technical Report 262, MIT, April 1980.

47. Pagenkopf, J.R. and Fong, H.L.M., "Assessment of Hydrothermal Models for Cooling Impoundment Ecosystem Analysis," presented at the Minnesota Lakes Conference, ASCE, Minneapolis, Minn., June 1981.

48. Paily, P.P., Macagno, E.O. and Kennedy, J.F., "Winter Regime Surface Heat Loss from Heated Streams," Iowa Institute of Hydraulics Research, Report No. 155, 1974.

49. Panofsky, H.A., "Determination of Stress from Wind and Temperature Measurements," Quart. J. Roy. Meteorol. Soc., Vol. 89, p. 85-94, 1963.

50. Priestley, C.H.B. and Taylor, J.B., "On the Assessment of Surface Heat Flux and Evaporation Using Large-Scale Parameters," Monthly Weather Review, Vol. 100, No. 2, p. 81-92, 1972.

51. Quinn, F.H., "An Improved Aerodynamic Evaporation Technique for Large Lakes with Application to the International Field Year for the Great Lakes," Water Resources Research, Vol. 15, No. 4, p. 935-40, 1979.

52. Resch, F.J. and Selva, J.P., "Turbulent Air-Water Mass Transfer Under Varied Stratification Conditions," Journal of Geophysical Research, Vol. 84, No. C7, p.3205, 1979.

53. Rimsha, V.A. and Donchenko, R.V., "The Investigation of Heat Loss from Free Water Surfaces in Wintertime," (in Russian) Trudy Leningrad Gosub- Gidrol. Inst. 64, 1957.

54. Rohwer, E., "Evaporation from Free Water Surfaces," U.S. Dept. of Agriculture, Technical Bulletin No. 271, 1931.

55. Ryan, P.J. and Harleman, D.R.F., "An Analytical and Experimental Study of Transient Cooling Pond Behavior," R.M. Parsons Laboratory, Technical Report No. 161, MIT, 1973.

56. Ryan, P.J., Stolzenbach, K.D. and Harleman, D.R.F., "Surface Heat Loss from Cooling Ponds," Water Resour. Res., Vol. 10, p. 930, 1974.

57. Shulyakovsky, L.G., "Formula for Computing Evaporation with Allowance for Temperature of Free Water Surface," Soviet Hydrology Selected Papers, Issue No. 6, 1969.

58. Throne, R.F., "How to Predict Cooling Lake Action," Power, p. 86-89, September 1951.

59. Turner, J.S., Buoyancy Effects in Fluids, Cambridge University Press, Cambridge, England, 1973.

60. Ward, G.H., "Accuracy of the Harbeck Diagram for Forced Evaporation," Journal of the Energy Division, ASCE, Vol. 106, No. EY1, p. 23, 1980.

61. Watanabe, M., Harleman, D.R.F. and Connor, J.J., "Finite Element Model for Transient Two-Layer Cooling Pond Behavior," M.I.T., Department of Civil Engineering, R.M. Parsons Laboratory for Water Resources and Hydrodynamics Technical Report No. 202, July 1975.

62. Weeks, W.F. et al., "Wintertime Dissipation of Heat from a Thermally Polluted River," Water Resources Research, Vol. 7, No. 6, 1971.

63. Weisman, R.N., "Comparison of Warm Water Evaporation Equations," Jour. Hydraulics Div., ASCE, Vol. 101, No. HY10, p. 1303-1313, 1975.

64. Weisman, R.N. and Brutsaert, W., "Evaporation and Cooling of a Lake Under Unstable Atmospheric Conditions," Water Resources Research, Vol. 9, No. 5, 1973.

65. Wengefeld, P. and Plate, E.J., "Evaporation from a Water Current Under the Influence of Wind-Induced Waves," IAHR Congress, Baden Baden, Germany, 1977.

66. West, R.E., "Field Investigation of Cooling Tower and Cooling Pond Plumes," EPA-600-17-78-059, 1978.

67. Winter, T.C., "Uncertainties in Estimating the Water Balance of Lakes," Water Resources Bulletin, Vol. 17, p. 82, 1981.

68. Wunderlich, W.O., "Heat and Mass Transfer Between a Water Surface and the Atmosphere," Engineering Laboratory, Tennessee Valley Authority, Lab. Report No. 14, 1972.